Expanding Molecular Designs for Mechanochromic Polymers

Thesis by

Yan Sun

In Partial Fulfillment of the Requirements for

the degree of

Doctor of Philosophy

CALIFORNIA INSTITUTE OF TECHNOLOGY

Pasadena, California

2026

(Defended Apr 27, 2026)

Yan Sun
ORCID: 0000-0002-3882-131X

ACKNOWLEDGEMENTS

I would first like to thank my advisor, Professor Maxwell Robb. I am deeply grateful for the scientific training I received under his guidance throughout my graduate studies at Caltech. Under his mentorship, I grew not only in my knowledge of chemistry, but also in how I think about research and approach scientific questions. I still remember our first one-on-one conversation by the Millikan pond, when I first saw the care and thoughtfulness he brings to mentoring his students. Throughout my time in the Robb group, Max has taught me far more than science alone. He has shaped the way I think about research, mentorship, and my future. What I have learned from him will continue to shape me throughout my life and career.

I am deeply grateful to my thesis committee, Professor Hosea Nelson, Professor Lu Wei, and Professor Brian Stoltz, for their time, guidance, and thoughtful feedback throughout my graduate studies. I truly appreciate each annual committee meeting and the valuable suggestions they gave me. Their encouragement to take on the greatest challenges in my career is something I will always remember.

I would also like to thank my undergraduate advisors, Professor Xin-Yuan Liu and Professor Kaka Zhang, for giving me the opportunity to work in their laboratories. Under their guidance, I gained my first real experience in scientific research and developed a much deeper interest in chemistry and functional materials. Their encouragement and support gave me the confidence to continue this path and pursue my PhD.

I would also like to thank all members of the Robb group for making the lab such a supportive, thoughtful, and enjoyable place. I would especially like to thank my mentor, Molly McFadden, who taught me so much when I first joined the lab. She is an exceptional chemist and a generous mentor. Her patience, guidance, and willingness to share her knowledge shaped my early years in the lab. I am also deeply grateful to Ross Barber, who offered tremendous help whenever my synthesis was not working and always had thoughtful suggestions for how to move forward. I am also deeply grateful to Skylar Osler, Stella Luo, and Debbie Tseng. They helped me at many important moments in my research, and their suggestions often helped me move forward when I felt stuck. Their support carried me through many of the challenges I faced throughout my graduate school. I would also like to thank May Zeng, Peng Liu, Anna Overholts, Brooke Versaw, Corey Husic, Nathan Ballinger, Analiese Wiedenbeck, Liam Ordner, Varun Gupta, Madison Patch, Audrey Conner, Jolly Patro, and

Wendy Granados Razo. Each of them helped me in different ways at different moments, and their kindness made a real difference during my time in graduate school. They shaped not only my time in the lab, but also the way I will move forward in science.

Beyond the lab, I would like to thank all of my friends at Caltech for bringing so much joy to my life outside of the lab. I will always remember the game nights with Yuxing, Zhiyang, Jee Won, Stella, and Changfan, as well as the karaoke nights with May, Ziyang, Hao, Kaiwen, and Hengyu. I am also grateful for the fun of playing softball with Churchgoers and following sports with Nathan and Liam. I am especially grateful to Molly, Ross, Stella, and Skylar for the friendship and laughter that we shared in office 311.

Above all, I would like to thank my parents for supporting me from the very beginning of my journey in chemistry and for always encouraging me to continue my studies. Their love and unwavering support gave me strength through the most difficult times in graduate school. I will always be grateful for their faith in me and for everything they have done for me.

Finally, I would like to thank my partner, Katie, for always standing by me and supporting me in every part of life. She has made my life brighter in countless ways and has given me the courage to face the many challenges of graduate school. I am deeply grateful to have shared both the joys and challenges with her. Her love and support have been a constant source of strength throughout this journey.

ABSTRACT

In the field of polymer mechanochemistry, mechanical force is harnessed to promote selective chemical transformations in the stress-sensitive molecules known as mechanophores. Mechanochromic mechanophores, which produce visible optical changes in polymeric materials in response to mechanical force, are particularly attractive for applications in force sensing, damage reporting, and patterning. This dissertation explores new molecular design strategies for mechanochromic polymers, elucidates fundamental understanding of mechanophore reactivity, and develops systems capable of responding to discrete stimuli and exhibiting multistage coloration.

Unlike typical angular naphthopyrans that exhibit photochromic and mechanochromic behavior, constitutionally isomeric linear naphthopyrans and 2*H*-1-benzopyrans are commonly considered non-photochromic at ambient temperature, while their mechanochemical activity has not been studied. In Chapter 1, we demonstrate that linear naphthopyrans incorporating an electron-donating amine substituent do in fact undergo a ring-opening reaction upon photoirradiation with UV light and upon mechanical activation, resulting in pronounced photochromic and mechanochromic behavior. In Chapter 2, we report that the indole-fused 2*H*-1-benzopyran mechanophore undergoes a ring-opening reaction under force to generate a yellow-colored merocyanine dye, which is further reversibly transformed to a purple-colored dye upon the introduction of acid, enabling a multi-staged coloration.

In contrast to conventional mechanochromic mechanophores, the mechanically gated photoswitching strategy, which decouples mechanochemical activation from the chromogenic response, enables mechanophores with high force-specificity and a high degree of modularity. Chapter 3 describes a mechanically gated 3*H*-anthra[2,1-*b*]pyran photoswitch that enables a three-stage coloration process. Mechanochemical activation of the photoinert mechanophore in the polymer generates a yellow-colored 3*H*-anthrapyran photoswitch, which can subsequently undergo a photochemical ring-opening reaction producing an orange-red colored merocyanine dye. Chapter 4 further expands this concept through the design of a naphthopyran mechanophore bearing a furan–maleimide Diels–Alder adduct whose active photochromism is regulated by mechanical force, providing a new approach to multistate stimuli-responsive polymers.

PUBLISHED CONTENT AND CONTRIBUTIONS

Sun, Y.; McFadden, M. E.; Osler, S. K.; Barber, R. W.; Robb, M. J. Anomalous Photochromism and Mechanochromism of a Linear Naphthopyran Enabled by a Polarizing Dialkylamine Substituent. *Chem. Sci.* **2023**, *14*, 10494–10499. DOI: 10.1039/D3SC03790H
Y. S. designed the research, performed the experiments, and wrote the manuscript.

Sun, Y.; Razo, W. G.; Luo, S. M.; Osler, S. K.; Robb, M. J. Mechanochemical Activation of an Indole-Fused 2*H*-Benzopyran Generates an Acidochromic Merocyanine Dye Enabling Multicolor Chromomorphic Materials. *Polym. Chem.* **2025**, *16*, 4128–4135. DOI: 10.1039/D5PY00746A
Y. S. designed the research, performed the experiments, and wrote the manuscript.

TABLE OF CONTENTS

C h a p t e r 1

ANOMALOUS PHOTOCHROMISM AND MECHANOCHROMISM OF A LINEAR NAPHTHOPYRAN ENABLED BY A POLARIZING DIALKYLAMINE SUBSTITUENT

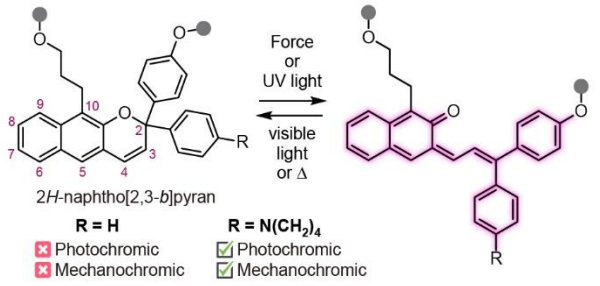

This chapter has been reprinted from Sun, Y.; McFadden, M. E.; Osler, S. K.; Barber, R. W.; Robb, M. J. *Chem. Sci.* **2023**, *14*, 10494–10499.

In contrast to common angular naphthopyrans that exhibit strong photochromic and mechanochromic behavior, constitutionally isomeric linear naphthopyrans are typically not photochromic, due to the putative instability of the completely dearomatized merocyanine product. The photochemistry of linear naphthopyrans is thus relatively understudied compared to angular naphthopyrans, while the mechanochromism of linear naphthopyrans remains completely unexplored. Here we demonstrate that the incorporation of a polarizing dialkylamine substituent enables photochromic and mechanochromic behavior from polymers containing a novel linear naphthopyran motif. In solution phase experiments, a Lewis acid trap was necessary to observe accumulation of the merocyanine product upon

photochemical and ultrasound-induced mechanochemical activation. However, the same linear naphthopyran molecule incorporated as a crosslinker in polydimethylsiloxane elastomers renders the materials photochromic and mechanochromic without the addition of any trapping agent. This study provides insights into the photochromic and mechanochromic reactivity of linear naphthopyrans that have conventionally been considered functionally inert, adding a new class of naphthopyran molecular switches to the repertoire of stimuli-responsive polymers.

1.1 Introduction

Naphthopyrans are molecular switches that undergo a 6π electrocyclic ring-opening reaction upon external stimulation to generate highly colored merocyanine dyes.[1] The photochemical ring-opening reaction of naphthopyrans upon irradiation with UV light has been extensively studied.[2,3] More recently, it was discovered that naphthopyrans respond similarly to mechanical force as the external stimulus, enabling new opportunities to use these versatile switches for stress sensing applications in polymers.[4] The nascent field of polymer mechanochemistry explores chemical transformations that are promoted selectively by mechanical force in privileged stress-sensitive molecules called mechanophores.[5–7] Mechanochromic mechanophores generate colored products upon mechanochemical activation, facilitating the straightforward visualization of stress and/or strain in materials.[8] A rapidly growing class of mechanochromic mechanophores includes spiropyran,[9–11] spirothiopyran,[12] rhodamine,[13–15] oxazine,[16,17] π-extended anthracene adducts,[18,19] triarylmethanes,[20] and diarylbibenzofuranone,[21,22] among others. Our group has been particularly interested in naphthopyrans due to their synthetic modularity and

structural diversity, providing access to mechanochromic mechanophores and materials with a wide range of functional properties.[23–28]

The vast majority of studies on the photochromism and mechanochromism of naphthopyran have focused on the so-called angular naphthopyrans (Scheme 1.1).[1] Angular naphthopyrans have been extensively studied and developed as photoswitches for commercial applications in photochromic lenses.[3] The mechanochemical ring-opening reaction of angular 3*H*-naphtho[1,2-*b*]pyran in polymeric materials was first reported in 2016.[4] In 2021, a closely related angular 2*H*-naphtho[2,1-*b*]pyran scaffold was also demonstrated to exhibit mechanochromic reactivity,[25,26] complementing the well-known photochromic behavior. However, the mechanochemical reactivity of a structurally isomeric linear 2*H*-naphtho[2,3-*b*]pyran scaffold has not been studied (Scheme 1.1b). These so-called linear naphthopyrans contain a pyran ring that is linearly oriented with respect to the naphthalene nucleus. In contrast to the angular naphthopyrans, linear naphthopyrans do not typically exhibit photochromic behavior at ambient temperature because the ring-opening reaction results in

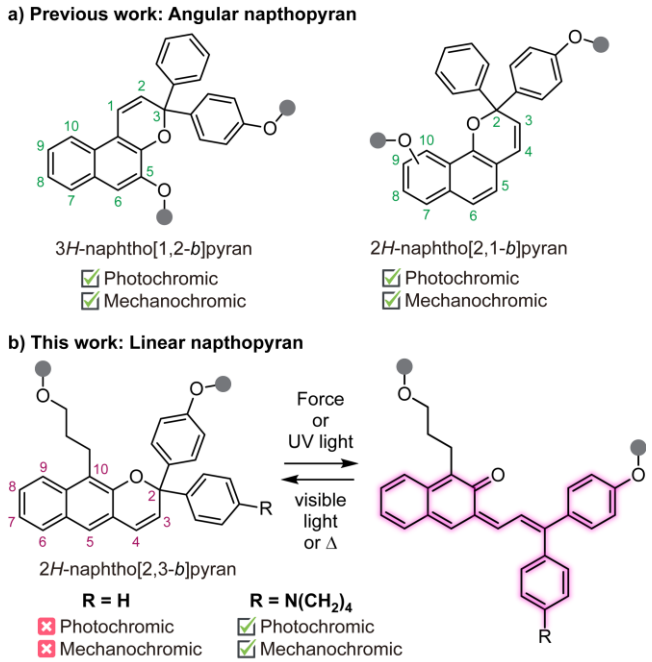

Scheme 1.1 Naphthopyran isomers and their stimuli-responsive behavior. (a) Angular naphthopyrans undergo ring-opening reactions with UV light or mechanical force. (b) Photochromism and mechanochromism of linear 2*H*-naphthopyran is enabled upon introduction of an electron donating dialkylamine substituent.

complete dearomatization of the naphthalene core.[1] Therefore, linear naphthopyrans have received relatively little attention as photoswitches and their mechanochemical reactivity is unknown.

We recently demonstrated that mechanical force is capable of promoting the dual ring-opening reaction of naphthodipyran, which diverges from the photochemical reaction where the concurrent ring opening of both pyran units is inaccessible.[27] Trapping the putatively unstable dimerocyanine product using a Lewis acid proved critical for observing its formation in solution upon ultrasound-induced mechanochemical activation. Incorporation of an electron rich dialkylamine substituent at the *para*-position of the pendant aryl groups enables complexation of the merocyanine product with boron trifluoride, which significantly slows or even eliminates thermal reversion.[29] Encouraged by these results, we hypothesized that the ring-opening reaction of an appropriately substituted linear naphthopyran may be observable upon trapping with boron trifluoride. Herein, we study the photochemical and mechanochemical reactivity of polymers containing a linear naphthopyran unit. In solution, a polarizing dialkylamine substituent is indeed demonstrated to turn on the photochromic and mechanochromic behavior of linear naphthopyran in the presence of boron trifluoride. Notably, however, silicone elastomers crosslinked with the same dialkylamine-substituted linear naphthopyran motif also exhibit photochromism and mechanochromism in the absence of any trapping agent.

1.2 Results and Discussion

Density functional theory calculations using the constrained geometries simulate external force (CoGEF) method were first performed to investigate the mechanochemical reactivity

of linear naphthopyran.[30,31] Models of targeted linear 2*H*-naphtho[2,3-*b*]pyrans containing *para*-H and *para*-pyrrolidine substituents are both predicted to undergo ring-opening reactions upon mechanical elongation to generate the anticipated merocyanine products (Figure 1.1 and Figure S1.1). The mechanochemical ring-opening reactions of the linear naphthopyran derivatives with *para*-H and *para*-pyrrolidine substitution occur with a maximum force (F_{max}) of 4.5 and 4.2 nN, respectively, which are similar to F_{max} values predicted by CoGEF for other naphthopyran mechanophores.[31]

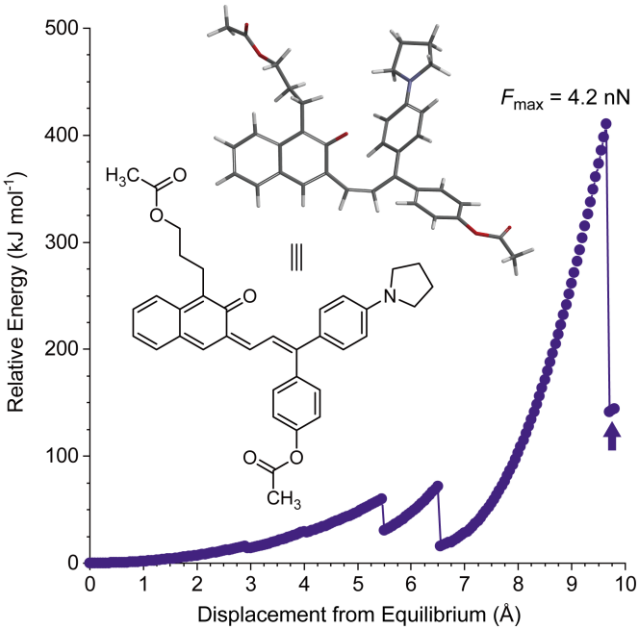

Figure 1.1 Density functional theory (DFT) calculations using the constrained geometries simulate external force (CoGEF) method performed on a linear 2*H*-naphtho[2,3-*b*]pyran model containing a pyrrolidine substituent predict a ring-opening reaction upon mechanical elongation. The structure of the predicted merocyanine product is shown, corresponding to the position in the profile denoted by the arrow. The features at ~5.5 and 6.5 Å displacement correspond to conformational changes. Calculations were performed at the B3LYP/6-31G* level of theory.

Encouraged by these computational results, we next set out to experimentally investigate the photochemical and mechanochemical reactivity of linear naphthopyran. Polymers in dilute solution undergo rapid extension upon ultrasonication with elongational forces maximized near the chain midpoint.[32] Therefore, poly(methyl acrylate) polymers containing a chain-centered linear naphthopyran unit (**PMA-LNP** and **PMA-PyLNP**) were designed and synthesized, along with polymer **PMA-Control** containing a pyrrolidine-substituted linear naphthopyran unit at the chain-end, which does not experience mechanical force upon

Scheme 1.2 Synthesis of poly(methyl acrylate) polymers incorporating a linear 2*H*-naphthopyran unit.

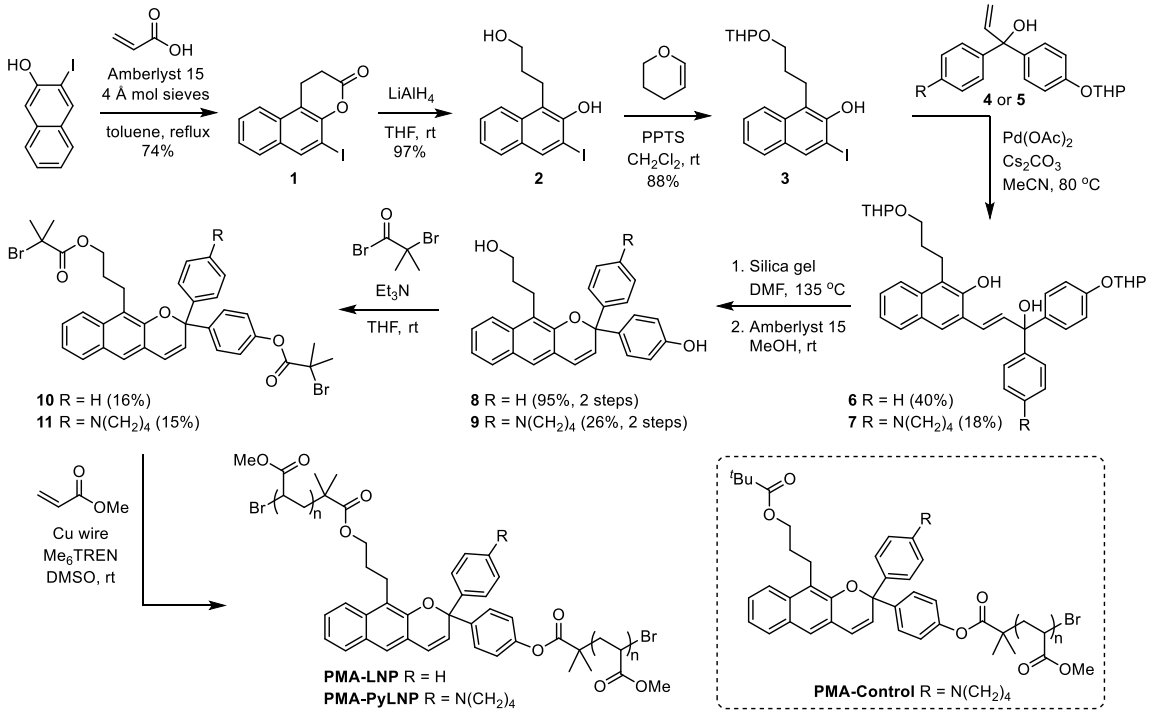

ultrasonication (Scheme 1.2).[7] Naphthopyrans are typically synthesized via an acid-catalyzed reaction between a naphthol and a propargyl alcohol.[33] However, this protocol is not effective for the synthesis of linear 2*H*-naphtho[2,3-*b*]pyrans.[34] We therefore employed an alternative Heck coupling strategy for the construction of the linear naphthopyran scaffold.[35,36] Synthesis commenced by reacting 1-iodo-2-naphthol with acrylic acid to generate lactone **1**, followed by reduction with LAH to afford tethered alcohol **2**. Protection of the primary alcohol with tetrahydropyran (THP) furnished naphthol **3**, which was engaged in a cross-coupling reaction with allylic alcohols **4** or **5** containing a *para*-H or *para*-pyrrolidine substituent, respectively, to afford the corresponding Heck products **6** and **7**. Naphthopyran formation and THP removal was then accomplished in a two-step sequence using silica gel in DMF at 135 °C and Amberlyst 15 in methanol at room temperature, respectively. Linear

naphthopyran diols **8** and **9** were esterified with bromoisobutyryl bromide to afford bis-initiators **10** and **11**, which were employed in the controlled radical polymerization of methyl acrylate using copper wire and Me_6TREN in DMSO[37] to furnish polymers **PMA-LNP** (M_n = 132 kDa; $Đ$ = 1.12) and **PMA-PyLNP** (M_n = 262 kDa; $Đ$ = 1.15) containing a chain-centered linear naphthopyran unit with *para*-H and *para*-pyrrolidine substituents, respectively. Polymer **PMA-Control** (M_n = 238 kDa; $Đ$ = 1.09) containing a pyrrolidine-substituted linear naphthopyran unit at the chain end was synthesized in a similar fashion starting from the naphthopyran with a single α-bromo ester initiating group.

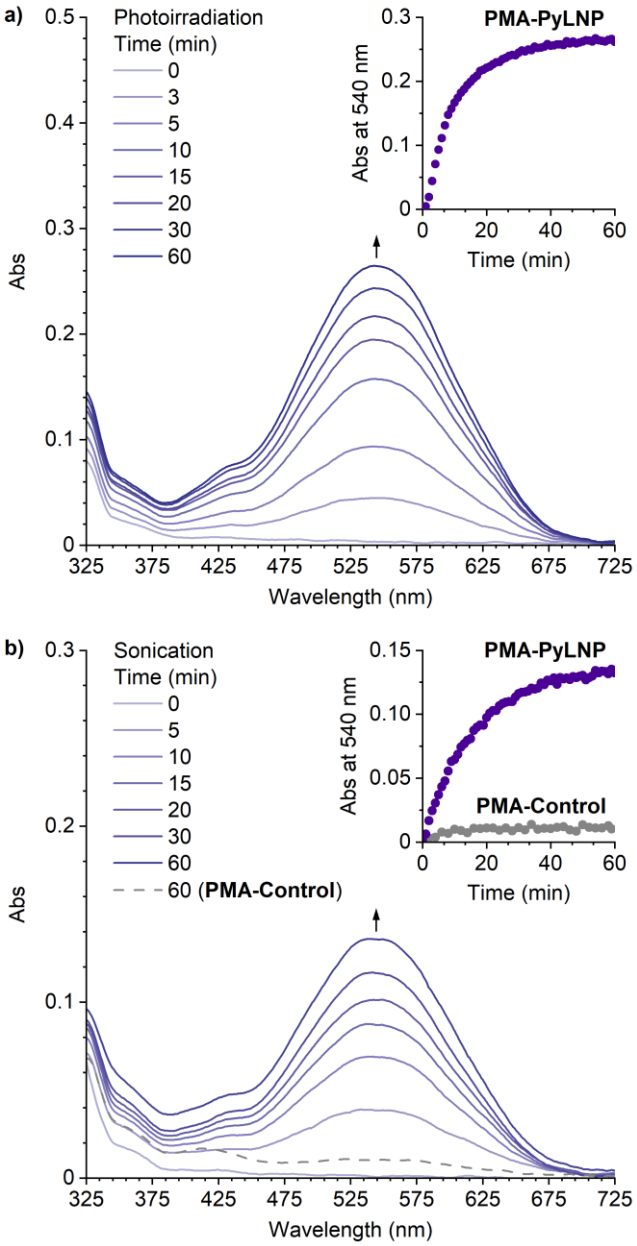

Figure 1.2 UV-vis absorption spectra of **PMA-PyLNP** in CH_3CN with 0.5 mM $BF_3{\cdot}Et_2O$ during (a) photoirradiation at −30 °C with 311 nm UV light, and (b) continuous ultrasonication at −15 °C. Ultrasonication of **PMA-Control** results in negligible merocyanine formation. Insets show absorbance at 540 nm as a function of photoirradiation or sonication time.

The photochemical and mechanochemical reactivity of the linear naphthopyrans was evaluated by subjecting dilute solutions of the polymers (2 mg/mL in CH_3CN with 30 mM BHT) to photoirradiation with 311 nm UV light at −30 °C or continuous ultrasonication at −15 °C and UV-vis absorption spectra were recorded synchronously using a continuous flow setup.[23,25] No photochromic or mechanochromic response was observed for **PMA-LNP** under these conditions or when similar experiments were performed in the presence of 0.5 mM $BF_3{\cdot}Et_2O$ (Figure S1.2). Likewise, no changes in absorption were observed upon photoirradiation or ultrasonication of **PMA-PyLNP** in the absence of $BF_3{\cdot}Et_2O$ (Figure S1.3). However, photoirradiation of **PMA-PyLNP** in the presence of 0.5 mM $BF_3{\cdot}Et_2O$ resulted in a new visible absorption peak at 540 nm (Figure 1.2a). An identical absorption spectrum was generated upon ultrasound-induced mechanochemical activation of **PMA-PyLNP** in the presence of 0.5 mM $BF_3{\cdot}Et_2O$ (Figure 1.2b). The products were found to be thermally persistent with no thermal reversion of the trapped merocyanine observed upon cessation of ultrasonication (Figure S1.4). Importantly, ultrasonication of **PMA-Control** under the same conditions in the presence of 0.5 mM $BF_3{\cdot}Et_2O$ resulted in negligible changes in absorption, confirming that mechanical force is responsible for the reaction of **PMA-PyLNP** upon ultrasonication in the presence of $BF_3{\cdot}Et_2O$ (Figure 1.2b and Figure S1.5).

We next explored the potential of the linear naphthopyran mechanophore to serve as a molecular force probe for visualizing stress or strain in solid polymeric materials. Esterification of diol **9** with 4-pentenoic anhydride afforded bis-alkene-functionalized linear naphthopyran **Crosslinker-PyLNP**, which was covalently incorporated into elastomeric polydimethylsiloxane (PDMS) networks via Pt-catalyzed hydrosilylation (Figure 1.3a).[11]

Interestingly, mechanical activation of the PDMS film via compression using an embossed stamp resulted in purple coloration where force was applied, and a similar chromogenic response was observed upon irradiation with UV light through a simple photomask (Figure 1.3b). The purple color generated upon photochemical or mechanochemical activation faded completely after ~20 min. These results contrast those above for the photochemical and mechanochemical activation of **PMA-PyLNP** in solution, in which merocyanine accumulation was only observed in the presence of $BF_3{\cdot}Et_2O$. Thermal reversion of naphthopyran-derived merocyanine dyes is significantly slower in bulk polymeric materials,[24] but that is unlikely to completely account for the differences between solution and solid state activation. The pyrrolidine substituent presumably favors a zwitterionic form of the merocyanine that regains some degree of aromaticity in comparison to the quinoidal form typical of angular naphthopyran derived merocyanines. The anionic oxygen atom of the zwitterion may also engage in a stabilizing interaction with the oxophilic silicon atoms in the PDMS network. We note that PDMS materials incorporating a linear naphthopyran

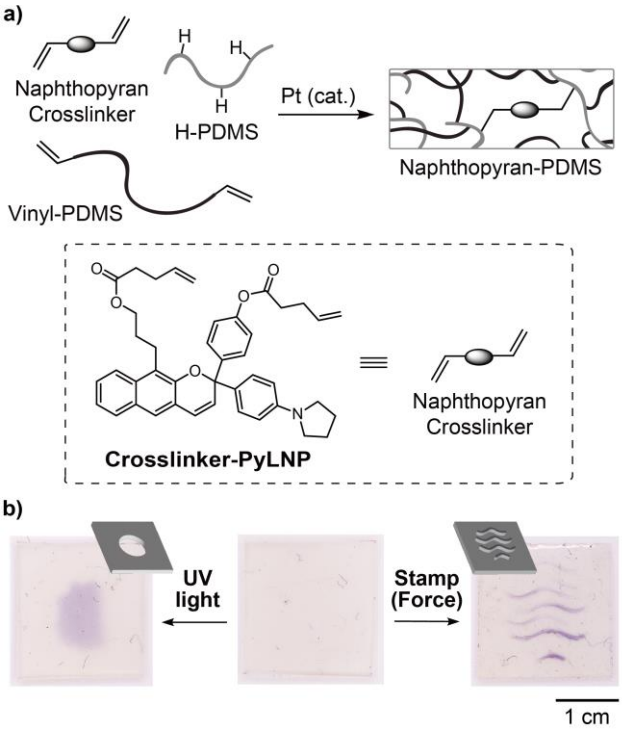

Figure 1.3 (a) PDMS networks covalently crosslinked with linear 2*H*-naphthopyran mechanophore **Crosslinker-PyLNP** (1.5 wt%) prepared via Pt-catalyzed hydrosilylation. (b) Photographs of the material before and after irradiation with 365 nm UV light for 120 s through a photomask, and after mechanical force applied via compression (2×) using an embossed stamp. Schematic representations of the photomask and stamp are shown.

crosslinker without a pyrrolidine substituent (*para*-H) were prepared in a similar fashion as above, but did not exhibit any photochromic or mechanochromic behavior (Figure S1.6).

1.3 Conclusions

Unlike typical angular naphthopyrans that exhibit photochromic and mechanochromic behavior, structurally isomeric linear 2*H*-naphtho[2,3-*b*]pyrans are poorly developed because they are commonly considered non-photochromic at ambient temperature, while their mechanochemical activity has not been studied. Here we investigate the photochemical and mechanochemical reactivity of a linear naphthopyran covalently incorporated into polymers and demonstrate that a polarizing dialkylamine substituent enables both photochromic and mechanochromic behavior in solution using UV light and ultrasonication, respectively. Accumulation of the merocyanine dye in solution is attributed to complexation of the ring-opened product with boron trifluoride, which renders it thermally persistent. However, elastomeric polydimethylsiloxane (PDMS) materials incorporating the linear naphthopyran unit as a crosslinker also exhibit photochromic and mechanochromic properties in the absence of any trapping agent. The polarizing dialkylamine substituent may favor the zwitterionic form of the merocyanine dye, regaining some aromaticity and potentially leading to a stabilizing interaction between the anionic oxygen atom and the oxophilic silicon atoms in the PDMS matrix. This study expands knowledge of the reactivity of linear naphthopyrans that have conventionally been overlooked as photoswitches and adds a new class of naphthopyran mechanophores to the catalog for designing stimuli-responsive polymers.

1.4 Supplementary Figures

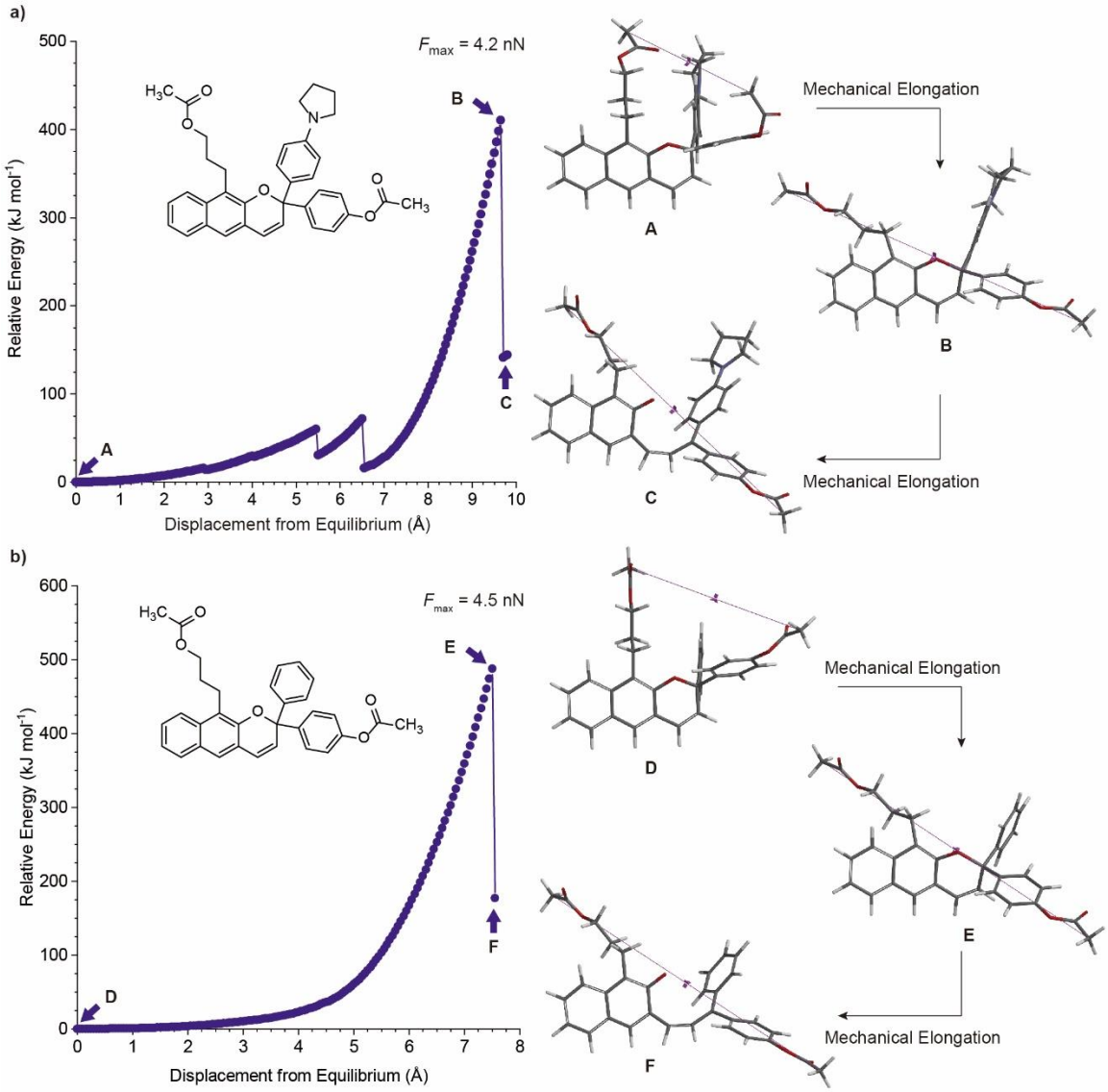

Figure S1.1 Density functional theory (DFT) calculations using the constrained geometries simulate external force (CoGEF) method performed on linear 2*H*-naphtho[2,3-*b*]pyran models with (a) *para*-pyrrolidine, and (b) *para*-H substitution predict a ring-opening reaction upon mechanical elongation. The structures at various points in the CoGEF profile are shown at right, corresponding to the positions denoted by the arrows. Calculations were performed

at the B3LYP/6-31G* level of theory. The carbon atoms of the terminal methyl groups were used to define the distance constraint.

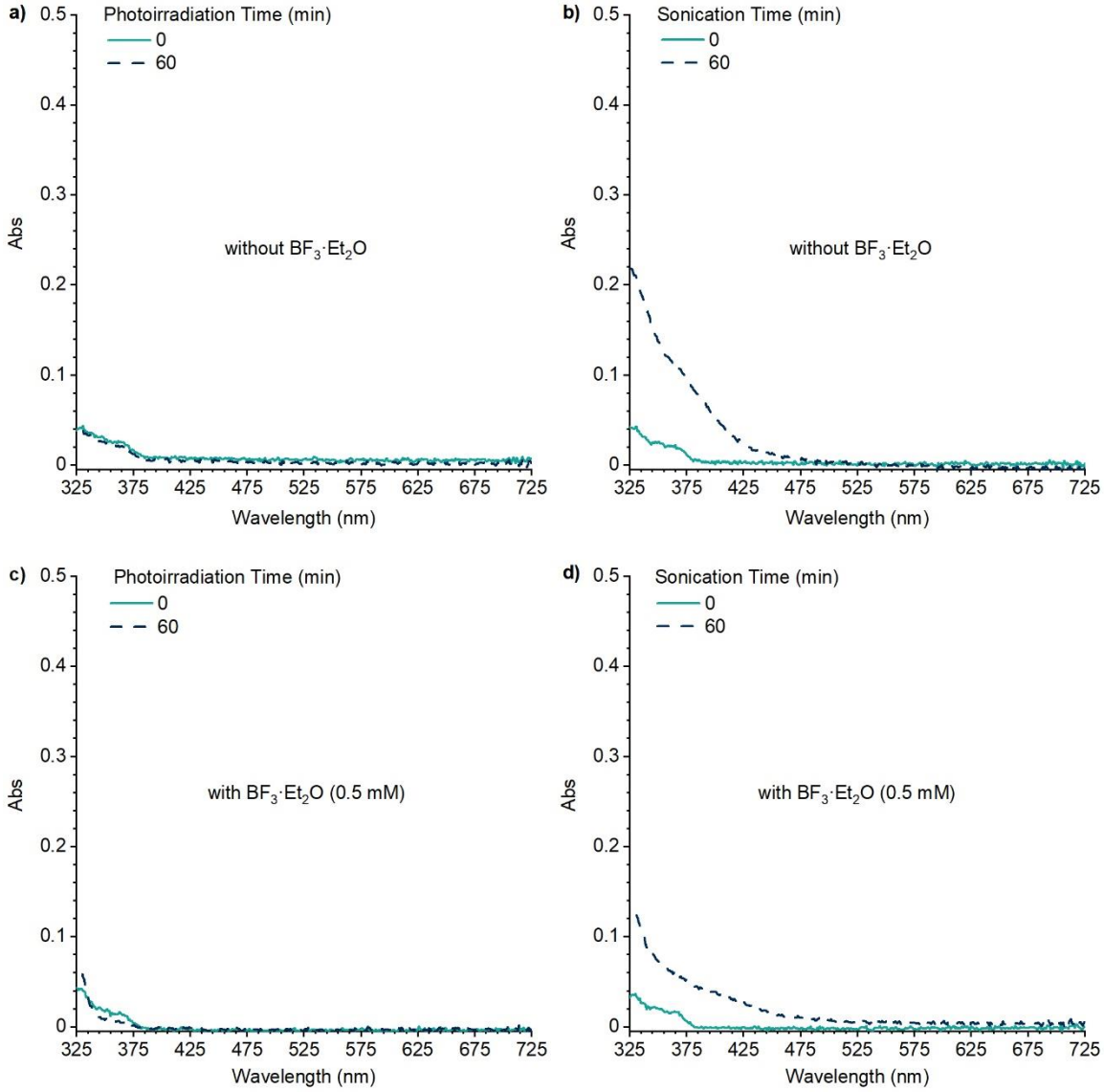

Figure S1.2 Comparison of the photochemical and mechanochemical reactivity of **PMA-LNP** in the presence or absence of $BF_3{\cdot}Et_2O$. UV-vis absorption spectra of **PMA-LNP** in CH_3CN (2 mg/mL with 30 mM BHT) before and after (a) photoirradiation at −30 °C with 311 nm UV light, and (b) continuous ultrasonication at −15 °C for 60 min. UV-vis absorption

spectra of **PMA-LNP** in CH_3CN (2 mg/mL with 30 mM BHT) with 0.5 mM $BF_3 \cdot Et_2O$ before and after (c) photoirradiation at −30 °C with 311 nm UV light, and (d) continuous ultrasonication at −15 °C for 60 min. No photochromic or mechanochromic response was observed under any conditions.

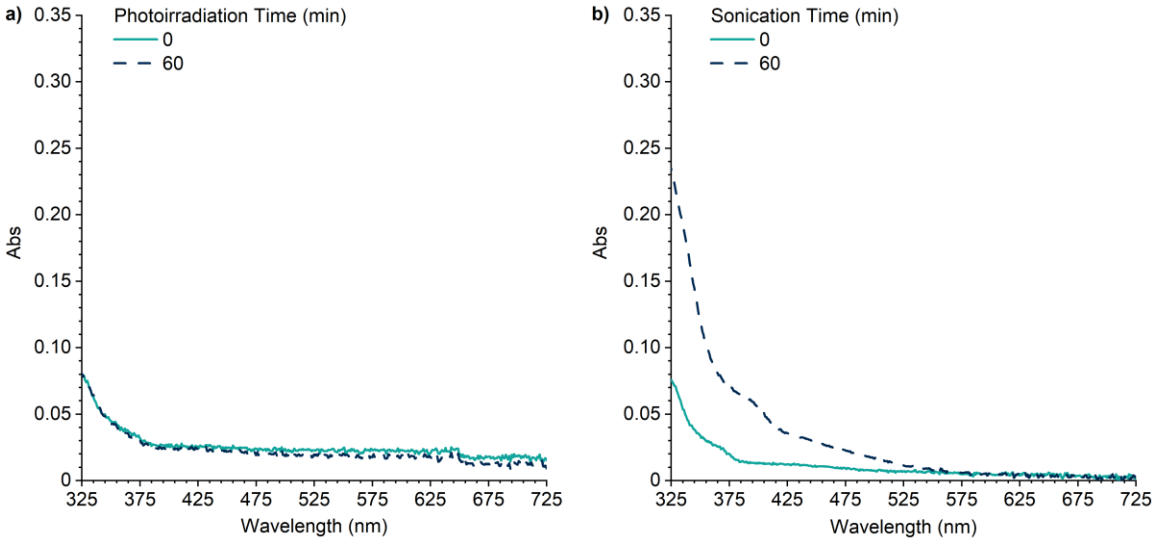

Figure S1.3 UV-vis absorption spectra of **PMA-PyLNP** in CH_3CN (2 mg/mL with 30 mM BHT) before and after (a) photoirradiation at −30 °C with 311 nm UV light, and (b) continuous ultrasonication at −15 °C for 60 min. No photochromic or mechanochromic response was observed from **PMA-PyLNP** in the absence of $BF_3 \cdot Et_2O$.

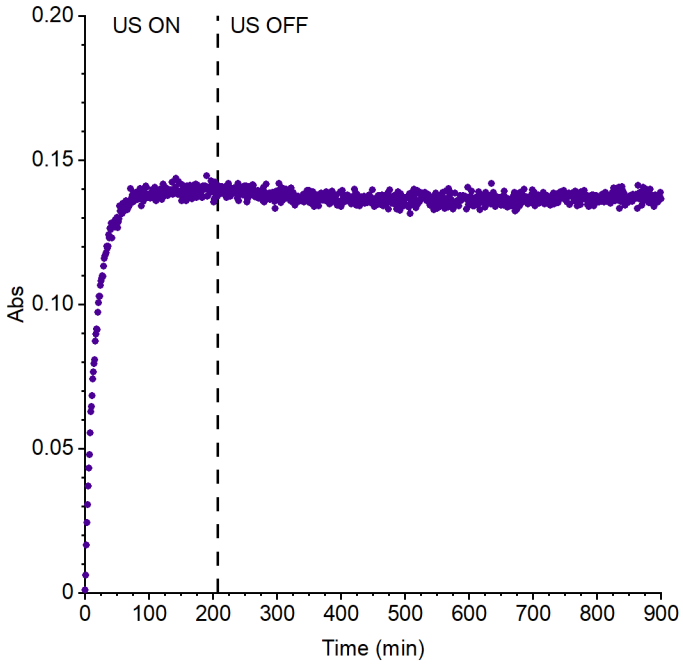

Figure S1.4 Absorbance recorded at 540 nm during ultrasonication of **PMA-PyLNP** in CH_3CN (2 mg/mL with 30 mM BHT) in the presence of 0.5 mM $BF_3 \cdot Et_2O$, and then after cessation of ultrasonication. Ultrasound-induced mechanochemical activation of **PMA-PyLNP** produces a persistent merocyanine product with no thermal reversion observed upon cessation of ultrasonication. Absorption was monitored at λ_{max}.

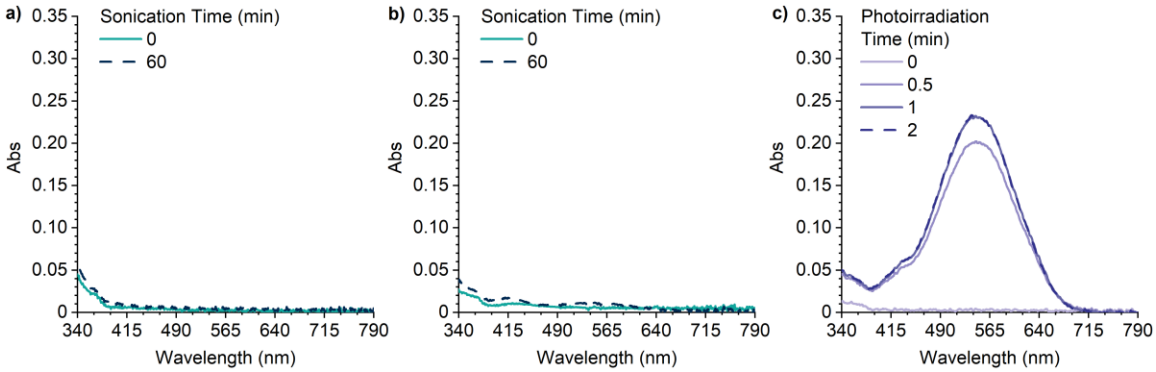

Figure S1.5 UV-vis absorption spectra of **PMA-Control** in CH_3CN (2 mg/mL with 30 mM BHT) before and after continuous ultrasonication at −15 °C for 60 min (a) without $BF_3{\cdot}Et_2O$, and (b) in the presence of 0.5 mM $BF_3{\cdot}Et_2O$. No changes in absorption are observed for **PMA-Control** upon ultrasonication in direct contrast to **PMA-PyLNP**, which contains the linear naphthopyran mechanophore near the chain midpoint where it is susceptible to mechanical force. (c) UV-vis absorption spectra of **PMA-Control** in CH_3CN (2 mg/mL with 30 mM BHT) in the presence of 0.5 mM $BF_3{\cdot}Et_2O$ before and after irradiation with 311 nm UV light, confirming the presence of the linear naphthopyran moiety at the polymer chain end. For this experiment, photoirradiation was performed in a quartz cuvette at room temperature without use of the flow setup.

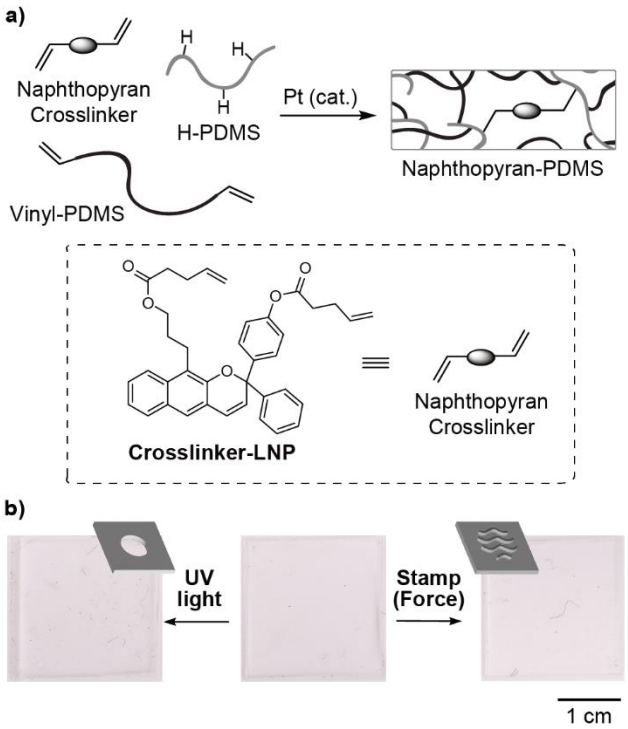

Figure S1.6 (a) PDMS networks covalently crosslinked with linear 2*H*-naphthopyran mechanophore **Crosslinker-LNP** (1.0 wt%) without a *para*-pyrrolidine substituent prepared via Pt-catalyzed hydrosilylation. (b) Photographs of the material before and after photoirradiation with 365 nm UV light for 120 s through a photomask, and after mechanical force applied via compression (2×) using an embossed stamp. Schematic representations of the photomask and stamp are shown. No photochromic or mechanochromic response is observed in contrast to the analogous materials incorporating **Crosslinker-PyLNP** with a polarizing dialkylamine substituent.

1.5 Experimental Section

1.5.1 General Experimental Details

Reagents from commercial sources were used without further purification unless otherwise stated. Methyl acrylate was passed through a short plug of basic alumina to remove inhibitor immediately prior to use. Amberlyst 15 was washed with acetone prior to use. Copper wire was soaked in 1 M HCl for 30 min and then rinsed consecutively with water and acetone immediately prior to use. Dry solvents were obtained from a Pure Process Technology solvent purification system. All reactions were performed under a N_2 atmosphere unless specified otherwise. Column chromatography was performed on a Biotage Isolera system using SiliCycle SiliaSep HP flash cartridges.

NMR spectra were recorded using a 400 MHz Bruker Avance III HD with Prodigy Cryoprobe or a 600 MHz Varian spectrometer with 5 mm triple resonance inverse probe. All ^{1}H NMR spectra are reported in δ units, parts per million (ppm), and were measured relative to the signals for residual chloroform (7.26 ppm), acetone (2.05 ppm), dichloromethane (5.32 ppm), or dimethyl sulfoxide (2.50 ppm) in deuterated solvent. All ^{13}C NMR spectra were measured in deuterated solvents and are reported in ppm relative to the signals for chloroform (77.16 ppm), acetone (206.26 ppm), dichloromethane (54.00 ppm), or dimethyl sulfoxide (39.52 ppm).

High resolution mass spectra (HRMS) were obtained from a Waters LCT Premier XE time-of-flight mass spectrometer equipped with an electrospray ionization (ESI) probe, a JEOL JMS-600H magnetic sector mass spectrometer equipped with a FAB+ probe, or via direct

injection on an Agilent 1260 Infinity II Series HPLC coupled to a 6230 LC/TOF system in electrospray ionization (ESI+) mode.

Analytical gel permeation chromatography (GPC) was performed using an Agilent 1260 series pump equipped with two Agilent PLgel MIXED-B columns (7.5 x 300 mm), an Agilent 1200 series diode array detector, a Wyatt 18-angle DAWN HELEOS light scattering detector, and a Optilab rEX differential refractive index detector. The mobile phase was THF at a flow rate of 1 mL/min. Molecular weights and molecular weight distributions were calculated by light scattering using a dn/dc value of 0.062 mL/g (25 °C) for poly(methyl acrylate).

UV-vis absorption spectra were recorded on a Thermo Scientific Evolution 220 spectrometer.

Ultrasound experiments were performed using a Vibra Cell 505 liquid processor equipped with a 0.5-inch diameter solid probe (part #630-0217), sonochemical adapter (part #830-00014), and a Suslick reaction vessel made by the Caltech glass shop (analogous to vessel #830-00014 from Sonics and Materials). Polymer solutions were continuously sampled for UV-vis analysis using a Cole Parmer Masterflex L/S pump system (item #EW-77912-10) composed of an L/S pump head (part #77390-00) and L/S precision variable speed drive (part #07528-20) using 4x6 mm PTFE tubing (part #77390-60) and a quartz flow-through cell (Starna, part #583.4-Q-10/Z8.5), which was connected using M6-threaded PTFE tubing (Starna, part #M6-SET). A Thermo Scientific EK45 Immersion Cooler (part #3281452) was used to maintain a constant temperature bath for sonication experiments. Photoirradiation with UV light was performed using either a DR/9W-UVA 365 nm lamp or a Philips PL-S

9W/01/2P UVB bulb with a narrow emission of 305–315 nm and a peak at 311 nm under ambient conditions unless indicated otherwise.

1.5.2 Synthesis and Characterization of Initiators and Polymers

Scheme S1.1 Synthesis of compounds used in this study not described in Scheme 1.2.

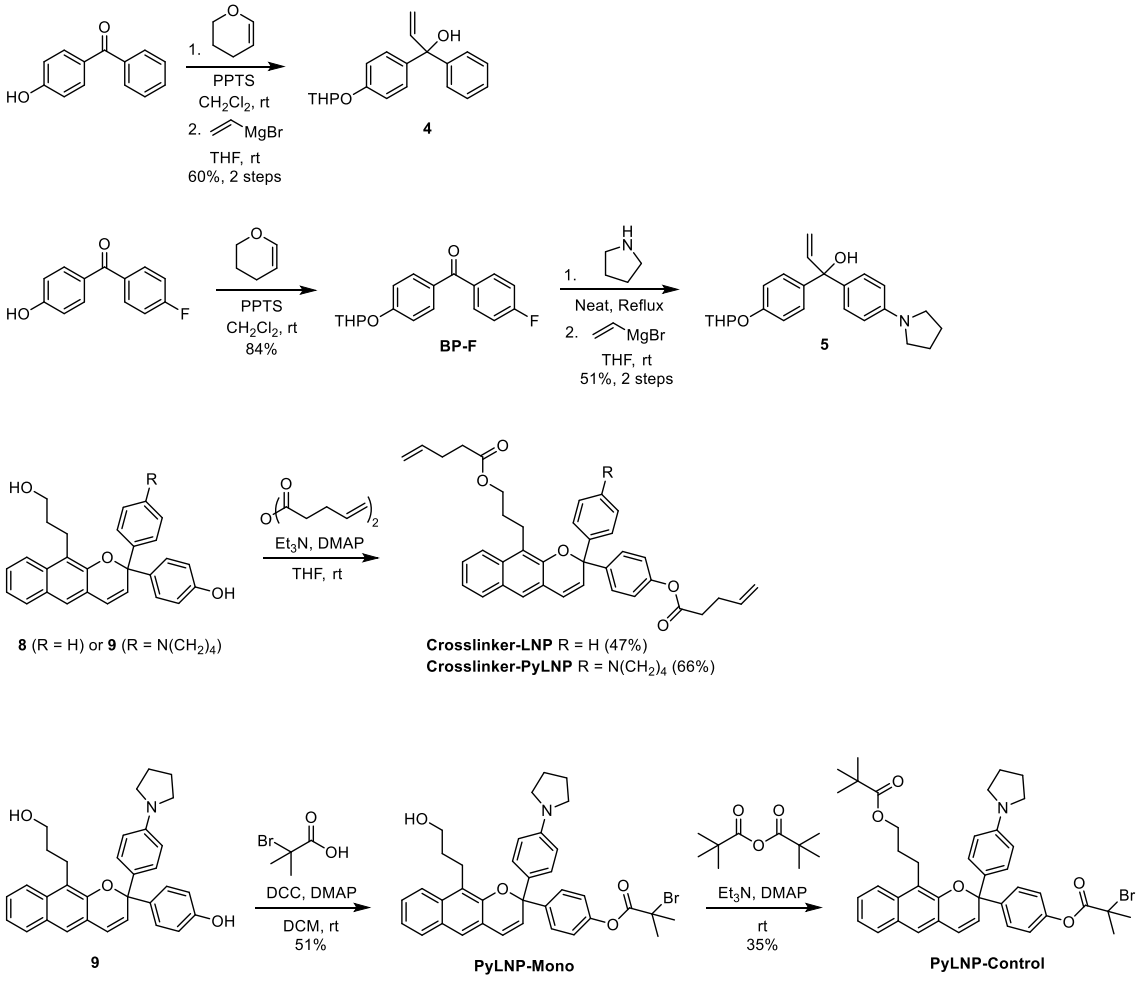

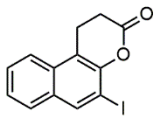

1

5-iodo-1,2-dihydro-3H-benzo[f]chromen-3-one (1). A flame-dried 10 mL round-bottom flask equipped with a stir bar was charged with 3-iodonaphthalen-2-ol (200 mg, 0.741 mmol), Amberlyst 15 (200 mg), and 4 Å molecular sieves (200 mg). The flask was evacuated and backfilled with N_2 three times. Dry toluene (2 mL) was then added via syringe, followed by the addition of acrylic acid (0.10 mL, 1.5 mmol) under N_2. After stirring at reflux overnight, the flask was removed from heat and the crude mixture was filtered, concentrated under reduced pressure, and purified by column chromatography on silica gel (0–15% ethyl acetate/hexanes) to produce the title compound **1** as a pale yellow solid (177 mg, 74%).

TLC (25% EtOAc/hexanes): $R_f = 0.50$

^{1}H NMR (400 MHz, Chloroform-*d*) δ: 8.28 (s, 1H), 7.84 (d, $J = 8.5$ Hz, 1H), 7.71 (d, $J = 8.2$ Hz, 1H), 7.61 – 7.53 (m, 1H), 7.50 – 7.43 (m, 1H), 3.34 (t, $J = 7.6$ Hz, 2H), 2.89 (dd, $J = 8.2$, 6.7 Hz, 2H).

^{13}C{^{1}H} NMR (101 MHz, Chloroform-*d*) δ: 167.4, 147.9, 138.7, 132.1, 130.9, 127.74, 127.66, 126.0, 122.9, 116.9, 84.7, 28.7, 20.6.

HRMS (FD, *m/z*): calcd for $[C_{13}H_9IO_2]^{+\cdot}$ $(M)^{+\cdot}$, 323.9647; found, 323.9644.

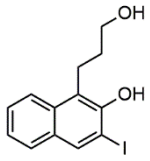

2

1-(3-hydroxypropyl)-3-iodonaphthalen-2-ol (2). A flame-dried 250 mL round-bottom flask equipped with a stir bar was charged with lithium aluminum hydride (700 mg, 18.4 mmol). The flask was evacuated and backfilled with N_2 three times and then dry THF (60 mL) was added via syringe. The flask was cooled in an ice bath and a solution of **1** (3.03 g, 9.35 mmol) in dry THF (20 mL) was added dropwise via syringe. After complete addition, the mixture was warmed to room temperature and stirred for 1 h. The flask was subsequently cooled in ice and ethyl acetate (20 mL) was added dropwise followed by a 10% aqueous solution of Rochelle's salt (100 mL). The mixture was stirred at room temperature overnight followed by addition of 1 M HCl (50 mL). The crude mixture was concentrated under reduced pressure and partitioned between water and ethyl acetate. The aqueous layer was discarded and the organic layer was washed with water and then dried over Na_2SO_4, filtered, and concentrated under reduced pressure. The crude product was purified by column chromatography (0–30% EtOAc/hexanes) to afford the title product as a yellow solid (2.98 g, 97%).

TLC (50% EtOAc/hexanes): $R_f = 0.56$

^{1}H NMR (400 MHz, Chloroform-*d*) δ: 8.22 (s, 1H), 7.88 (d, $J = 8.6$ Hz, 1H), 7.67 (d, $J = 8.1$ Hz, 1H), 7.53 – 7.45 (m, 1H), 7.38 – 7.29 (m, 1H), 3.64 (t, $J = 5.8$ Hz, 2H), 3.39 (dd, $J = 7.3$, 6.1 Hz, 2H), 2.09 – 1.95 (m, 2H).

$^{13}C\{^{1}H\}$ NMR (101 MHz, Chloroform-*d*) δ: 150.1, 137.4, 133.3, 130.9, 127.7, 127.0, 123.9, 123.0, 119.2, 89.3, 61.0, 30.7, 21.8.

HRMS (ESI, *m/z*): calcd for $[C_{13}H_{12}IO_2]^-$ $(M-H)^-$, 326.9887; found, 326.9884.

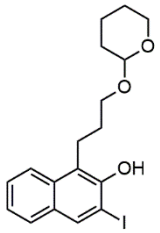

3

3-iodo-1-(3-((tetrahydro-2H-pyran-2-yl)oxy)propyl)naphthalen-2-ol (3). A flame-dried 100 mL round-bottom flask equipped with a stir bar was charged with **2** (3.08 g, 9.39 mmol) and pyridinium *p*-toluenesulfonate (PPTS, 689 mg, 2.75 mmol). The flask was evacuated and backfilled with N_2 three times. Dry CH_2Cl_2 (20 mL) was added via syringe, followed by the addition of 3,4-dihydro-2*H*-pyran (0.80 mL, 9.1 mmol). After stirring at room temperature overnight, the mixture was concentrated under reduced pressure and partitioned between water and CH_2Cl_2. The aqueous phase was discarded and the organic phase was dried over Na_2SO_4, filtered, and concentrated under reduced pressure. The crude product was purified by column chromatography (0–15% EtOAc/hexanes) to afford the title product as yellow solid (3.40 g, 88%).

TLC (10% EtOAc/hexanes): R_f = 0.31

^{1}H NMR (400 MHz, Chloroform-*d*) δ: 8.22 (s, 1H), 7.88 (d, *J* = 8.6 Hz, 1H), 7.67 (d, *J* = 8.1 Hz, 1H), 7.48 (ddd, *J* = 8.4, 6.8, 1.3 Hz, 1H), 7.32 (ddd, *J* = 8.1, 6.9, 1.1 Hz, 1H), 7.29 (s, 1H),4.67 (dd, *J* = 4.6, 3.0 Hz, 1H), 3.93 (ddd, *J* = 11.0, 6.3, 3.7 Hz, 1H), 3.78 (dt, *J* = 10.2, 5.5 Hz, 1H), 3.60 – 3.50 (m, 1H), 3.46 (dt, *J* = 10.2, 5.8 Hz, 1H), 3.26 (t, *J* = 7.0 Hz, 2H),

2.08 – 1.99 (m, 2H), 1.98 – 1.86 (m, 1H), 1.86 – 1.78 (m, 1H), 1.79 – 1.68 (m, 1H), 1.63 – 1.56 (m, 3H).

$^{13}C\{^{1}H\}$ NMR (101 MHz, Chloroform-*d*) δ: 150.1, 137.3, 133.3, 130.9, 127.7, 126.9, 123.8, 123.1, 119.9, 99.1, 89.5, 65.9, 62.9, 30.7, 28.9, 25.4, 22.5, 19.7.

HRMS (FD, *m/z*): calcd for $[C_{18}H_{21}IO_3]^{+\cdot}$ $(M)^{+\cdot}$, 412.0535; found, 412.0539.

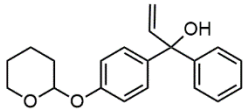

4

1-phenyl-1-(4-((tetrahydro-2H-pyran-2-yl)oxy)phenyl)prop-2-en-1-ol (4). A flame-dried round-bottom flask equipped with a stir bar was charged with 4-hydroxybenzophenone (2.03 g, 10.3 mmol) and pyridinium *p*-toluenesulfonate (PPTS, 400 mg, 1.59 mmol). The flask was evacuated and backfilled with N_2 three times. Dry CH_2Cl_2 (20 mL) was added via syringe followed by the addition of 3,4-dihydro-2*H*-pyran (1.0 mL, 11 mmol). After stirring at room temperature overnight, the mixture was concentrated under reduced pressure and partitioned between water and CH_2Cl_2. The aqueous phase was discarded and the organic phase was dried over Na_2SO_4, filtered, and concentrated under reduced pressure. Next, the crude yellow oil was added to a flame-dried round-bottom flask equipped with a stir bar and the flask was evacuated and backfilled with N_2 three times. Dry THF (20 mL) was added via syringe and the flask was cooled in an ice bath followed by the slow addition of vinylmagnesium bromide (1 M in THF, 12 mL, 12 mmol). After complete addition, the reaction mixture was allowed to warm to room temperature and stirred for 5 h. The flask was cooled in an ice bath and water was added dropwise. The crude reaction mixture was concentrated under reduced

pressure and partitioned between water and ethyl acetate. The aqueous phase was discarded and the organic phase was dried over Na_2SO_4, filtered, and concentrated under reduced pressure. The crude product was purified by column chromatography (0–30% EtOAc/hexanes) to afford the title product as yellow oil (1.91 g, 60%).

TLC (20% EtOAc/hexanes): $R_f = 0.57$

^{1}H NMR (400 MHz, DMSO-d_6) δ: 7.37 – 7.26 (m, 4H), 7.25 – 7.17 (m, 3H), 6.98 – 6.89 (m, 2H), 6.52 (dd, J = 16.9, 10.7 Hz, 1H), 5.86 (s, 1H), 5.43 (t, J = 3.4 Hz, 1H), 5.24 – 5.11 (m, 2H), 3.74 (ddd, J = 12.0, 8.7, 3.6 Hz, 1H), 3.52 (dt, J = 10.8, 4.4 Hz, 1H), 1.93 – 1.66 (m, 3H), 1.65 – 1.39 (m, 3H).

^{13}C{^{1}H} NMR (101 MHz, DMSO-d_6) δ: 155.2, 147.1, 144.6, 140.1, 127.9, 127.7, 126.6, 126.4, 115.6, 112.7, 95.7, 77.6, 61.5, 29.9, 24.7, 18.7.

HRMS (ESI, *m/z*): calcd for $[C_{20}H_{22}NaO_3]^+$ $(M+Na)^+$, 333.1461; found, 333.1462.

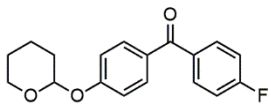

BP-F

(4-fluorophenyl)(4-((tetrahydro-2H-pyran-2-yl)oxy)phenyl)methanone (BP-F). A flame-dried 100 mL round-bottom flask equipped with a stir bar was charged with 4-fluoro-4'-hydroxybenzophenone (4.08 g, 18.9 mmol) and pyridinium *p*-toluenesulfonate (PPTS, 690 mg, 2.75 mmol). The flask was evacuated and backfilled with N_2 three times. Dry CH_2Cl_2 (20 mL) was added via syringe followed by addition of 3,4-dihydro-2*H*-pyran (2.5 mL, 27 mmol). After stirring at room temperature overnight, the mixture was concentrated under reduced pressure and partitioned between water and CH_2Cl_2. The aqueous phase was

discarded and the organic phase was dried over Na_2SO_4, filtered and concentrated under reduced pressure. The crude product was purified by column chromatography (0–15% EtOAc/hexanes) to afford the title product as white solid (4.74 g, 84%).

TLC (10% EtOAc/hexanes): R_f = 0.49

^{1}H NMR (400 MHz, Chloroform-*d*) δ: 7.87 – 7.74 (m, 4H), 7.20 – 7.07 (m, 4H), 5.54 (t, J_{HH} = 3.2 Hz, 1H), 3.88 (ddd, J_{HH} = 11.4, 9.8, 3.1 Hz, 1H), 3.64 (ddd, J_{HH} = 11.3, 4.0, 1.4 Hz, 1H), 2.09 – 1.95 (m, 1H), 1.93 – 1.86 (m, 2H), 1.78 – 1.65 (m, 2H), 1.65 – 1.59 (m, 1H).

^{13}C{^{1}H} NMR (101 MHz, Chloroform-*d*) δ: 194.4, 165.2 (d, J_{CF} = 253 Hz), 160.9, 134.5 (d, J_{CF} = 3.1 Hz), 132.5 (d, J_{CF} = 8.9 Hz), 132.4, 130.8, 116.0, 115.5 (d, J_{CF} = 21.8 Hz), 96.2, 62.2, 30.2, 25.2, 18.6.

HRMS (FD, *m/z*): calcd for $[C_{18}H_{17}FO_3]^{+\cdot}$ $(M)^{+\cdot}$, 300.1162; found, 300.1159.

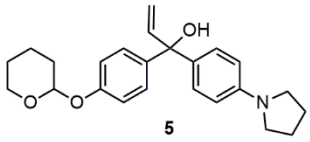

5

1-(4-(pyrrolidin-1-yl)phenyl)-1-(4-((tetrahydro-2H-pyran-2-yl)oxy)phenyl)prop-2-en-1-ol (5). A flame-dried round-bottom flask equipped with a stir bar was charged with **BP-F** (6.50 g, 21.7 mmol) and the flask was evacuated and backfilled with N_2 three times. Pyrrolidine (5 mL) was then added via syringe. After stirring at reflux for 1 h, the flask was removed from heat and the crude mixture was diluted with CH_2Cl_2. The organic phase was washed with sat. $NaHCO_3$ (aq), dried over Na_2SO_4, filtered, and concentrated under reduced pressure. Next, the crude yellow solid was added to a flame-dried round-bottom flask equipped with a stir bar and the flask was evacuated and backfilled with N_2 three times. Dry

THF (100 mL) was added via syringe and the flask was cooled in an ice bath, followed by the slow addition of vinylmagnesium bromide (1 M in THF, 24 mL, 24 mmol). After complete addition, the reaction mixture was allowed to warm to room temperature and stirred for 1 h. The flask was again cooled in an ice bath and water was added dropwise. The crude mixture was concentrated under reduced pressure and partitioned between water and ethyl acetate. The aqueous phase was discarded and the organic phase was dried over Na_2SO_4, filtered, and concentrated under reduced pressure. The crude product was purified by column chromatography (0–15% EtOAc/hexanes) to afford the title product as yellow oil (4.23 g, 51%).

TLC (20% EtOAc/hexanes): $R_f = 0.46$

^{1}H NMR (400 MHz, CD_2Cl_2) δ: 7.31 – 7.22 (m, 2H), 7.21 – 7.12 (m, 2H), 7.01 – 6.91 (m, 2H), 6.52 – 6.42 (m, 3H), 5.38 (t, *J* = 3.4 Hz, 1H), 5.28 (dd, *J* = 17.1, 1.5 Hz, 1H), 5.23 (dd, *J* = 10.5, 1.5 Hz, 1H), 3.92 (ddd, *J* = 11.5, 9.4, 3.2 Hz, 1H), 3.59 (ddd, *J* = 11.4, 4.2, 1.5 Hz, 1H), 3.31 – 3.22 (m, 4H), 2.28 (s, 1H), 2.05 – 1.93 (m, 5H), 1.89 – 1.77 (m, 2H), 1.73 – 1.50 (m, 3H).

^{13}C{^{1}H} NMR (101 MHz, Chloroform-*d*) δ: 156.14, 156.11, 147.2, 144.4, 139.6, 132.84, 132.82, 128.18, 128.16, 128.12, 115.93, 115.91, 112.9, 111.2, 96.51, 96.47, 79.1, 62.2, 47.7, 30.5, 25.6, 25.4, 19.0.

HRMS (ESI, *m/z*): calcd for $[C_{24}H_{30}NO_3]^+$ $(M+H)^+$, 380.2220; found, 380.2231.

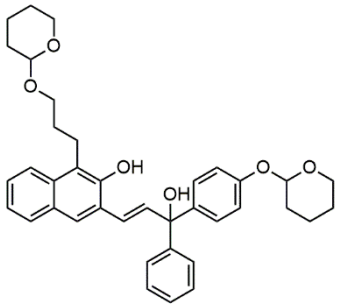

6

(E)-3-(3-hydroxy-3-phenyl-3-(4-((tetrahydro-2H-pyran-2-yl)oxy)phenyl)prop-1-en-1-yl)-1-(3-((tetrahydro-2H-pyran-2-yl)oxy)propyl)naphthalen-2-ol (6). A flame-dried round-bottom flask equipped with a stir bar was charged with **3** (100 mg, 0.243 mmol), **4** (83 mg, 0.27 mmol), $Pd(OAc)_2$ (16 mg, 0.071 mmol), and Cs_2CO_3 (78 mg, 0.24 mmol). The flask was evacuated and backfilled with N_2 three times followed by addition of dry CH_3CN (2 mL) via syringe. After stirring at 80 °C for 1.5 h, the flask was removed from heat and the crude mixture was diluted with ethyl acetate and washed with water. The aqueous phase was discarded and the organic phase was dried over Na_2SO_4, filtered, and concentrated under reduced pressure. The crude product was purified by column chromatography (0–25% EtOAc/hexanes) to afford the title product as yellow solid (58 mg, 40%).

TLC (25% EtOAc/hexanes): $R_f = 0.27$

^{1}H NMR (400 MHz, Acetone-d_6) δ: 7.99 – 7.91 (m, 2H), 7.80 (d, J = 7.4 Hz, 1H), 7.56 – 7.52 (m, 2H), 7.46 – 7.38 (m, 3H), 7.36 – 7.12 (m, 6H), 7.04 – 6.94 (m, 2H), 5.43 (t, J = 3.4 Hz, 1H), 4.64 (dd, J = 4.2, 2.8 Hz, 1H), 3.89 – 3.72 (m, 3H), 3.55 (ddd, J = 11.4, 4.3, 1.3 Hz, 1H), 3.50 – 3.42 (m, 2H), 3.21 (td, J = 7.3, 2.6 Hz, 2H), 2.00 – 1.92 (m, 3H), 1.89 – 1.45 (m, 13H).

$^{13}C\{^{1}H\}$ NMR (101 MHz, Acetone-d_6) δ: 157.0, 151.1, 148.5, 141.4, 139.2, 133.6, 130.2, 129.4, 129.07, 129.06, 128.6, 128.5, 127.86, 127.85, 127.4, 126.7, 125.4, 124.68, 124.67, 123.9, 123.6, 120.9, 116.6, 99.4, 97.0, 79.2, 67.1, 62.6, 62.4, 31.4, 31.1, 26.2, 26.0, 22.2, 20.2, 19.6.

HRMS (ESI, *m/z*): calcd for $[C_{38}H_{41}O_5]^+$ $(M\text{-}OH)^+$, 577.2949; found, 577.2954.

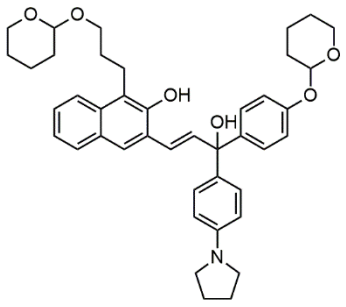

7

(E)-3-(3-hydroxy-3-(4-(pyrrolidin-1-yl)phenyl)-3-(4-((tetrahydro-2H-pyran-2-yl)oxy)phenyl)prop-1-en-1-yl)-1-(3-((tetrahydro-2H-pyran-2-yl)oxy)propyl)naphthalen-2-ol (7). A flame-dried round-bottom flask equipped with a stir bar was charged with **3** (200 mg, 0.485 mmol), **5** (200 mg, 0.528 mmol), $Pd(OAc)_2$ (33 mg, 0.15 mmol), and Cs_2CO_3 (160 mg, 0.492 mmol). The flask was evacuated and backfilled with N_2 three times followed by addition of dry CH_3CN (2 mL) via syringe. After stirring at 80 °C for 1.5 h, the flask was removed from heat and the crude mixture was diluted with ethyl acetate and washed with water. The aqueous phase was discarded and the organic phase was dried over Na_2SO_4, filtered, and concentrated under reduced pressure. The crude product was purified by column chromatography (0–25% EtOAc/hexanes) to afford the title product as yellow solid (57 mg, 18%).

TLC (25% EtOAc/hexanes): R_f = 0.30

^{1}H NMR (400 MHz, Acetone-d_6) δ: 7.98 – 7.89 (m, 2H), 7.83 – 7.75 (m, 2H), 7.45 – 7.36 (m, 3H), 7.32 – 7.24 (m, 3H), 7.20 (d, *J* = 15.8 Hz, 1H), 7.10 (d, *J* = 15.8 Hz, 1H), 7.02 – 6.94 (m, 2H), 6.56 – 6.45 (m, 2H), 5.42 (t, *J* = 3.4 Hz, 1H), 4.63 (dd, *J* = 4.2, 2.9 Hz, 1H), 4.53 (s, 1H), 3.91 – 3.69 (m, 3H), 3.55 (dt, *J* = 11.5, 4.6 Hz, 1H), 3.49 – 3.42 (m, 2H), 3.27 – 3.12 (m, 6H), 2.01 – 1.91 (m, 6H), 1.89 – 1.47 (m, 12H).

^{13}C{^{1}H} NMR (101 MHz, Acetone-d_6) δ: 156.7, 151.2, 147.8, 142.0, 140.1, 135.0, 133.5, 130.3, 129.3, 128.98, 128.97, 128.8, 128.7, 126.6, 125.2, 123.8, 123.67, 123.66, 123.56, 120.9, 116.40, 116.38, 111.8, 99.4, 97.1, 79.2, 67.1, 62.6, 62.4, 48.2, 31.4, 31.1, 26.2, 26.02, 25.97, 22.2, 20.2, 19.6.

HRMS (ESI, *m/z*): calcd for $[C_{42}H_{48}NO_5]^+$ $(M-OH)^+$, 646.3527; found, 646.3546.

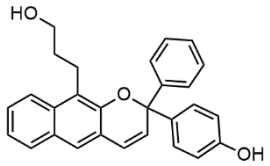

8

4-(10-(3-hydroxypropyl)-2-phenyl-2H-benzo[g]chromen-2-yl)phenol (8) A flame-dried round bottom flask equipped with a stir bar was charged with **6** (46 mg, 0.077 mmol) and silica gel (150 mg). The flask was evacuated and backfilled with N_2 three times followed by addition of dry DMF (5 mL) via syringe. The reaction mixture was stirred at 135 °C for 40 h. After cooling to room temperature, Amberlyst 15 (100 mg) and methanol (10 mL) were added and the reaction mixture was stirred at room temperature for 60 h. The crude mixture was filtered and the filtrate was diluted with DCM and washed consecutively with 10% LiCl

solution and water. The organic layer was dried over Na_2SO_4, filtered, and concentrated under reduced pressure. The crude mixture was purified by column chromatography (0–40% EtOAc/hexanes) to afford title compound as a pale yellow solid (30 mg, 95%).

TLC (50% EtOAc/hexanes): R_f = 0.44

^{1}H NMR (400 MHz, CD_2Cl_2) δ: 7.88 (d, *J* = 8.6 Hz, 1H), 7.72 (d, *J* = 8.1 Hz, 1H), 7.48 – 7.38 (m, 4H), 7.35 – 7.23 (m, 6H), 6.84 (d, *J* = 9.9 Hz, 1H), 6.76 – 6.70 (m, 2H), 6.38 (d, *J* = 9.8 Hz, 1H), 3.61 – 3.46 (m, 2H), 3.36 – 3.13 (m, 2H), 1.93 – 1.75 (m, 2H).

^{13}C{^{1}H} NMR (101 MHz,CD_2Cl_2) δ: 156.4, 148.1, 145.3, 136.9, 133.9, 132.1, 130.4, 129.4, 129.1, 128.8, 128.1, 127.3, 126.9, 124.8, 124.5, 124.3, 123.7, 122.3, 122.0, 115.6, 83.9, 62.1, 32.9, 21.1. A small grease peak is present at 30.2 ppm in the included spectrum.

HRMS (ESI, *m/z*): calcd for $[C_{28}H_{25}O_3]^+$ $(M+H)^+$, 409.1798; found, 409.1804.

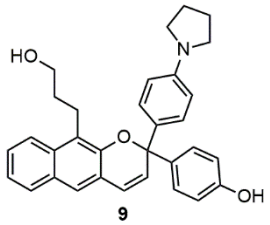

9

4-(10-(3-hydroxypropyl)-2-(4-(pyrrolidin-1-yl)phenyl)-2H-benzo[g]chromen-2-yl)phenol (9) A flame-dried round bottom flask equipped with a stir bar was charged with **7** (58 mg, 0.087 mmol) and silica gel (180 mg). The flask was evacuated and backfilled with N_2 three times followed by addition of dry DMF (5 mL) via syringe. The reaction mixture was stirred at 135 °C for 2 h. After cooling to room temperature, Amberlyst 15 (500 mg) and methanol (5 mL) were added and the reaction mixture was stirred at room temperature for 1

h. The crude mixture was filtered and the filtrate was diluted with DCM and washed consecutively with 10% LiCl solution and water. The organic layer was dried over Na_2SO_4, filtered, and concentrated under reduced pressure. The crude mixture was purified by column chromatography (0–40% EtOAc/hexanes) to afford title compound as a yellow solid (11 mg, 26%).

TLC (50% EtOAc/hexanes): $R_f = 0.50$

^{1}H NMR (400 MHz, Acetone-d_6) δ: 8.32 (s, 1H), 7.94 (d, J = 8.6 Hz, 1H), 7.73 (d, J = 8.1 Hz, 1H), 7.47 (s, 1H), 7.41 – 7.36 (m, 1H), 7.35 – 7.31 (m, 2H), 7.30 – 7.24 (m, 3H), 6.85 (d, J = 9.8 Hz, 1H), 6.81 – 6.76 (m, 2H), 6.50 – 6.44 (m, 2H), 6.40 (d, J = 9.8 Hz, 1H), 3.71 – 3.62 (m, 2H), 3.57 – 3.51 (m, 1H), 3.25 – 3.12 (m, 6H), 1.99 – 1.91 (m, 4H), 1.87 – 1.75 (m, 2H).

^{13}C{^{1}H} NMR (101 MHz, Acetone-d_6) δ: 157.4, 148.8, 148.2, 137.8, 134.3, 133.9, 132.5, 130.6, 129.3, 129.1, 128.8, 126.8, 124.5, 124.2, 124.0, 123.9, 123.4, 123.1, 115.6, 111.8, 83.8, 62.6, 48.1, 34.1, 26.0, 22.1.

HRMS (ESI, *m/z*): calcd for $[C_{32}H_{32}NO_3]^+$ $(M+H)^+$, 478.2382; found, 478.2377.

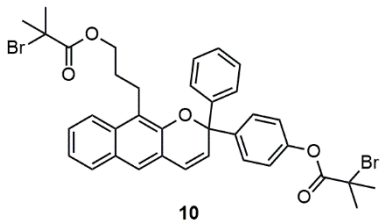

10

3-(2-(4-((2-bromo-2-methylpropanoyl)oxy)phenyl)-2-phenyl-2H-benzo[g]chromen-10-yl)propyl 2-bromo-2-methylpropanoate (10). An oven-dried 20 mL vial equipped with a

stir bar was charged with diol **8** (25 mg, 0.061 mmol) and the vial was evacuated and backfilled with N_2 three times. Dry THF (5 mL) was added via syringe followed by addition of Et_3N (20 μL, 0.14 mmol) and then α-bromoisobutyryl bromide (20 μL, 0.162 mmol). After stirring at room temperature overnight, the solid precipitate was filtered off and discarded. The filtrate was diluted with ethyl acetate and washed with water. The organic layer was dried over Na_2SO_4, filtered, and concentrated under reduced pressure. The crude mixture was purified by column chromatography (0–15% EtOAc/hexanes) to afford title compound as a pale yellow solid (7 mg, 16%).

TLC (25% EtOAc/hexanes): R_f = 0.67

^{1}H NMR (400 MHz, CD_2Cl_2) δ: 7.88 (d, *J* = 8.7 Hz, 1H), 7.73 (d, *J* = 8.0 Hz, 1H), 7.55 – 7.39 (m, 6H), 7.37 – 7.24 (m, 4H), 7.13 – 7.06 (m, 2H), 6.90 (d, *J* = 9.9 Hz, 1H), 6.35 (d, *J* = 9.8 Hz, 1H), 4.26 (t, *J* = 6.3 Hz, 2H), 3.25 – 3.14 (m, 2H), 2.03 (s, 6H), 1.95 – 1.88 (m, 8H).

^{13}C{^{1}H} NMR (101 MHz, CD_2Cl_2) δ: 172.1, 170.7, 150.7, 147.8, 145.1, 143.4, 133.8, 131.7, 130.3, 129.2, 128.9, 128.9, 128.3, 127.6, 127.0, 125.0, 124.9, 124.3, 123.5, 122.4, 122.2, 121.3, 83.3, 66.7, 56.9, 56.2, 31.2, 31.0, 30.3, 29.4, 22.0.

HRMS (ESI, *m/z*): calcd for $[C_{36}H_{35}Br_2O_5]^+$ $(M+H)^+$, 705.0851; found, 705.0848.

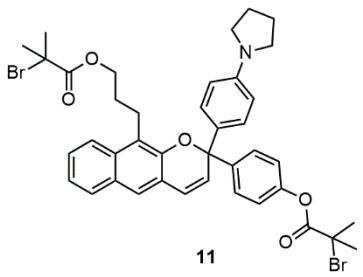

11

3-(2-(4-((2-bromo-2-methylpropanoyl)oxy)phenyl)-2-(4-(pyrrolidin-1-yl)phenyl)-2H-benzo[g]chromen-10-yl)propyl 2-bromo-2-methylpropanoate (11). A flame-dried round bottom flask equipped with a stir bar was charged with diol **9** (42 mg, 0.088 mmol) and the flask was evacuated and backfilled with N_2 three times. Dry THF (6 mL) was added via syringe followed by addition of Et_3N (50 μL, 0.36 mmol). The flask was cooled in an ice bath and α-bromoisobutyryl bromide (50 μL, 0.40 mmol) was added slowly. After stirring at room temperature overnight, the solid precipitate was filtered off and discarded. The filtrate was diluted with ethyl acetate and washed with water. The organic layer was dried over Na_2SO_4, filtered, and concentrated under reduced pressure. The crude mixture was purified by column chromatography (0–30% EtOAc/hexanes) to afford the title compound as a pale yellow solid (10 mg, 15%).

TLC (15% EtOAc/hexanes): R_f = 0.50

^{1}H NMR (400 MHz, CD_2Cl_2) δ: 7.87 (d, *J* = 8.5 Hz, 1H), 7.72 (d, *J* = 8.0 Hz, 1H), 7.56 – 7.50 (m, 2H), 7.45 – 7.38 (m, 2H), 7.36 – 7.25 (m, 3H), 7.15 – 7.05 (m, 2H), 6.86 (d, *J* = 9.8 Hz, 1H), 6.63 (bs, 2H), 6.30 (d, *J* = 9.7 Hz, 1H), 4.26 (t, *J* = 6.3 Hz, 2H), 3.35 – 3.24 (m, 4H), 3.20 (t, *J* = 7.9 Hz, 2H), 2.04 (s, 6H), 2.02 – 1.97 (m, 4H), 1.96 – 1.92 (m, 2H), 1.91 – 1.88 (m, 6H).

^{13}C{^{1}H} NMR (101 MHz, Chloroform-*d*) δ: 171.9, 170.3, 149.9, 147.8, 143.8, 133.5, 131.9, 129.7, 128.72, 128.67, 128.5, 126.3, 124.3, 123.8, 123.6, 123.0, 122.2, 121.4, 120.7, 111.2, 83.1, 66.4, 56.2, 55.5, 47.7, 30.94, 30.92, 30.8, 28.9, 25.6, 21.6. A small grease peak is present at 29.8 ppm in the included spectrum.

HRMS (ESI, *m/z*): calcd for $[C_{40}H_{42}Br_2NO_5]^+$ $(M+H)^+$, 774.1430; found, 774.1412.

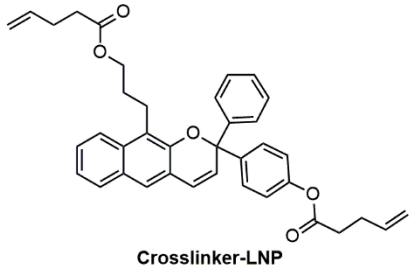

Crosslinker-LNP

3-(2-(4-(pent-4-enoyloxy)phenyl)-2-phenyl-2H-benzo[g]chromen-10-yl)propyl pent-4-enoate (Crosslinker-LNP). An oven-dried 20 mL vial equipped with a stir bar was charged with diol **8** (30 mg, 0.074 mmol) and DMAP (2.0 mg, 0.016 mmol). The vial was evacuated and backfilled with N_2 three times. Dry THF (5 mL) was then added via syringe followed by the addition of Et_3N (50 µL, 0.36 mmol) and 4-pentenoic anhydride (40 µL, 0.22 mmol). After stirring at room temperature overnight, the filtrate was diluted with ethyl acetate and washed with water. The organic layer was dried over Na_2SO_4, filtered, and concentrated under reduced pressure. The crude mixture was purified by column chromatography (0–10% EtOAc/hexanes) to afford title compound as a pale yellow solid (20 mg, 47%).

TLC (20% EtOAc/hexanes): R_f = 0.61

^{1}H NMR (400 MHz, CD_2Cl_2) δ: 7.85 (d, *J* = 8.6 Hz, 1H), 7.72 (d, *J* = 8.2 Hz, 1H), 7.52 – 7.38 (m, 6H), 7.37 – 7.25 (m, 4H), 7.06 – 7.00 (m, 2H), 6.88 (d, *J* = 9.8 Hz, 1H), 6.36 (d, *J* = 9.8 Hz, 1H), 5.94 – 5.74 (m, 2H), 5.16 – 4.93 (m, 4H), 4.16 (t, *J* = 6.3 Hz, 2H), 3.24 – 3.09 (m, 2H), 2.67 – 2.59 (m, 2H), 2.52 – 2.41 (m, 2H), 2.41 – 2.27 (m, 4H), 1.92 – 1.82 (m, 2H).

^{13}C{^{1}H} NMR (101 MHz, CD_2Cl_2) δ: 173.4, 171.9, 150.7, 147.8, 145.2, 143.0, 137.6, 137.1, 133.8, 131.8, 130.2, 129.2, 128.8, 128.7, 128.2, 127.5, 126.9, 125.0, 124.8, 124.3, 123.5, 122.5, 122.3, 121.9, 116.1, 115.6, 83.2, 64.9, 34.1, 30.3, 29.5, 29.42, 29.35, 22.0.

HRMS (ESI, *m/z*): calcd for $[C_{38}H_{37}O_5]^+$ $(M+H)^+$, 573.2641; found, 573.2631.

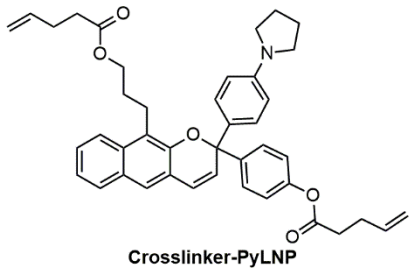

3-(2-(4-(pent-4-enoyloxy)phenyl)-2-(4-(pyrrolidin-1-yl)phenyl)-2H-benzo[g]chromen-10-yl)propyl pent-4-enoate (Crosslinker-PyLNP). A flame-dried 25 mL round bottom flask equipped with a stir bar was charged with diol **9** (60 mg, 0.13 mmol) and DMAP (2.0 mg, 0.016 mmol). The flask was evacuated and backfilled with N_2 three times. Dry THF (10 mL) was added via syringe followed by the addition of Et_3N (50 μL, 0.36 mmol) and 4-pentenoic anhydride (60 μL, 0.33 mmol). After stirring at room temperature overnight, the filtrate was diluted with ethyl acetate and washed with water. The organic layer was dried over Na_2SO_4, filtered, and concentrated under reduced pressure. The crude mixture was purified by column chromatography (0–15% EtOAc/hexanes) to afford title compound as a pale yellow solid (55 mg, 66%).

TLC (15% EtOAc/hexanes): $R_f = 0.50$

^{1}H NMR (400 MHz, CD_2Cl_2) δ: 7.84 (d, J = 8.5 Hz, 1H), 7.71 (d, J = 8.2 Hz, 1H), 7.52 – 7.47 (m, 2H), 7.43 – 7.37 (m, 2H), 7.33 – 7.23 (m, 3H), 7.08 – 6.99 (m, 2H), 6.84 (d, J = 9.8 Hz, 1H), 6.56 – 6.43 (m, 2H), 6.32 (d, J = 9.8 Hz, 1H), 5.98 – 5.55 (m, 2H), 5.18 – 4.94 (m,

4H), 4.16 (t, J = 6.4 Hz, 2H), 3.30 – 3.19 (m, 4H), 3.16 (t, J = 7.9 Hz, 2H), 2.70 – 2.60 (m, 2H), 2.51 – 2.42 (m, 2H), 2.41 – 2.28 (m, 4H), 1.99 – 1.91 (m, 4H), 1.91 – 1.80 (m, 2H).

$^{13}C\{^{1}H\}$ NMR (101 MHz, Chloroform-*d*) δ: 173.3, 171.6, 149.8, 147.9, 147.3, 143.4, 137.0, 136.4, 133.5, 132.0, 130.9, 129.7, 128.7, 128.6, 128.3, 126.2, 124.2, 123.7, 123.6, 123.0, 122.2, 121.6, 121.2, 116.1, 115.5, 111.1, 83.1, 64.7, 47.6, 33.8, 33.7, 29.1, 29.03, 29.01, 25.6, 21.6. A small grease peak is present at 29.8 ppm in the included spectrum.

HRMS (ESI, *m/z*): calcd for $[C_{42}H_{44}NO_5]^+$ $(M+H)^+$, 642.3219; found, 642.3221.

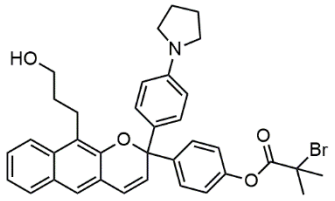

PyLNP-Mono

4-(10-(3-hydroxypropyl)-2-(4-(pyrrolidin-1-yl)phenyl)-2H-benzo[g]chromen-2-yl)phenyl 2-bromo-2-methylpropanoate (PyLNP-Mono). An oven-dried 20 mL vial equipped with a stir bar was charged with diol **9** (30 mg, 0.063 mmol), DMAP (2.0 mg, 0.016 mmol), and dicyclohexylcarbodiimide (DCC, 15 mg, 0.073 mmol). The vial was evacuated and backfilled with N_2 three times and dry DCM (3 mL) was added via syringe. The vial was opened briefly and α-Bromoisobutyric acid (12 mg, 0.072 mmol) was added under a flow of nitrogen. After stirring at room temperature for 2 h, the solid precipitate was filtered off and discarded. The filtrate was diluted with DCM (20 mL) and washed with water. The organic layer was dried over Na_2SO_4, filtered, and concentrated under reduced pressure. The crude

mixture was purified by column chromatography (0–20% EtOAc/hexanes) to afford the title compound as a pale purple solid (20 mg, 51%).

TLC (25% EtOAc/hexanes): R_f = 0.40

^{1}H NMR (400 MHz, CD_2Cl_2) δ: 7.88 (d, *J* = 8.6 Hz, 1H), 7.72 (d, *J* = 8.2 Hz, 1H), 7.57 – 7.49 (m, 2H), 7.45 – 7.37 (m, 2H), 7.33 – 7.25 (m, 3H), 7.14 – 7.03 (m, 2H), 6.85 (d, *J* = 9.8 Hz, 1H), 6.61 (bs, 2H), 6.34 (d, *J* = 9.8 Hz, 1H), 3.55 (td, *J* = 6.2, 1.9 Hz, 2H), 3.31 – 3.24 (m, 4H), 3.19 (t, *J* = 7.4 Hz, 2H), 2.04 (s, 6H), 2.01 – 1.95 (m, 4H), 1.85 – 1.76 (m, 2H).

^{13}C{^{1}H} NMR (101 MHz, Chloroform-*d*) δ: 170.4, 150.0, 147.9, 147.5, 143.3, 133.5, 131.7, 130.5, 129.9, 128.7, 128.6, 128.5, 126.3, 124.3, 123.9, 123.8, 123.3, 121.9, 121.5, 120.7, 111.2, 83.6, 61.9, 55.5, 47.7, 32.5, 30.7, 25.6, 20.7. A small grease peak is present at 29.9 ppm in the included spectrum.

HRMS (ESI, *m/z*): calcd for $[C_{36}H_{37}BrNO_4]^+$ $(M+H)^+$, 626.1900; found, 626.1885.

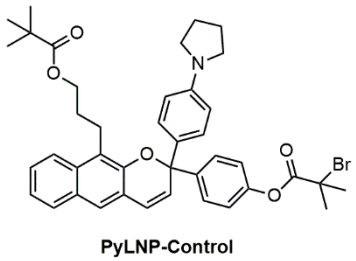

PyLNP-Control

3-(2-(4-((2-bromo-2-methylpropanoyl)oxy)phenyl)-2-(4-(pyrrolidin-1-yl)phenyl)-2H-benzo[g]chromen-10-yl)propyl pivalate (PyLNP-Control). An oven-dried 20 mL vial equipped with a stir bar was charged with **PyLNP-Mono** (25 mg, 0.040 mmol) and DMAP (3.0 mg, 0.025 mmol). The vial was evacuated and backfilled with N_2 three times. Pivalic anhydride (1.0 mL, 4.9 mmol) was added via syringe followed by the addition of Et_3N (10

μL, 0.072 mmol). After stirring at room temperature for 4 h, the solution was diluted with ethyl acetate (20 mL) and washed with water. The organic layer was dried over Na_2SO_4, filtered, and concentrated under reduced pressure. The crude mixture was purified by column chromatography (0–10% EtOAc/hexanes) to afford title compound as a pale yellow solid (10 mg, 35% yield).

TLC (10% EtOAc/hexanes): R_f = 0.44

^{1}H NMR (400 MHz, CD_2Cl_2) δ: 7.85 (d, *J* = 8.6 Hz, 1H), 7.72 (d, *J* = 8.1 Hz, 1H), 7.56 – 7.49 (m, 2H), 7.44 – 7.36 (m, 2H), 7.35 – 7.25 (m, 3H), 7.14 – 7.05 (m, 2H), 6.85 (d, *J* = 9.8 Hz, 1H), 6.55 (bs, 2H), 6.31 (d, *J* = 9.7 Hz, 1H), 4.15 (t, *J* = 6.3 Hz, 2H), 3.32 – 3.21 (m, 4H), 3.16 (t, *J* = 8.0 Hz, 2H), 2.05 (s, 6H), 2.01 – 1.94 (m, 4H), 1.93 – 1.82 (m, 2H), 1.20 (s, 9H).

^{13}C{^{1}H} NMR (101 MHz, CD_2Cl_2) δ: 178.9, 170.8, 150.4, 148.1, 144.4, 133.8, 132.5, 130.2, 129.1, 128.9, 128.6, 126.7, 124.6, 124.5, 124.1, 123.5, 122.8, 122.3, 121.2, 112.0, 83.4, 65.0, 56.3, 48.7, 39.2, 31.0, 29.6, 27.6, 25.9, 22.1. A small grease peak is present at 30.2 ppm in the included spectrum.

HRMS (ESI, *m/z*): calcd for $[C_{41}H_{45}BrNO_5]^+$ $(M+H)^+$, 710.2476; found, 710.2466.

General Procedure for the Synthesis of Poly(Methyl Acrylate) (PMA) Polymers Incorporating a Linear Naphthopyran Unit. Polymers were synthesized by controlled radical polymerization following the procedure by Nguyen *et al*.[38] A flame-dried Schlenk flask equipped with a stir bar was charged with freshly cut 20 G copper wire (2 cm), initiator, DMSO, and methyl acrylate. The flask was sealed and the solution was degassed via three freeze-pump-thaw cycles, then backfilled with nitrogen and warmed to room temperature.

Me_6TREN was added via microsyringe and the reaction was stirred at room temperature for the indicated amount of time. Upon completion of the polymerization, the flask was opened to atmosphere and diluted with a minimal amount of DCM. The polymer was precipitated 3x into methanol cooled with dry ice and then dried under vacuum. The GPC traces for each polymer are shown below in Figure S7.

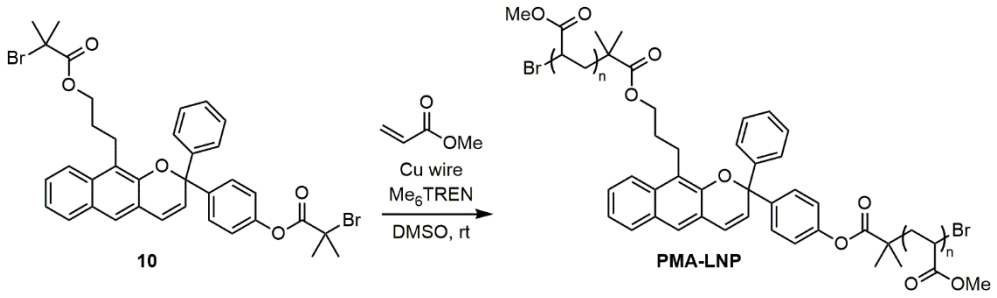

PMA-LNP. Synthesized according to the general procedure using bis-initiator **10** (3.0 mg, 0.0042 mmol), Me_6TREN (4.5 µL, 0.017 mmol), DMSO (1.20 mL), and methyl acrylate (1.20 mL, 13.3 mmol). Polymerization for 70 min afforded the title polymer as a tacky pale yellow solid (300 mg, 27%). M_n = 132 kg/mol, $Đ$ = 1.12.

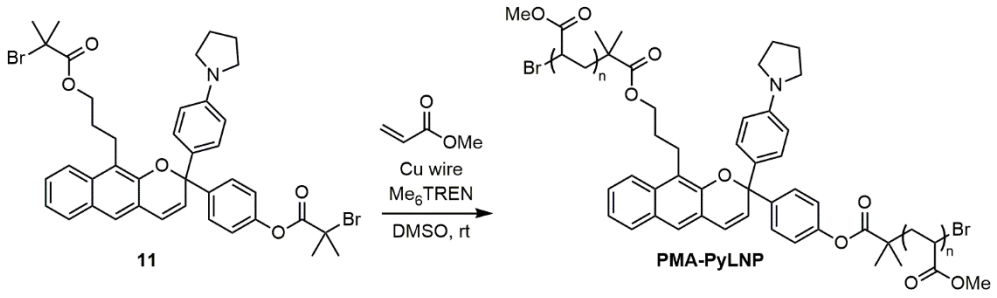

PMA-PyLNP. Synthesized according to the general procedure using bis-initiator **11** (4.3 mg, 0.0056 mmol), Me_6TREN (6.0 µL, 0.022 mmol), DMSO (1.50 mL), and methyl acrylate

(1.50 mL, 16.7 mmol). Polymerization for 60 min afforded the title polymer as a tacky pale yellow solid (570 mg, 40%). M_n = 262 kg/mol, $Đ$ = 1.15.

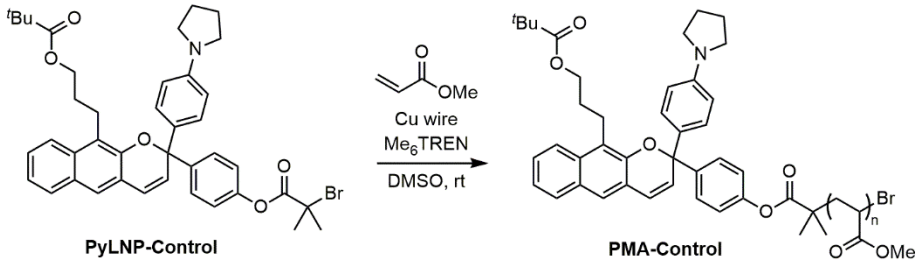

PMA-Control. Synthesized according to the general procedure using mono-functional initiator **PyLNP-Control** (2.0 mg, 0.0028 mmol), Me_6TREN (3.0 µL, 0.011 mmol), DMSO (0.75 mL), and methyl acrylate (0.75 mL, 8.5 mmol). Polymerization for 60 min afforded the title polymer as a tacky pale yellow solid (160 mg, 22%). M_n = 238 kg/mol, $Đ$ = 1.09.

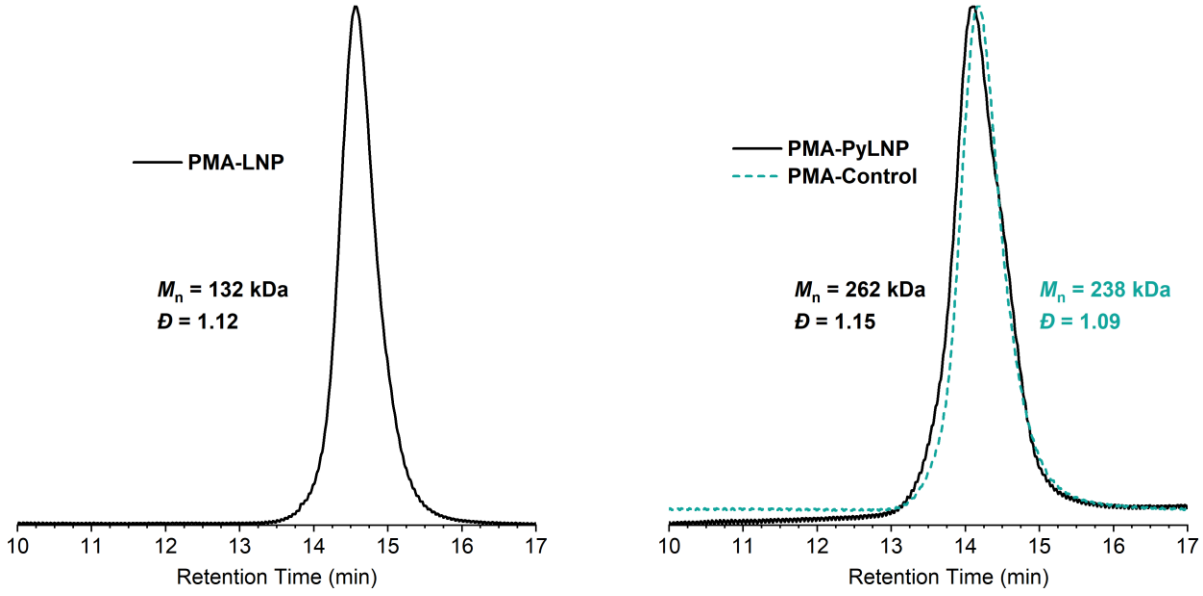

Figure S1.7 GPC traces (RI response) normalized to peak height for **PMA-LNP**, **PMA-PyLNP**, and **PMA-Control**.

1.5.4 PDMS Materials

PDMS materials incorporating linear naphthopyrans (1.0−1.5 wt%) were prepared following previously reported procedures using the two-part Sylgard® 184 elastomer kit (Dow Corning).[4,39] PDMS sheets approximately 0.5 mm thick were cut into 2 cm x 2 cm samples for testing.

General Procedure for Preparation of PDMS Materials. A representative procedure is provided for the preparation of PDMS materials incorporating linear naphthopyran crosslinker **Crosslinker-PyLNP**. Naphthopyran crosslinker **Crosslinker-PyLNP** (26 mg) was dissolved in xylenes (1.5 mL) in a 20 mL scintillation vial. Sylgard® 184 prepolymer base (1.704 g) was added and the mixture was thoroughly mixed in a vortex mixer to form a homogenous, pale yellow opaque dispersion. Sylgard® 184 curing agent (169.0 mg) was added and the contents were mixed using a vortex mixer. The mixture was pipetted onto a 5 cm x 5 cm Delrin plate which was placed inside a vacuum chamber and evacuated under high vacuum (< 50 mTorr) for 2 h. The Delrin plate was then transferred to an oven and cured at 80 ° C overnight. After curing, the plate was removed from the oven and the PDMS film was peeled off and cut into 2 cm x 2 cm samples with a razor blade. For the preparation of PDMS materials incorporating the crosslinker without a *para*-pyrrolidine substituent, a similar procedure was followed using linear naphthopyran crosslinker **Crosslinker-LNP** (10 mg), Sylgard® 184 prepolymer base (0.995 g), and Sylgard® 184 curing agent (101.5 mg) with a 2.5 cm x 2.5 cm Delrin plate.

Details of the Patterning Procedure Applied to PDMS Films. The stamp used in the patterning experiments to apply localized compression was 3D printed from poly(lactic acid)

with embossed features in the shape of a wavy pattern,[40] as illustrated in Figure 3 in the main text. The stamp was manually compressed into a 4 cm^2 film under a weight of ~72 kg to achieve mechanochemical activation without causing irreversible deformation or tearing of the PDMS. For the photopatterning experiment, a 4 cm^2 film was irradiated with 365 nm UV light for 120 s through a cardboard photomask containing a small central hole.

1.5.5 DFT Calculations (CoGEF)

CoGEF calculations were performed using Spartan ′20 Parallel Suite ang to previously reported methods.[31,41] Ground state energies were calculated using DFT at the B3LYP/6-31G* level of theory. Truncated models of each mechanophore with terminal acetoxy groups were used in the calculations. The equilibrium conformations of the unconstrained molecule were initially calculated using molecular mechanics (MMFF) followed by optimization of the equilibrium geometries using DFT (B3LYP/6-31G*). Starting from the equilibrium geometry of the unconstrained molecules (energy = 0 kJ/mol), the distance between the carbon atoms in the terminal methyl groups of the truncated structures was increased in increments of 0.05 Å and the energy was minimized at each step. The maximum force associated with the mechanochemical reaction was calculated from the slope of the curve immediately prior to bond cleavage.

1.5.6 Details for Photoirradiation and Sonication Experiments

To continuously monitor reaction progress by UV–vis absorption spectroscopy, a previously described experimental setup[23,42] was assembled using a peristaltic pump to transport the

solution from the reaction vessel through a quartz flow cell in a UV-vis spectrometer and return the solution to the reaction vessel. The flow rate through the system was maintained at 8 mL/min, corresponding to a setting of 50 RPM on the peristaltic pump at the selected occlusion. The UV-vis spectrometer was programmed to acquire full spectra at regular time intervals. Absorbance values were measured at 790 nm and subtracted from the absorbance values across the rest of the spectrum at each time point to account for drift during the experiments.

General Procedure for Sonication Experiments. A sonication vessel was placed onto the sonication probe and charged with a 2 mg/mL solution of polymer in CH_3CN containing 30 mM BHT (20.0 mL), which was added to minimize decomposition side reactions resulting from free radicals generated during sonication.[43,44] An additional 6.2 mL of solution was pumped into the dead space of the circulatory setup. If applicable, $BF_3{\cdot}Et_2O$ was added to the sonication vessel via microsyringe to provide a final concentration of 0.5 mM $BF_3{\cdot}Et_2O$. Teflon inlet and outlet tubes were inserted into the solution in the sonication vessel through punctured septa, and the pump was engaged to start the flow of solution through the system. The sonication vessel was submerged in a −45 °C bath and degassed by sparging with N_2 for 30 min. The inert gas line was then removed into the headspace of the reaction vessel and the system was maintained under an inert atmosphere throughout the sonication experiment. Continuous sonication was then initiated (20 kHz, 20% amplitude, 6.8 ± 0.5 W/cm^2 unless indicated otherwise). The temperature inside the reaction vessel equilibrated to −15 °C, as measured by a thermocouple inserted into the solution (Digi-Sense EW-91428-02 thermometer with Digi-Sense probe EW-08466-83). Reaction progress was monitored by

UV–vis absorption spectroscopy. The entire system was kept in the dark for the duration of the experiment. After completion of each experiment involving $BF_3 \cdot Et_2O$, the flow cell was purged sequentially with CH_3CN, deionized water, a saturated aqueous solution of $Ca(OH)_2$, deionized water, and finally CH_3CN to remove residual $BF_3 \cdot Et_2O$ and any potentially hazardous byproducts of sonication.[45] Sonication experiments on **PMA-LNP** were performed using a different sonication probe with an acoustic intensity of 10.5 ± 0.2 W/cm^2. Sonication intensity was calibrated via the literature method.[46]

General Procedure for Photoirradiation Experiments. Photoirradiation experiments were performed under conditions that closely mimic those of the ultrasonication experiments. A sonication vessel was placed onto the sonication probe and charged with a 2 mg/mL solution of polymer in CH_3CN containing 30 mM BHT (20.0 mL) for consistency with ultrasonication experiments. An additional 6.2 mL of solution was pumped into the dead space of the circulatory setup. If applicable, $BF_3 \cdot Et_2O$ was added to the sonication vessel via microsyringe to give a final concentration of 0.5 mM $BF_3 \cdot Et_2O$. Teflon inlet and outlet tubes were inserted into the solution in the sonication vessel through punctured septa, and the pump was engaged to start the flow of solution through the system. The sonication vessel was submerged in a −45 °C bath and degassed by sparging with N_2 for 30 min. The system was then maintained under an inert atmosphere throughout the photoirradiation experiment. Without sonication, the temperature inside the reaction vessel equilibrated to −30 °C. The vessel was then exposed to a UV light source (λ = 311 nm) positioned ~2 in away, which was also submerged in the cooling bath and encased within a quartz tube. Reaction progress

was monitored by UV-vis absorption spectroscopy. The entire system was protected from external light for the duration of the experiment.

1.6 ^{1}H and ^{13}C NMR Spectra

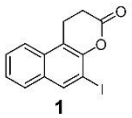

1

^{1}H (400 MHz, $CDCl_3$)

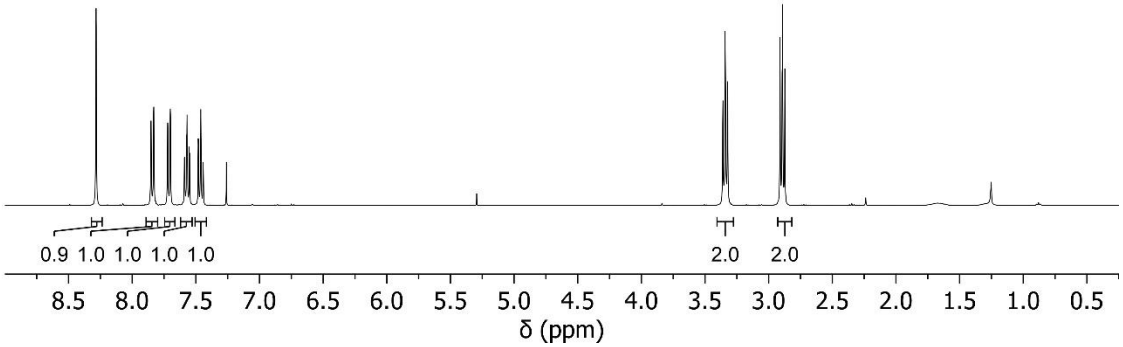

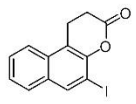

1

^{13}C (101 MHz, $CDCl_3$)

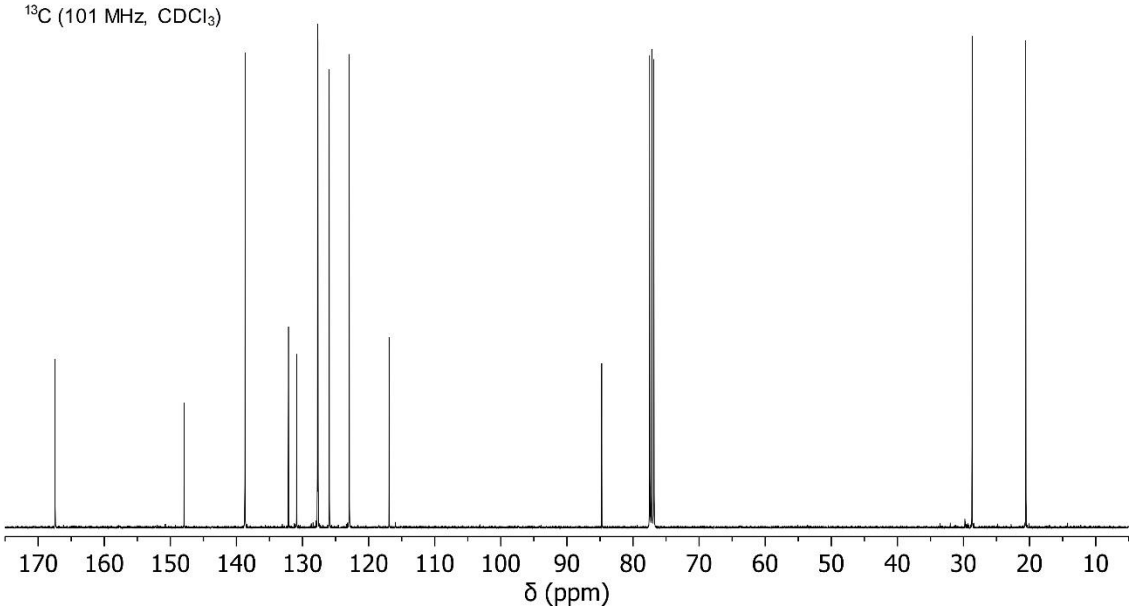

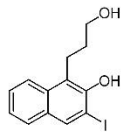

2

^{1}H (400 MHz, $CDCl_3$)

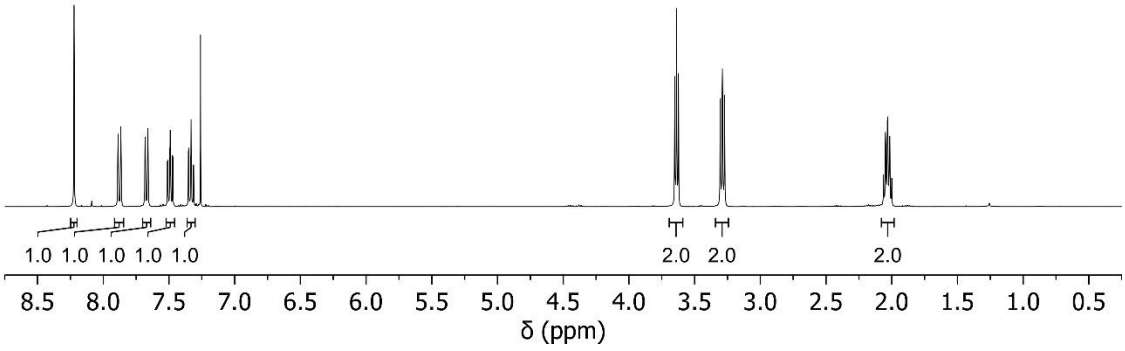

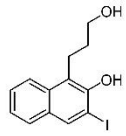

2

^{13}C (101 MHz, $CDCl_3$)

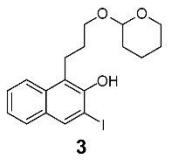

3

^{1}H (400 MHz, $CDCl_3$)

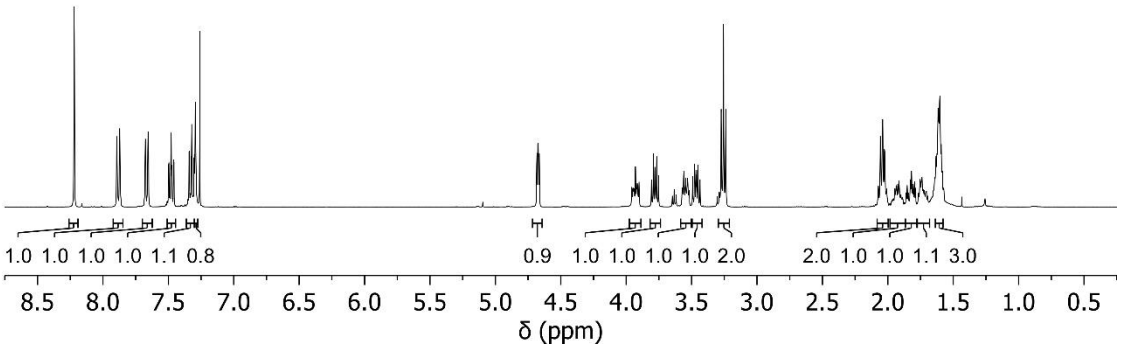

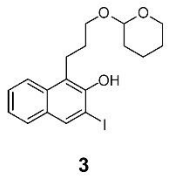

3

^{13}C (101 MHz, $CDCl_3$)

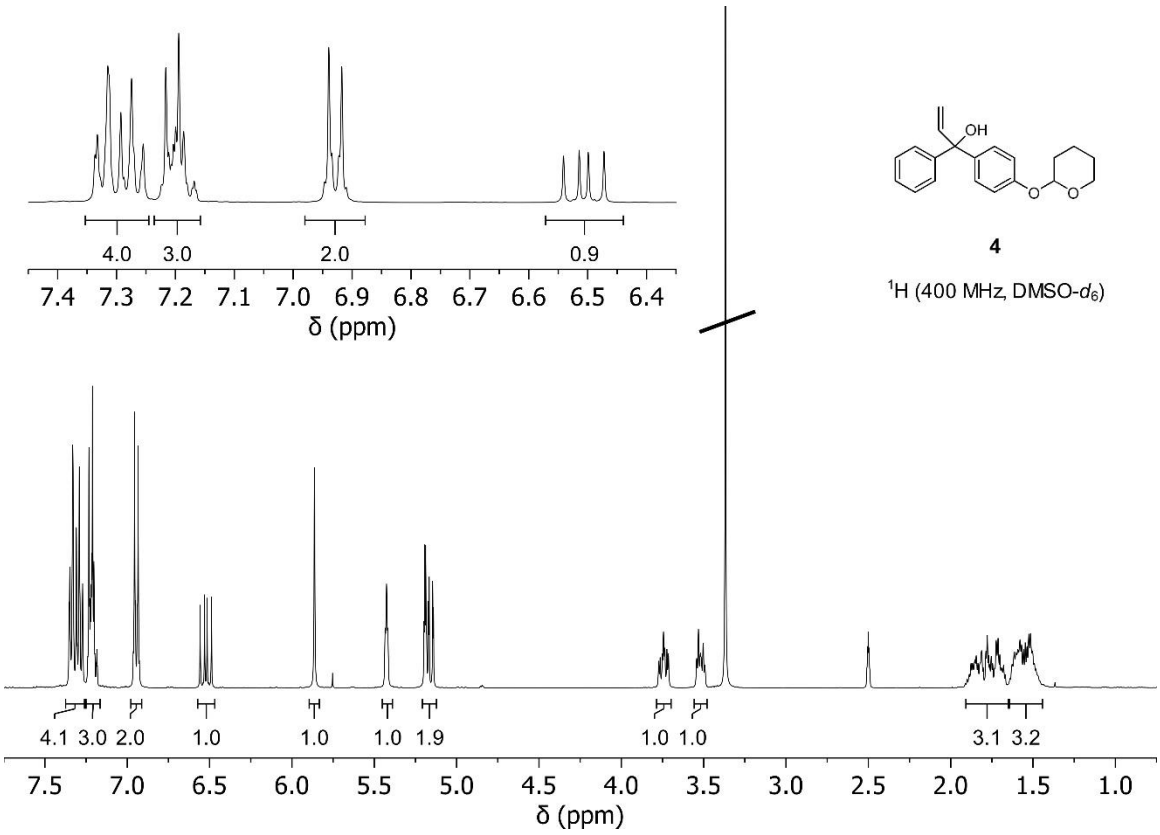
OH
O
O
4
^{1}H (400 MHz, DMSO-d_6)
4.0 3.0 2.0 0.9
7.4 7.3 7.2 7.1 7.0 6.9 6.8 6.7 6.6 6.5 6.4
δ (ppm)
4.1 3.0 2.0 1.0 1.0 1.0 1.9 1.0 1.0 3.1 3.2
7.5 7.0 6.5 6.0 5.5 5.0 4.5 4.0 3.5 3.0 2.5 2.0 1.5 1.0
δ (ppm)

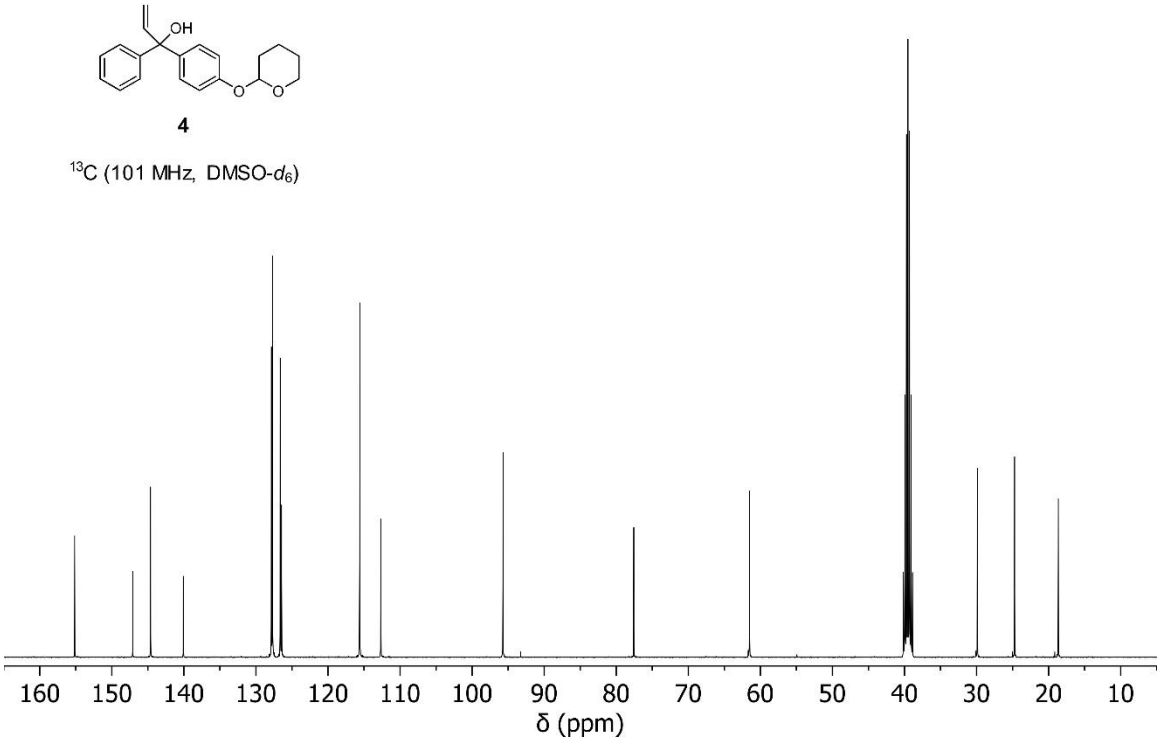
OH
O
O
4
^{13}C (101 MHz, DMSO-d_6)
160 150 140 130 120 110 100 90 80 70 60 50 40 30 20 10
δ (ppm)

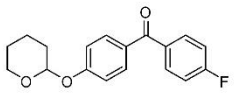

BP-F

^{1}H (400 MHz, $CDCl_3$)

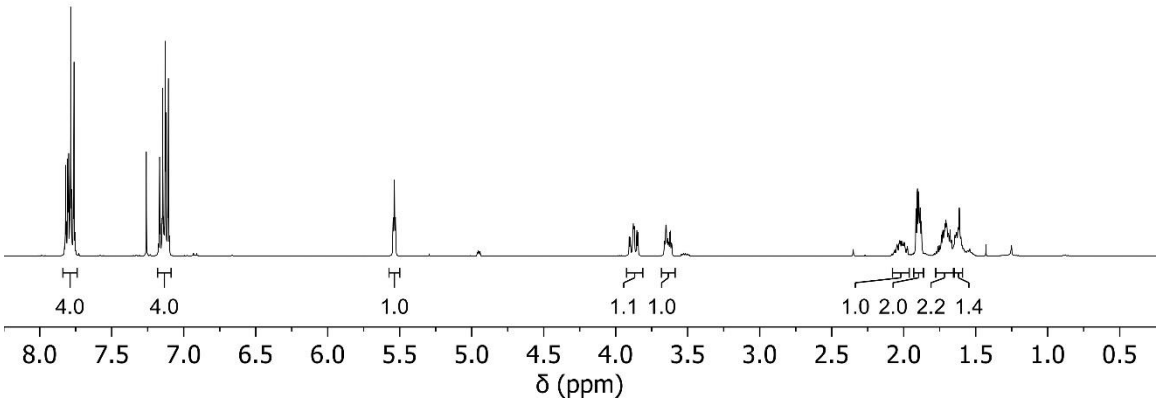

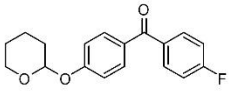

BP-F

^{13}C (101 MHz, $CDCl_3$)

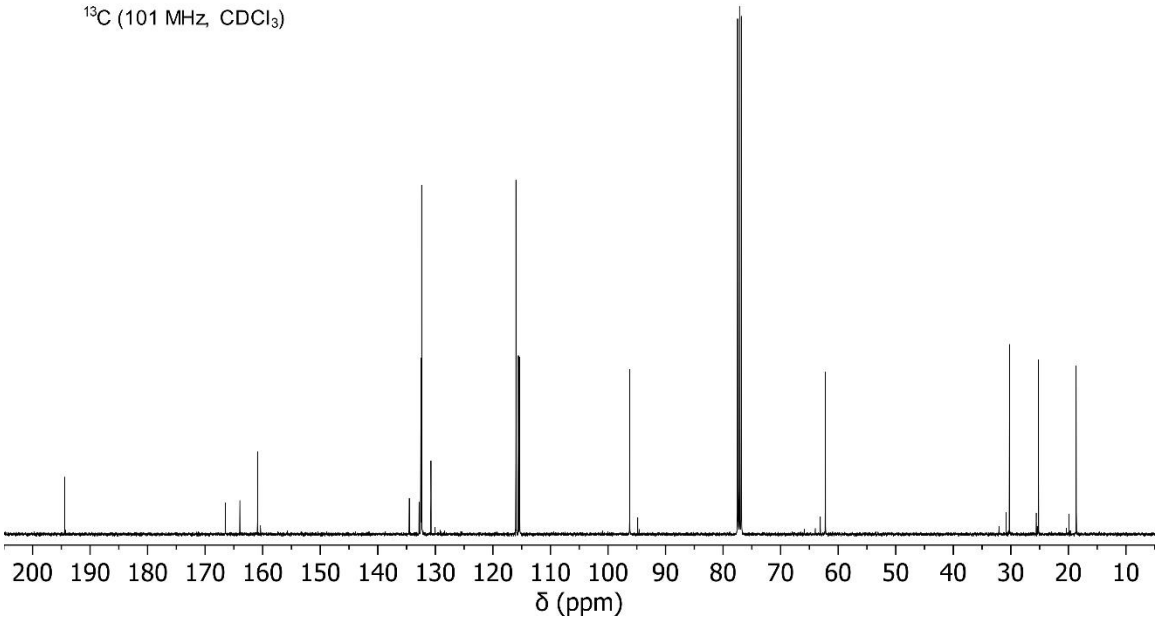

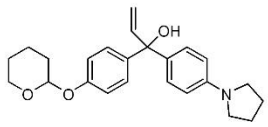

5

^{1}H (400 MHz, CD_2Cl_2)

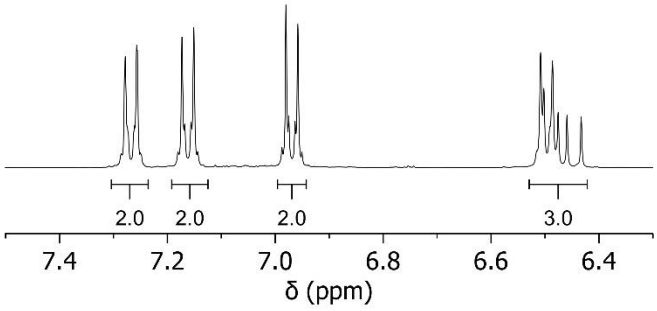

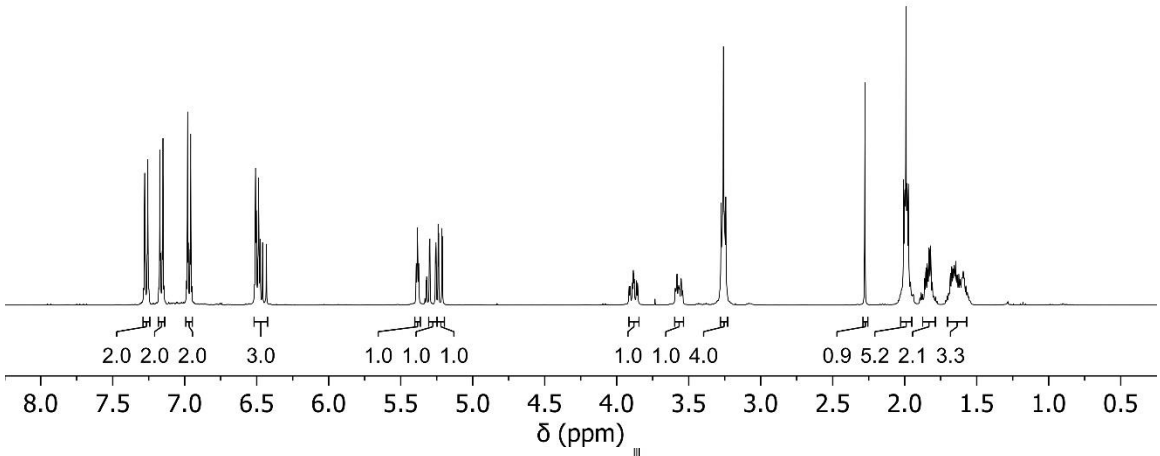

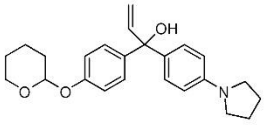

5

^{13}C (101 MHz, $CDCl_3$)

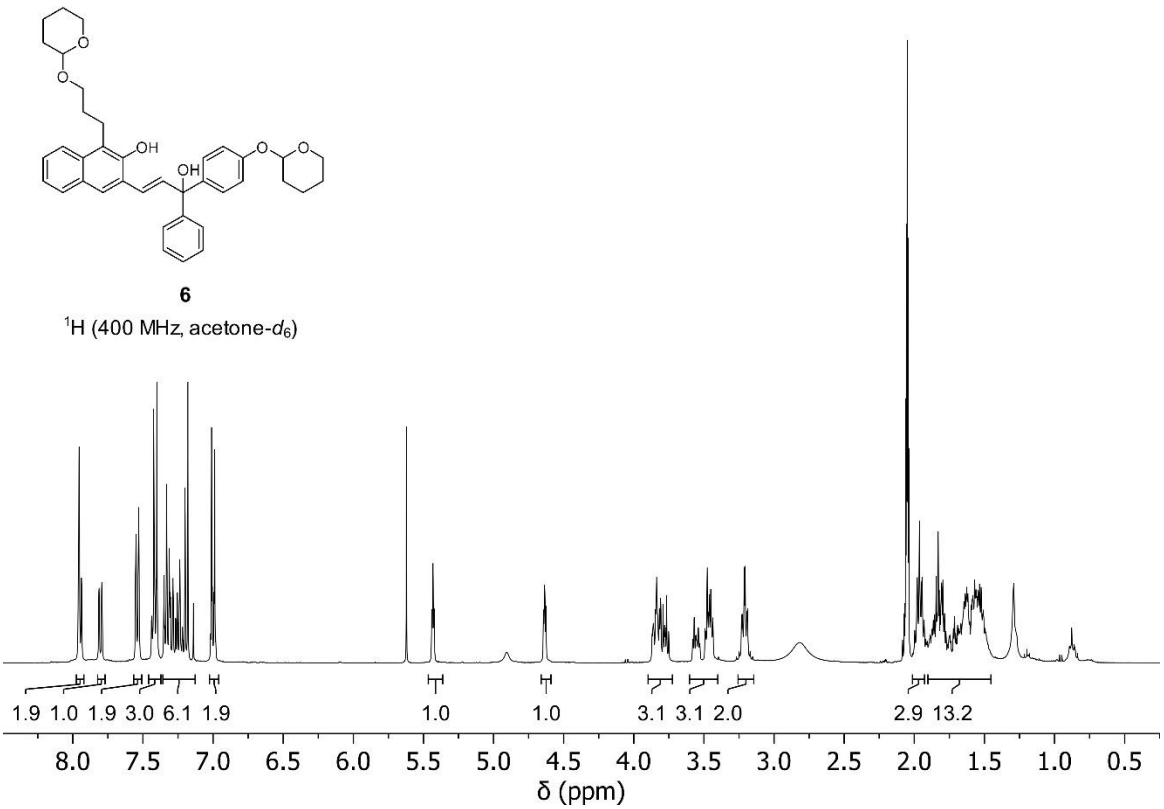
OH
OH
O
O
O
6
1H (400 MHz, acetone-d6)
1.9 1.0 1.9 3.0 6.1 1.9
1.0
1.0
3.1 3.1 2.0
2.9 13.2
8.0 7.5 7.0 6.5 6.0 5.5 5.0 4.5 4.0 3.5 3.0 2.5 2.0 1.5 1.0 0.5
δ (ppm)

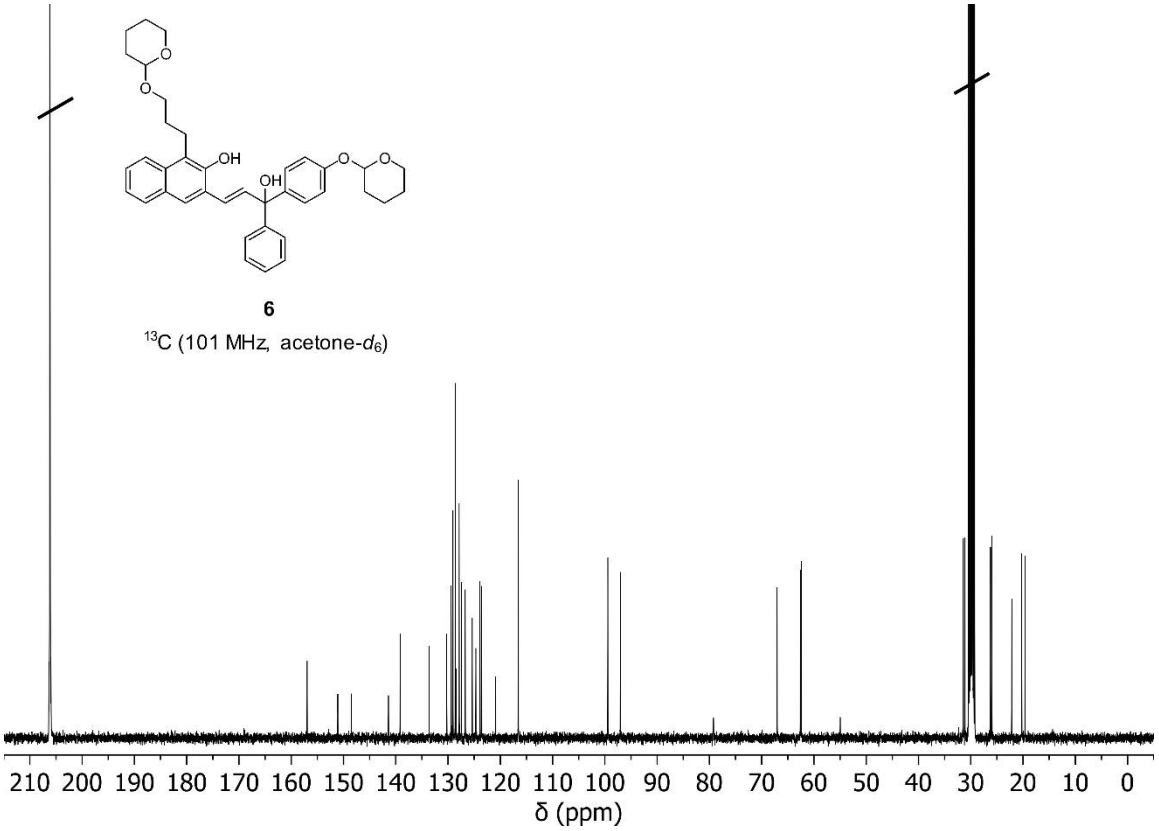
OH
OH
O
O
O
6
13C (101 MHz, acetone-d6)
210 200 190 180 170 160 150 140 130 120 110 100 90 80 70 60 50 40 30 20 10 0
δ (ppm)

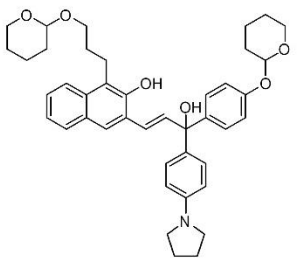

7

^{1}H (400 MHz, acetone-d_6)

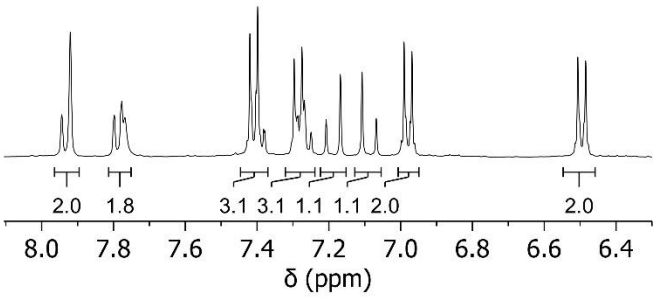

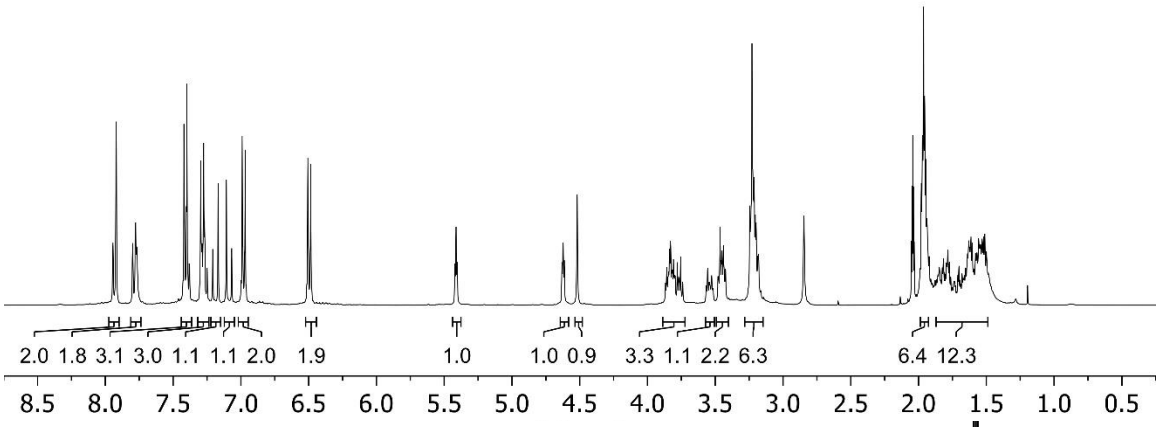

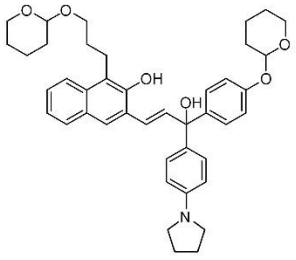

7

^{13}C (101 MHz, acetone-d_6)

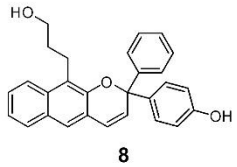

8

^{1}H (400 MHz, CD_2Cl_2)

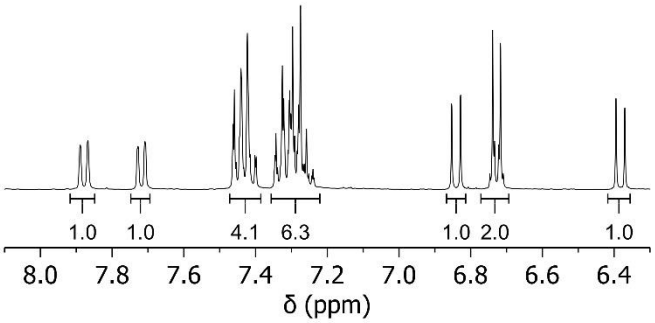

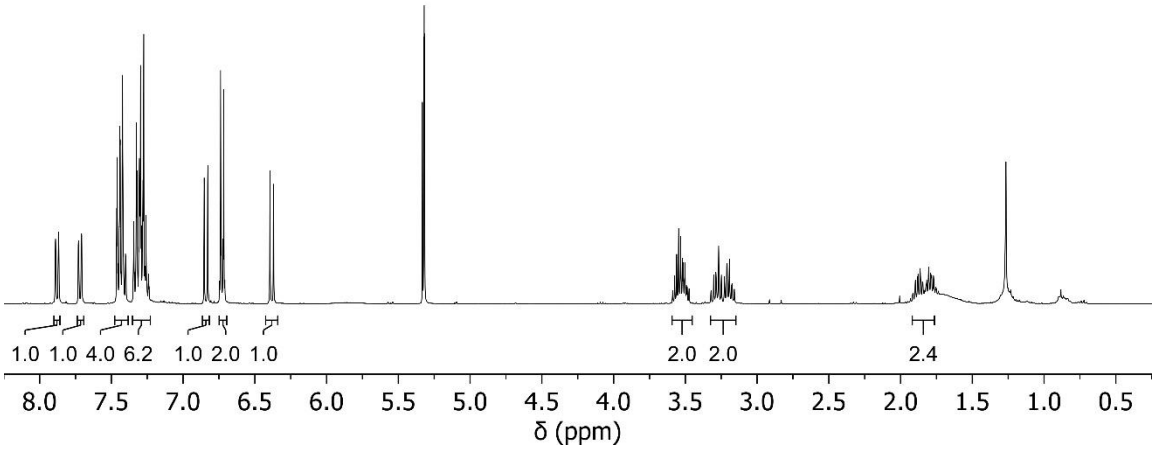

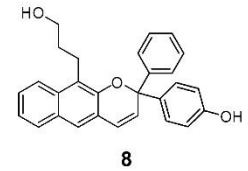

8

^{13}C (101 MHz, CD_2Cl_2)

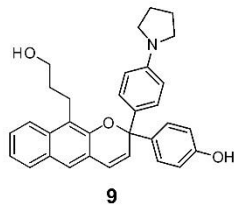

9

^{1}H (400 MHz, acetone-d_6)

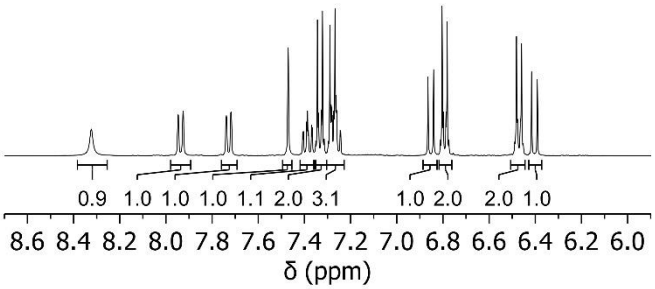

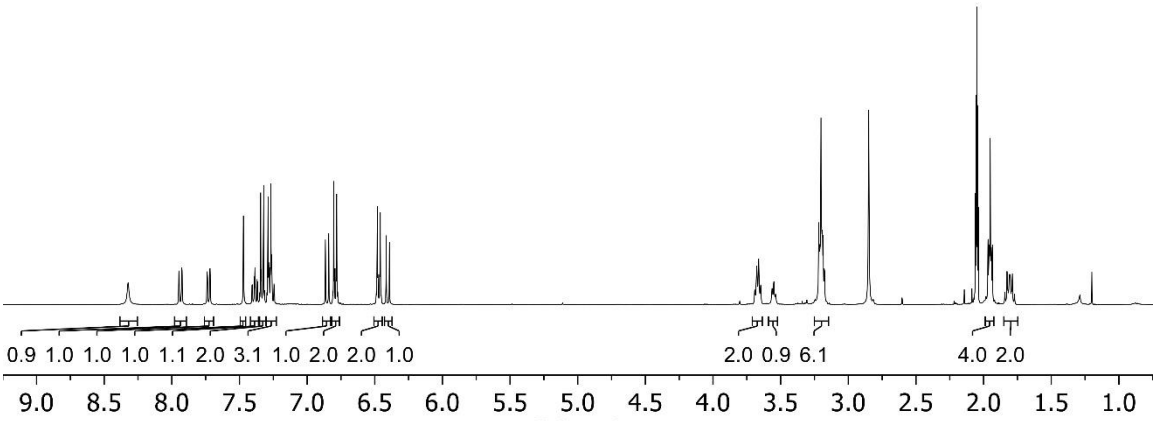

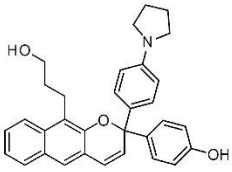

9

^{13}C (101 MHz, acetone-d_6)

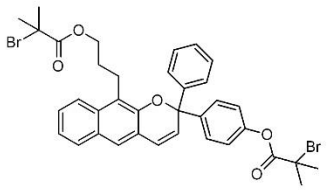

10

^{1}H (400 MHz, CD_2Cl_2)

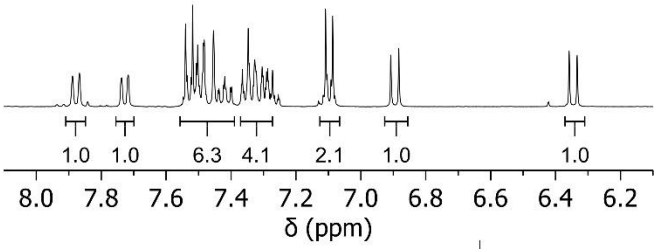

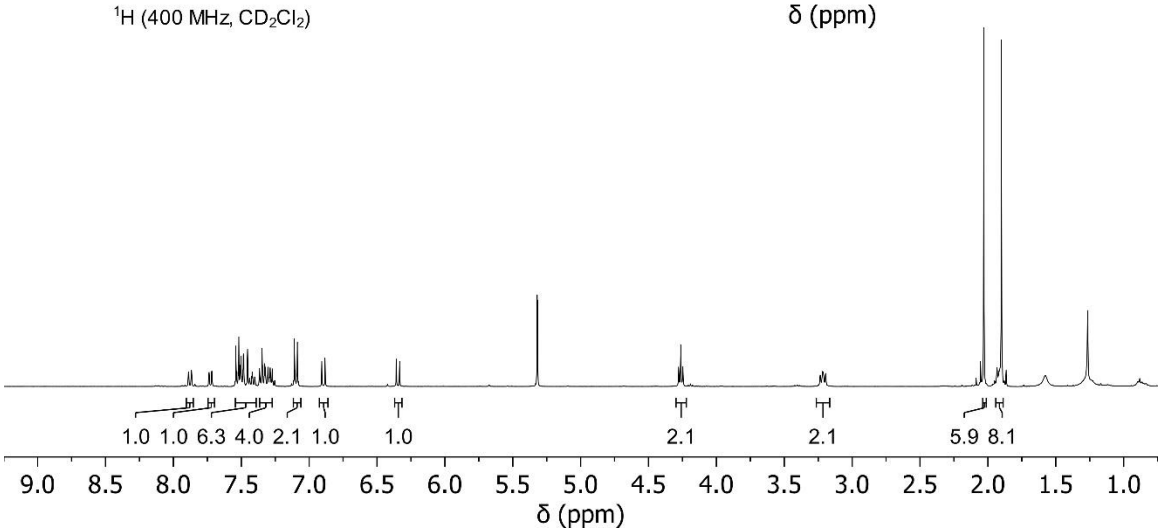

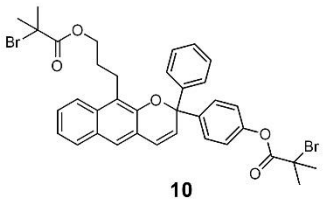

10

^{13}C (101 MHz, CD_2Cl_2)

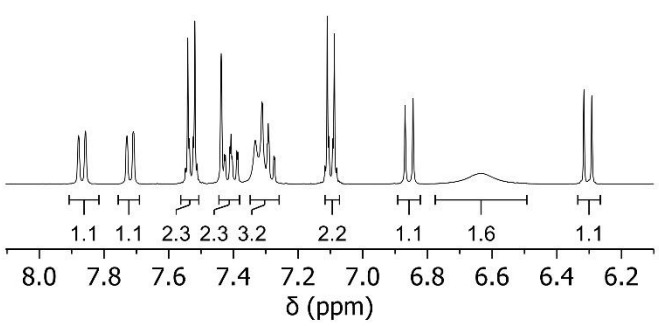

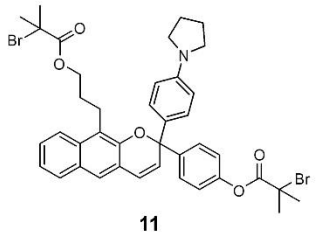

11

^{1}H (400 MHz, CD_2Cl_2)

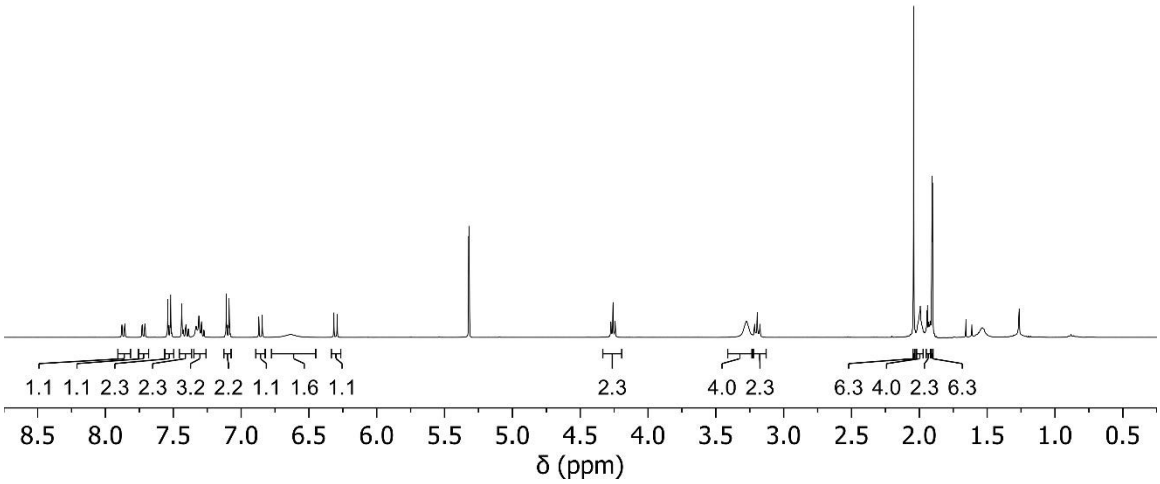

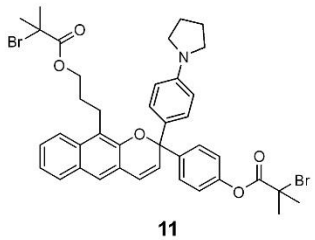

11

^{13}C (101 MHz, $CDCl_3$)

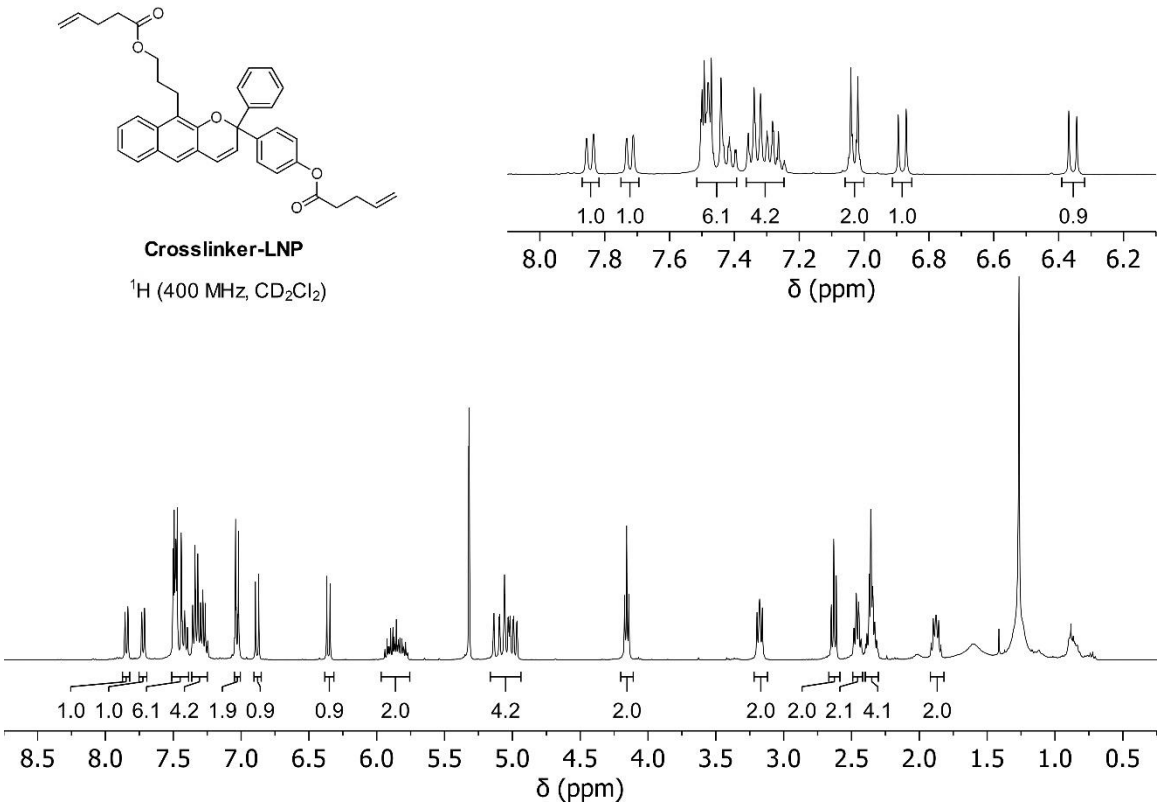
Crosslinker-LNP
^{1}H (400 MHz, CD_2Cl_2)
1.0 1.0 6.1 4.2 2.0 1.0 0.9
8.0 7.8 7.6 7.4 7.2 7.0 6.8 6.6 6.4 6.2
δ (ppm)
1.0 1.0 6.1 4.2 1.9 0.9 0.9 2.0 4.2 2.0 2.0 2.0 2.1 4.1 2.0
8.5 8.0 7.5 7.0 6.5 6.0 5.5 5.0 4.5 4.0 3.5 3.0 2.5 2.0 1.5 1.0 0.5
δ (ppm)

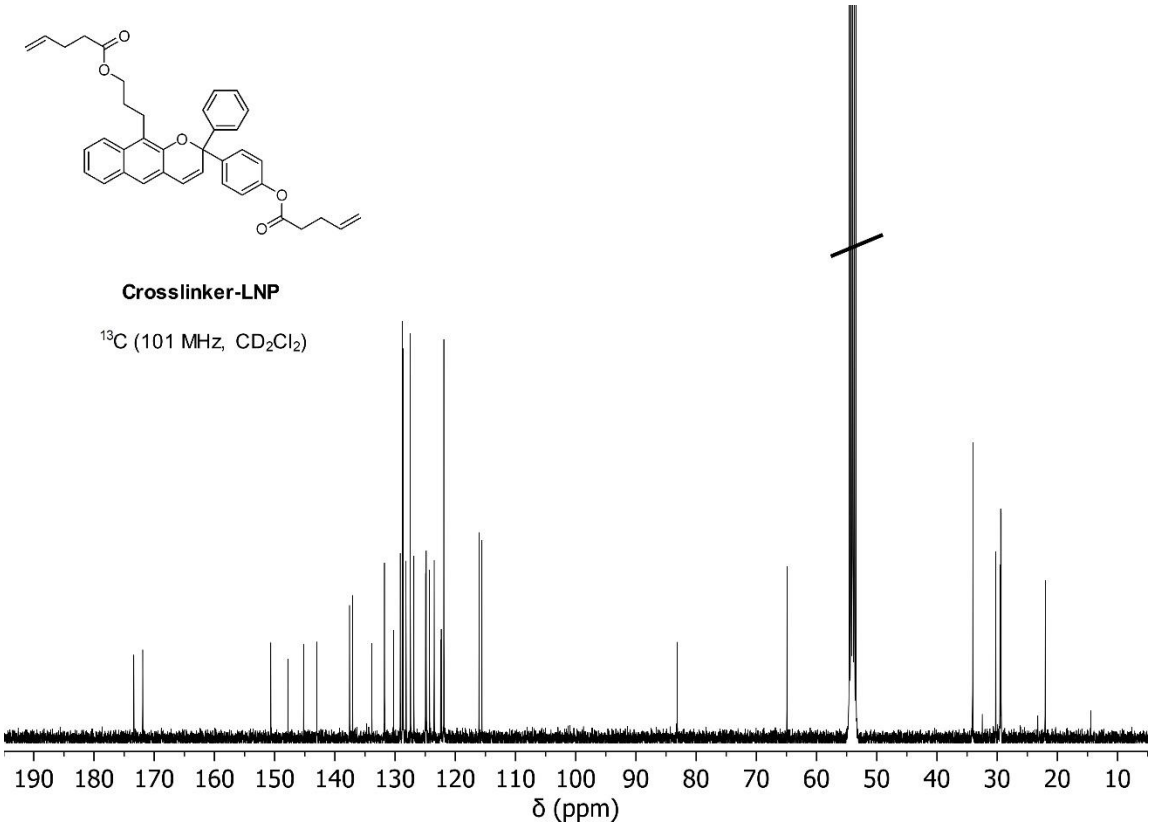
Crosslinker-LNP
^{13}C (101 MHz, CD_2Cl_2)
190 180 170 160 150 140 130 120 110 100 90 80 70 60 50 40 30 20 10
δ (ppm)

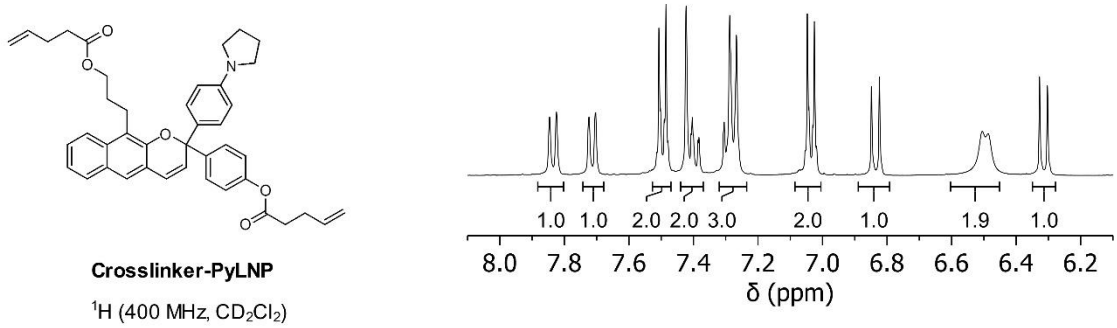

Crosslinker-PyLNP

^{1}H (400 MHz, CD_2Cl_2)

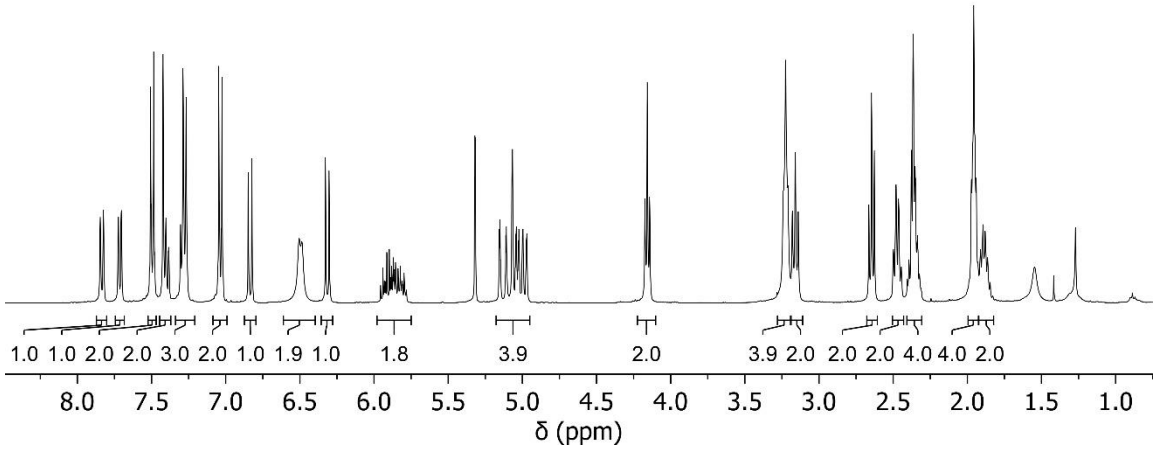

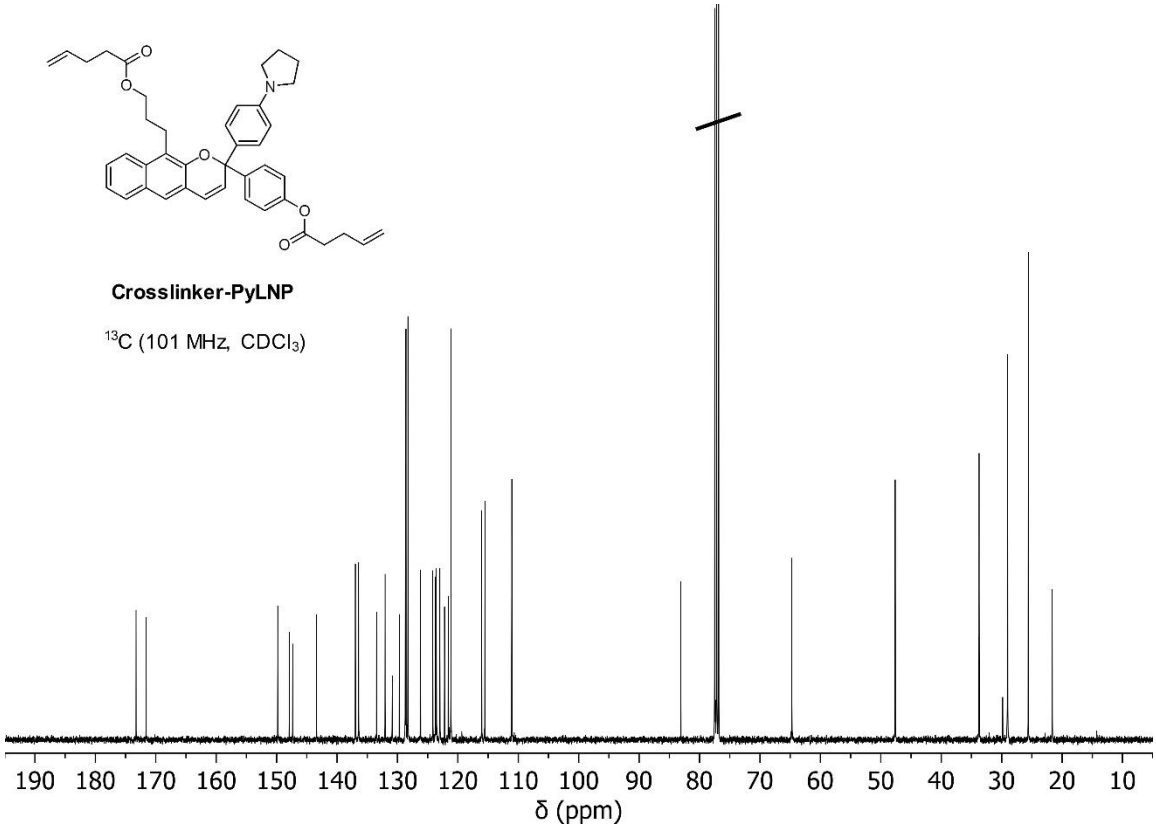

Crosslinker-PyLNP

^{13}C (101 MHz, $CDCl_3$)

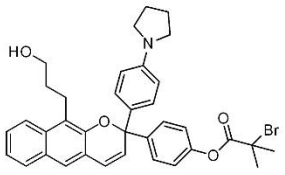

PyLNP-Mono

^{1}H (400 MHz, CD_2Cl_2)

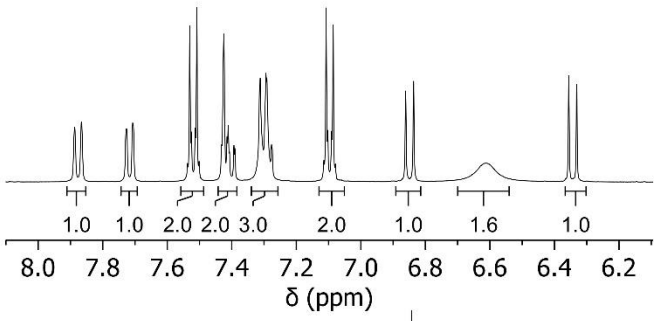

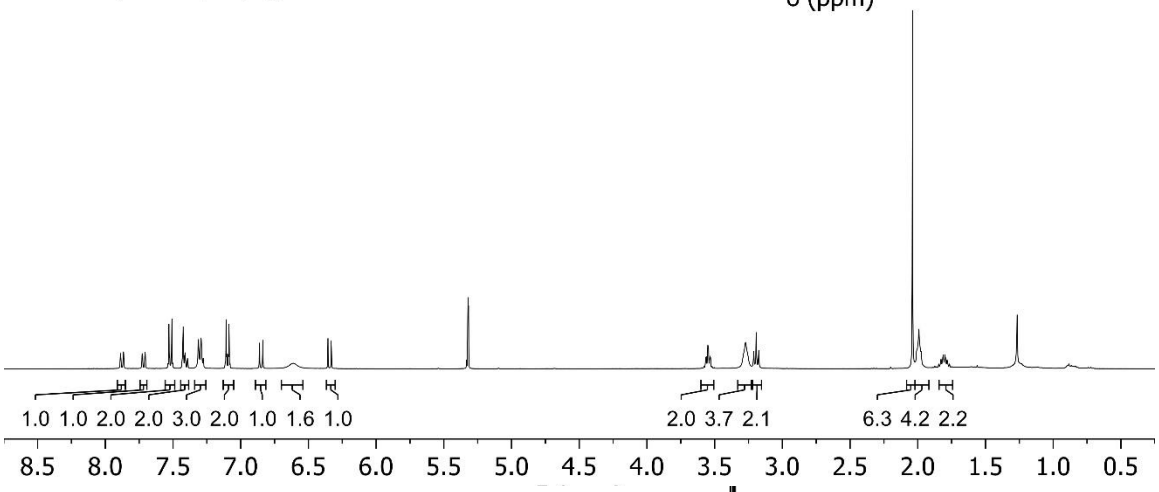

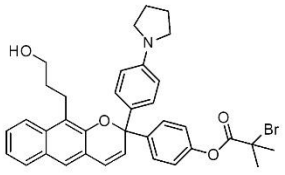

PyLNP-Mono

^{13}C (101 MHz, $CDCl_3$)

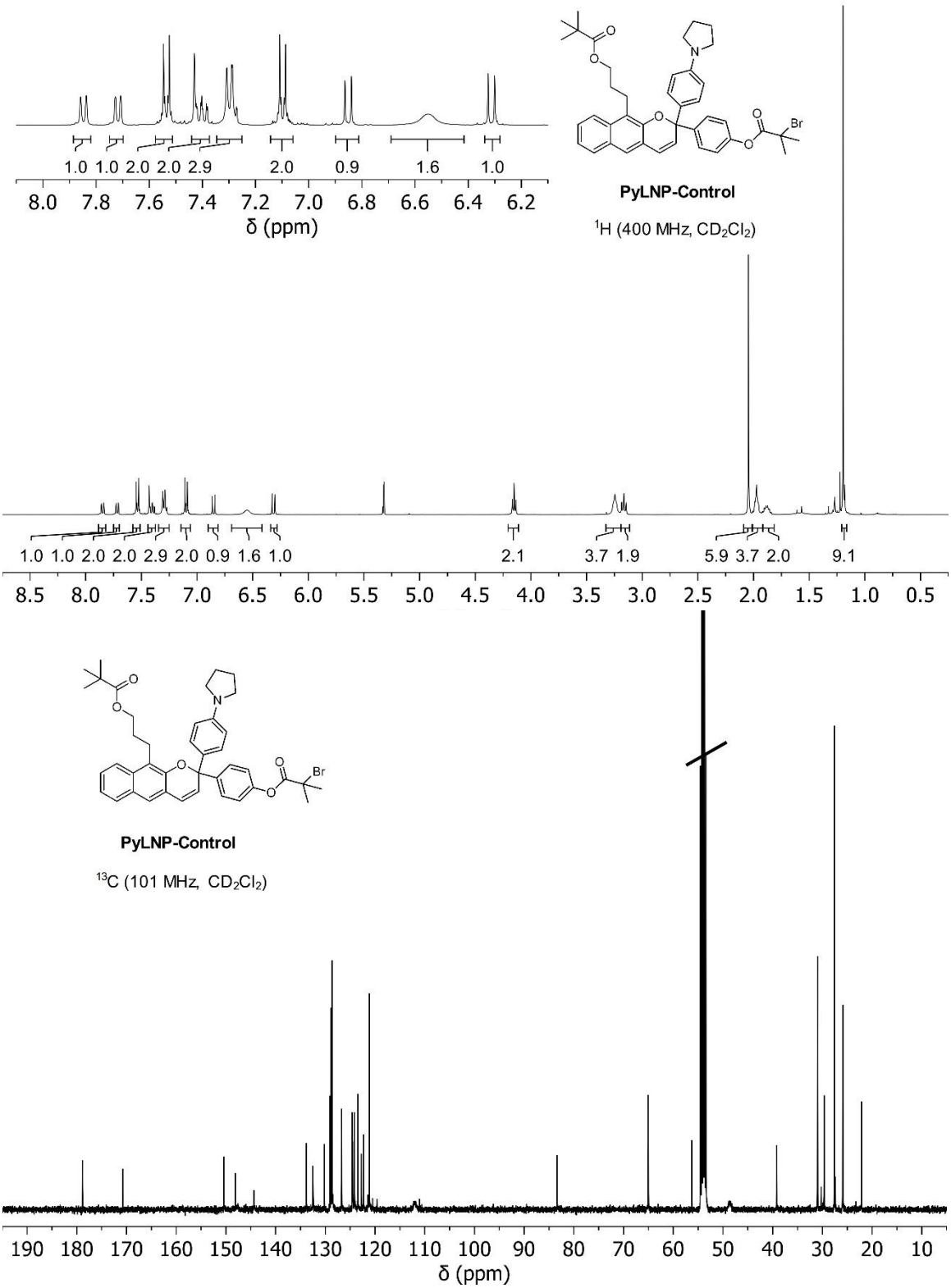
PyLNP-Control
^{1}H (400 MHz, CD_2Cl_2)
1.0 1.0 2.0 2.0 2.9 2.0 0.9 1.6 1.0
8.0 7.8 7.6 7.4 7.2 7.0 6.8 6.6 6.4 6.2
δ (ppm)
1.0 1.0 2.0 2.0 2.9 2.0 0.9 1.6 1.0
2.1
3.7 1.9
5.9 3.7 2.0
9.1
8.5 8.0 7.5 7.0 6.5 6.0 5.5 5.0 4.5 4.0 3.5 3.0 2.5 2.0 1.5 1.0 0.5
PyLNP-Control
^{13}C (101 MHz, CD_2Cl_2)
190 180 170 160 150 140 130 120 110 100 90 80 70 60 50 40 30 20 10
δ (ppm)

1.7 References

(1) Hepworth, J. D.; Heron, B. M. Photochromic Naphthopyrans. In *Functional Dyes*; Elsevier Science, 2006; pp 85–135. https://doi.org/10.1016/B978-044452176-7/50004-8.

(2) Van Gemert, B. Benzo and Naphthopyrans (Chromenes). In *Organic Photochromic and Thermochromic Compounds*; Springer: Boston, MA, 2002; pp 111–140.

(3) Corns, S. N.; Partington, S. M.; Towns, A. D. Industrial Organic Photochromic Dyes. *Color. Technol.* **2009**, *125* (5), 249–261. https://doi.org/10.1111/j.1478-4408.2009.00204.x.

(4) Robb, M. J.; Kim, T. A.; Halmes, A. J.; White, S. R.; Sottos, N. R.; Moore, J. S. Regioisomer-Specific Mechanochromism of Naphthopyran in Polymeric Materials. *J. Am. Chem. Soc.* **2016**, *138* (38), 12328–12331. https://doi.org/10.1021/jacs.6b07610.

(5) Beyer, M. K.; Clausen-Schaumann, H. Mechanochemistry: The Mechanical Activation of Covalent Bonds. *Chem. Rev.* **2005**, *105* (8), 2921–2948. https://doi.org/10.1021/cr030697h.

(6) Caruso, M. M.; Davis, D. A.; Shen, Q.; Odom, S. A.; Sottos, N. R.; White, S. R.; Moore, J. S. Mechanically-Induced Chemical Changes in Polymeric Materials. *Chem. Rev.* **2009**, *109*, 5755–5798. https://doi.org/10.1021/cr9001353.

(7) Li, J.; Nagamani, C.; Moore, J. S. Polymer Mechanochemistry: From Destructive to Productive. *Acc. Chem. Res.* **2015**, *48* (8), 2181–2190. https://doi.org/10.1021/acs.accounts.5b00184.

(8) Barber, R. W.; McFadden, M. E.; Hu, X.; Robb, M. J. Mechanochemically Gated Photoswitching: Expanding the Scope of Polymer Mechanochromism. *Synlett* **2019**, *30*, 1725–1732. https://doi.org/10.1055/s-0037-1611858.

(9) Potisek, S. L.; Davis, D. A.; Sottos, N. R.; White, S. R.; Moore, J. S. Mechanophore-Linked Addition Polymers. *J. Am. Chem. Soc.* **2007**, *129*, 13808–13809. https://doi.org/10.1021/ja076189x.

(10) Davis, D. A.; Hamilton, A.; Yang, J.; Cremar, L. D.; Van Gough, D.; Potisek, S. L.; Ong, M. T.; Braun, P. V.; Martínez, T. J.; White, S. R.; Moore, J. S.; Sottos, N. R. Force-Induced Activation of Covalent Bonds in Mechanoresponsive Polymeric Materials. *Nature* **2009**, *459* (7243), 68–72. https://doi.org/10.1038/nature07970.

(11) Gossweiler, G. R.; Hewage, G. B.; Soriano, G.; Wang, Q.; Welshofer, G. W.; Zhao, X.; Craig, S. L. Mechanochemical Activation of Covalent Bonds in Polymers with Full and Repeatable Macroscopic Shape Recovery. *ACS Macro Lett.* **2014**, *3*, 216–219. https://doi.org/10.1021/mz500031q.

(12) Zhang, H.; Gao, F.; Cao, X.; Li, Y.; Xu, Y.; Weng, W.; Boulatov, R. Mechanochromism and Mechanical-Force-Triggered Cross-Linking from a Single Reactive Moiety Incorporated into Polymer Chains. *Angew. Chem. Int. Ed.* **2016**, *55* (9), 3040–3044. https://doi.org/10.1002/anie.201510171.

(13) Wang, Z.; Ma, Z.; Wang, Y.; Xu, Z.; Luo, Y.; Wei, Y.; Jia, X. A Novel Mechanochromic and Photochromic Polymer Film: When Rhodamine Joins Polyurethane. *Adv. Mater.* **2015**, *27* (41), 6469–6474. https://doi.org/10.1002/adma.201503424.

(14) Wang, T.; Zhang, N.; Dai, J.; Li, Z.; Bai, W.; Bai, R. Novel Reversible Mechanochromic Elastomer with High Sensitivity: Bond Scission and Bending-Induced Multicolor Switching. *ACS Appl. Mater. Interfaces* **2017**, *9* (13), 11874–11881. https://doi.org/10.1021/acsami.7b00176.

(15) Wu, M.; Li, Y.; Yuan, W.; De Bo, G.; Cao, Y.; Chen, Y. Cooperative and Geometry-Dependent Mechanochromic Reactivity through Aromatic Fusion of Two Rhodamines in Polymers. *J. Am. Chem. Soc.* **2022**, *144* (37), 17120–17128. https://doi.org/10.1021/jacs.2c07015.

(16) Qian, H.; Purwanto, N. S.; Ivanoff, D. G.; Halmes, A. J.; Sottos, N. R.; Moore, J. S. Fast, Reversible Mechanochromism of Regioisomeric Oxazine Mechanophores: Developing in Situ Responsive Force Probes for Polymeric Materials. *Chem* **2021**, *7* (4), 1080–1091. https://doi.org/10.1016/j.chempr.2021.02.014.

(17) Qi, Q.; Sekhon, G.; Chandradat, R.; Ofodum, N. M.; Shen, T.; Scrimgeour, J.; Joy, M.; Wriedt, M.; Jayathirtha, M.; Darie, C. C.; Shipp, D. A.; Liu, X.; Lu, X. Force-Induced Near-Infrared Chromism of Mechanophore-Linked Polymers. *J. Am. Chem. Soc.* **2021**, *143* (42), 17337–17343. https://doi.org/10.1021/jacs.1c05923.

(18) Göstl, R.; Sijbesma, R. P. π-Extended Anthracenes as Sensitive Probes for Mechanical Stress. *Chem. Sci.* **2016**, *7* (1), 370–375. https://doi.org/10.1039/C5SC03297K.

(19) Baumann, C.; Stratigaki, M.; Centeno, S. P.; Göstl, R. Multicolor Mechanofluorophores for the Quantitative Detection of Covalent Bond Scission in Polymers. *Angew. Chem. Int. Ed.* **2021**, *60*, 13287–13293. https://doi.org/10.1002/anie.202101716.

(20) Hemmer, J. R.; Rader, C.; Wilts, B. D.; Weder, C.; Berrocal, J. A. Heterolytic Bond Cleavage in a Scissile Triarylmethane Mechanophore. *J. Am. Chem. Soc.* **2021**, *143* (45), 18859–18863. https://doi.org/10.1021/jacs.1c10004.

(21) Imato, K.; Irie, A.; Kosuge, T.; Ohishi, T.; Nishihara, M.; Takahara, A.; Otsuka, H. Mechanophores with a Reversible Radical System and Freezing-Induced Mechanochemistry in Polymer Solutions and Gels. *Angew. Chem. Int. Ed.* **2015**, *54* (21), 6168–6172. https://doi.org/10.1002/anie.201412413.

(22) Imato, K.; Kanehara, T.; Ohishi, T.; Nishihara, M.; Yajima, H.; Ito, M.; Takahara, A.; Otsuka, H. Mechanochromic Dynamic Covalent Elastomers: Quantitative Stress Evaluation and Autonomous Recovery. *ACS Macro Lett.* **2015**, *4* (11), 1307–1311. https://doi.org/10.1021/acsmacrolett.5b00717.

(23) McFadden, M. E.; Robb, M. J. Force-Dependent Multicolor Mechanochromism from a Single Mechanophore. *J. Am. Chem. Soc.* **2019**, *141* (29), 11388–11392. https://doi.org/10.1021/jacs.9b05280.

(24) Versaw, B. A.; McFadden, M. E.; Husic, C. C.; Robb, M. J. Designing Naphthopyran Mechanophores with Tunable Mechanochromic Behavior. *Chem. Sci.* **2020**, *11* (17), 4525–4530. https://doi.org/10.1039/D0SC01359E.

(25) Osler, S. K.; McFadden, M. E.; Robb, M. J. Comparison of the Reactivity of Isomeric 2H- and 3H-Naphthopyran Mechanophores. *J. Polym. Sci.* **2021**, *59*, 2537–2544. https://doi.org/10.1002/pol.20210417.

(26) McFadden, M. E.; Robb, M. J. Generation of an Elusive Permanent Merocyanine via a Unique Mechanochemical Reaction Pathway. *J. Am. Chem. Soc.* **2021**, *143* (21), 7925–7929. https://doi.org/10.1021/jacs.1c03865.
(27) McFadden, M. E.; Osler, S. K.; Sun, Y.; Robb, M. J. Mechanical Force Enables an Anomalous Dual Ring-Opening Reaction of Naphthodipyran. *J. Am. Chem. Soc.* **2022**, *144* (49), 22391–22396. https://doi.org/10.1021/jacs.2c08817.
(28) Osler, S. K.; McFadden, M. E.; Zeng, T.; Robb, M. J. Mechanochemical Reactivity of a Multimodal 2H-Bis-Naphthopyran Mechanophore. *Polym. Chem.* **2023**, *14* (22), 2717–2723. https://doi.org/10.1039/D3PY00344B.
(29) Guo, K.; Chen, Y. 'Locking and Unlocking Control' of Photochromism of Naphthopyran Derivative. *Journal of Physical Organic Chemistry* **2010**, *23* (3), 207–210. https://doi.org/10.1002/poc.1598.
(30) Beyer, M. K. The Mechanical Strength of a Covalent Bond Calculated by Density Functional Theory. *J. Chem. Phys.* **2000**, *112* (17), 7307–7312. https://doi.org/10.1063/1.481330.
(31) Klein, I. M.; Husic, C. C.; Kovács, D. P.; Choquette, N. J.; Robb, M. J. Validation of the CoGEF Method as a Predictive Tool for Polymer Mechanochemistry. *J. Am. Chem. Soc.* **2020**, *142* (38), 16364–16381. https://doi.org/10.1021/jacs.0c06868.
(32) May, P. A.; Moore, J. S. Polymer Mechanochemistry: Techniques to Generate Molecular Force via Elongational Flows. *Chem. Soc. Rev.* **2013**, *42*, 7497–7506. https://doi.org/10.1039/C2CS35463B.
(33) Zhao, W.; Carreira, E. M. Facile One-Pot Synthesis of Photochromic Pyrans. *Org. Lett.* **2003**, *5* (22), 4153–4154. https://doi.org/10.1021/ol035599x.
(34) Gabbutt, C. D.; Heron, B. M.; Instone, A. C.; Thomas, D. A.; Partington, S. M.; Hursthouse, M. B.; Gelbrich, T. Observations on the Synthesis of Photochromic Naphthopyrans. *Eur. J. Org. Chem.* **2003**, No. 7, 1220–1230. https://doi.org/10.1002/ejoc.200390176.
(35) Kicková, A.; Donovalová, J.; Kasák, P.; Putala, M. A Chiroptical Binaphthopyran Switch: Amplified CD Response in a Polystyrene Film. *New J. Chem.* **2010**, *34* (6), 1109. https://doi.org/10.1039/c0nj00102c.
(36) Tee, J. T.; Yaeghoobi, M.; Chee, C. F.; Rahman, N. Abd. Efficient One-Pot Synthesis of 2,2-Dimethyl-2H-Chromenes via Pd(II)-Catalyzed Coupling and SiO2-Promoted Condensation of o-Halophenols with 2-Methyl-3-Buten-2-Ol. *Synthetic Commun.* **2015**, *45* (16), 1920–1927. https://doi.org/10.1080/00397911.2015.1056371.
(37) Nguyen, N. H.; Rosen, B. M.; Lligadas, G.; Percec, V. Surface-Dependent Kinetics of Cu(0)-Wire-Catalyzed Single-Electron Transfer Living Radical Polymerization of Methyl Acrylate in DMSO at 25 °C. *Macromolecules* **2009**, *42* (7), 2379–2386. https://doi.org/10.1021/ma8028562.
(38) Nguyen, N. H.; Rosen, B. M.; Lligadas, G.; Percec, V. Surface-Dependent Kinetics of Cu(0)-Wire-Catalyzed Single-Electron Transfer Living Radical Polymerization of Methyl Acrylate in DMSO at 25 °C. *Macromolecules* **2009**, *42* (7), 2379–2386. https://doi.org/10.1021/ma8028562.
(39) Gossweiler, G. R.; Hewage, G. B.; Soriano, G.; Wang, Q.; Welshofer, G. W.; Zhao, X.; Craig, S. L. Mechanochemical Activation of Covalent Bonds in Polymers with Full and

Repeatable Macroscopic Shape Recovery. *ACS Macro Lett.* **2014**, *3* (3), 216–219. https://doi.org/10.1021/mz500031q.

(40) Overholts, A. C.; Granados Razo, W.; Robb, M. J. Mechanically Gated Formation of Donor–Acceptor Stenhouse Adducts Enabling Mechanochemical Multicolour Soft Lithography. *Nat. Chem.* **2023**, *15* (3), 332–338. https://doi.org/10.1038/s41557-022-01126-5.

(41) Beyer, M. K. The Mechanical Strength of a Covalent Bond Calculated by Density Functional Theory. *The Journal of Chemical Physics* **2000**, *112* (17), 7307–7312. https://doi.org/10.1063/1.481330.

(42) May, P. A.; Munaretto, N. F.; Hamoy, M. B.; Robb, M. J.; Moore, J. S. Is Molecular Weight or Degree of Polymerization a Better Descriptor of Ultrasound-Induced Mechanochemical Transduction? *ACS Macro Lett.* **2016**, *5* (2), 177–180. https://doi.org/10.1021/acsmacrolett.5b00855.

(43) Yang, J.; Horst, M.; Werby, S. H.; Cegelski, L.; Burns, N. Z.; Xia, Y. Bicyclohexene-*Peri* -Naphthalenes: Scalable Synthesis, Diverse Functionalization, Efficient Polymerization, and Facile Mechanoactivation of Their Polymers. *J. Am. Chem. Soc.* **2020**, *142* (34), 14619–14626. https://doi.org/10.1021/jacs.0c06454.

(44) Overholts, A. C.; McFadden, M. E.; Robb, M. J. Quantifying Activation Rates of Scissile Mechanophores and the Influence of Dispersity. *Macromolecules* **2022**, *55* (1), 276–283. https://doi.org/10.1021/acs.macromol.1c02232.

(45) McFadden, M. E.; Osler, S. K.; Sun, Y.; Robb, M. J. Mechanical Force Enables an Anomalous Dual Ring-Opening Reaction of Naphthodipyran. *J. Am. Chem. Soc.* **2022**, *144* (49), 22391–22396. https://doi.org/10.1021/jacs.2c08817.

(46) Berkowski, K. L.; Potisek, S. L.; Hickenboth, C. R.; Moore, J. S. Ultrasound-Induced Site-Specific Cleavage of Azo-Functionalized Poly(Ethylene Glycol). *Macromolecules* **2005**, *38* (22), 8975–8978. https://doi.org/10.1021/ma051394n.

C h a p t e r 2

MECHANOCHEMICAL ACTIVATION OF AN INDOLE-FUSED 2*H*-BENZOPYRAN GENERATES AN ACIDOCHROMIC MEROCYANINE DYE ENABLING MULTICOLOR CHROMOMORPHIC MATERIALS

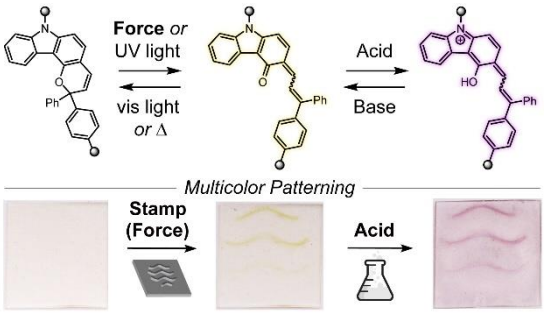

This chapter has been reprinted from Sun, Y.; Razo, W. G.; Luo, S. M.; Osler, S. K.; Robb, M. J. *Polym. Chem.* **2025**, *16*, 4128–4135.

Molecular switches based on the 2*H*-1-benzopyran (chromene) scaffold have been widely developed for their desirable photochromic and mechanochromic properties. Extended π-conjugation is necessary to stabilize the ring-opened merocyanine dye at room temperature leading to efficient switching under ambient conditions. To this end, naphthopyrans represent a special class of benzo-annulated benzopyrans that have been studied extensively as both photoswitches and more recently as mechanophores, generating intensely colored merocyanine dyes upon exposure to ultraviolet light or mechanical force, respectively. Alternative annulation strategies with judicious heteroatom substitution have also been

studied in the photochemistry literature, but the mechanochemistry of 2*H*-1-benzopyrans has yet to be explored. Here, we report the mechanochemical activation of an indole-fused 2*H*-1-benzopyran mechanophore that generates a yellow-colored merocyanine dye in polymers that is subsequently transformed to a purple-colored dye upon treatment with acid. Neutralization with base recovers the yellow-colored merocyanine isomer with *trans* exocyclic alkene geometry through an unusual acid-mediated alkene isomerization. This study expands the repertoire of mechanochromic mechanophores based on (hetero)annulated benzopyrans to enable multicolor chromomorphic behavior in response to both mechanical force and acid for applications in stimuli-responsive polymeric materials with complex switching properties.

2.1 Introduction

Responsive materials that undergo chemical or physical changes with external stimuli such as light, mechanical force, or changes in pH enable innovative applications in areas such as sensing,[1–3] bioimaging,[4,5] and molecular delivery.[6–8] Materials that produce a multi-staged response to discrete stimuli are particularly appealing, facilitating the storage of complex information and logic gate functions.[9–11] In the nascent field of polymer mechanochemistry, mechanical force is transduced via polymer chains to induce specific chemical transformations in stress-sensitive molecules termed mechanophores.[12–14] Mechanochromic mechanophores that produce changes in color upon mechanical activation have been widely developed as molecular force probes to enable the straightforward visualization of critical stress and/or strain in polymeric materials.[15] The expanding catalog of mechanochromic mechanophores includes naphthopyran,[16–23]

spiropyran,[24–26] spirothiopyran,[27] rhodamine,[28–30] oxazine,[31,32] π-extended anthracene adducts,[33,34] triarylmethanes,[35] and diarylbibenzofuranone,[36,37] among many others. While most mechanochromic mechanophores exhibit a binary response to force, those that are capable of generating multiple products or states with distinct colors remain limited.[17,21,38,39] On the other hand, combining mechanical force with a secondary stimulus represents an alternative strategy for achieving responsive materials with multicolor functionality. Acid, for example, has been extensively used as a simple yet powerful external stimulus to regulate chemical processes, inspiring the design of pH-responsive materials.[40] Thus, we envisioned that a mechanochromic mechanophore that also responds to changes in pH would engender a multi-staged color response to discrete stimuli and potentially enable more complex switching properties and applications.

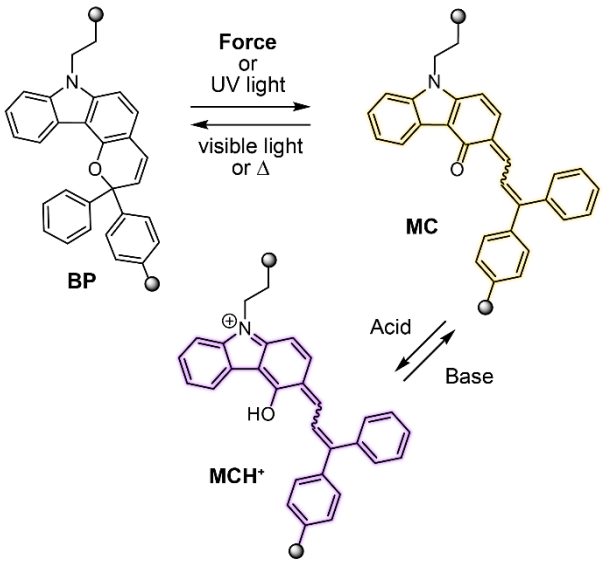

Scheme 2.1 Reactivity of an indole-fused 2*H*-1-benzopyran (**BP**) molecular switch generating a yellow-colored merocyanine dye (**MC**), which is further transformed to a purple-colored dye (**MCH**$^+$) upon treatment with acid. Subsequent neutralization with base regenerates yellow-colored **MC**. Further investigation indicates that the recovered **MC** is the isomer with *trans* exocyclic alkene geometry.

The 2*H*-1-benzopyran (chromene) scaffold has been widely developed as a class of molecular switches that undergo a 6π electrocyclic ring-opening reaction upon external stimulation to generate colored merocyanine dyes.[41] Although simple derivatives of benzopyran exhibit only weak photochromism under ambient conditions due to the

instability of the dearomatized merocyanine product,[41,42] judicious substitution, as in the case of benzo-annulation (i.e., naphthopyrans), engenders both strong photochromic and mechanochromic behavior.[43] However, in contrast to naphthopyran,[43] the mechanochemistry of 2*H*-1-benzopyran has not been investigated to date. Likewise, studies of the photochemistry of benzopyran remain relatively limited. Substitution of benzopyran with electron-donating groups including heteroannulation with furan and indole has been effectively employed to stabilize the photochemically generated merocyanine products.[42,44–46] We hypothesized that similarly substituted benzopyrans would also be mechanochemically active, enabling the ring-opening reaction to proceed under mechanical force. Moreover, the presence of a basic nitrogen atom, as in the case of the indole-annulated benzopyrans, may also serve to enable additional pH-responsive behavior to further modulate the accessible color states.

Herein, we report an indole-fused 2*H*-1-benzopyran mechanophore that undergoes a ring-opening reaction under force to generate a yellow-colored merocyanine dye, which is further reversibly transformed to a purple-colored dye upon the introduction of acid (Scheme 2.1). Neutralization with base recovers a thermally stable yellow-colored merocyanine dye with *trans* exocyclic alkene geometry. We demonstrate the multicolor chromogenic behavior of the indole-fused benzopyran mechanophore using solution-phase ultrasonication experiments in combination with acid and base treatment, and extend the reactivity to polydimethylsiloxane elastomers to achieve multi-staged, multicolor patterning. This study expands the toolbox of mechanochromic mechanophores to include

the understudied benzopyran scaffold and leverages distinct stimuli-responsive manifolds to enable polymeric materials with complex multicolor switching properties.

2.2 Results and Discussion

properties. We first investigated the mechanochemical reactivity of the indole-fused 2*H*-1-benzopyran scaffold *in silico* by performing density functional theory (DFT) calculations on a truncated model using the constrained geometries simulate external force (CoGEF) method.[47,48] We identified a benzopyran skeleton with indole fusion at the 7,8-positions and the N-atom bound to C(7), as illustrated in Scheme 1. A similar benzopyran compound was reported by Oliveira *et al.* to be photochemically active, producing a merocyanine dye with absorption maxima at 431 and 557 nm as well as relatively slow thermal reversion.[44] We evaluated a model of this benzopyran containing truncated polymer attachment positions at the N-atom of the carbazole fragment and at one of the phenyl groups on the pyran ring (Figure 2.1 and Figure S2.1). Upon mechanical elongation using the CoGEF protocol (B3LYP/6-31G*), a ring-opening reaction of the pyran occurs with a rupture force (F_{max}) of 4.9 nN. While the absolute forces calculated by CoGEF are

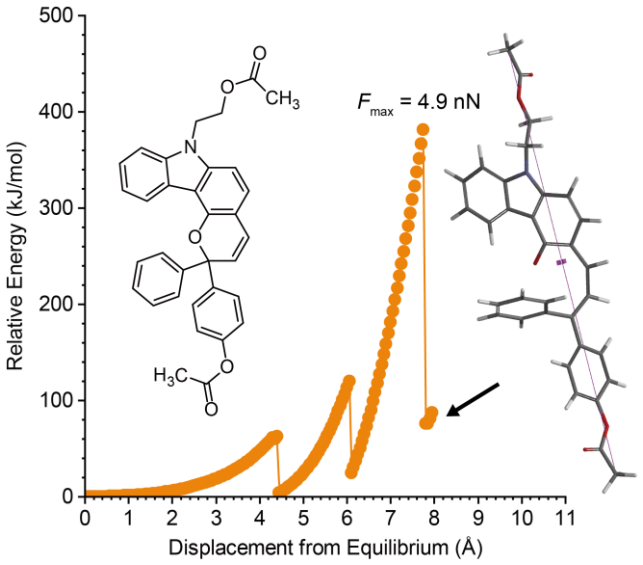

Figure 2.1 Density functional theory (DFT) calculations using the constrained geometries simulate external force (CoGEF) method performed on an indole-fused 2*H*-1-benzopyran model predicts merocyanine formation upon mechanical elongation. Structures of the benzopyran model and the predicted merocyanine product are shown. The features at ~4.4 and ~6.0 Å displacement correspond to conformational changes. Calculations were performed at the B3LYP/6-31G* level of theory. The carbon atoms of the terminal methyl groups define the distance constraint.

typically overestimated relative to experiments, they nevertheless provide a useful characterization of the relative reactivity of mechanophores.[48] The value of F_{max} predicted for the indole-fused benzopyran is comparable to F_{max} values predicted for other naphthopyran mechanophores, suggesting that the mechanochemical ring-opening reaction should be accessible experimentally.[16,18–20,22]

We next set out to synthesize the target indole-fused benzopyran compound and incorporate it into polymers to experimentally investigate the stimuli-responsive properties. Ultrasonication is routinely employed to mechanically activate polymers in dilute solution whereby cavitation-induced elongational force is maximized near the chain midpoint and is non-existent at the chain ends.[49] Thus, we sought to prepare poly(methyl acrylate) **P1** and control polymer **P2** containing the indole-fused 2*H*-1-benzopyran motif near the chain center and at the chain end, respectively (Scheme 2.2). Starting from 4-hydroxycarbazole **1**, an *N*-alkylation reaction with protected 2-iodoethanol followed by removal of the

Scheme 2.2 Synthesis of poly(methyl acrylate) polymers incorporating an indole-fused 2*H*-benzopyran unit.

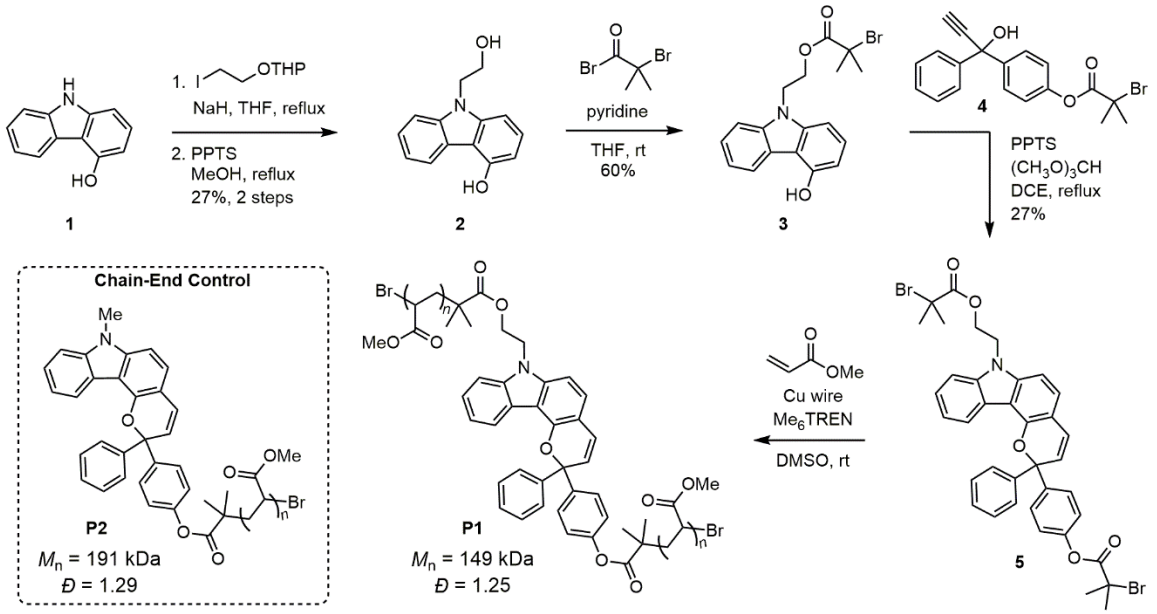

tetrahydropyran (THP) protecting group using pyridinium *p*-toluenesulfonate (PPTS) in methanol afforded carbazole diol **2**. Selective esterification of the alcohol using bromoisobutyryl bromide furnished monoester **3**. Next, reaction with propargyl alcohol **4** in the presence of PPTS and trimethyl orthoformate following Carreira's procedure[50] furnished benzopyran bis-initiator **5**, which was subsequently employed in the controlled radical polymerization of methyl acrylate using Cu wire and Me_6TREN in DMSO[51] to afford **P1** (M_n = 149 kDa; $Đ$ = 1.25) incorporating the benzopyran unit near the chain center. Control polymer **P2** (M_n = 191 kDa; $Đ$ = 1.29) incorporating the benzopyran unit at the chain end was prepared in a similar fashion from the benzopyran initiator containing an *N*-Me group.

The reactivity of the indole-fused benzopyran was initially investigated by subjecting a dilute solution of **P1** (2 mg/mL in CH_3CN with 30 mM BHT, −15 °C) to continuous ultrasonication (8.4 ± 0.4 W/cm^2) and aliquots were removed and analyzed by UV-vis absorption spectroscopy (Figure 2.2). A new visible absorption peak at 423 nm was generated upon ultrasound-induced mechanochemical activation of **P1** corresponding to the formation of merocyanine product **MC** (see Scheme 2.1 and Figure S2.2). In direct contrast, the control polymer **P2** containing the benzopyran unit at the chain end produced minimal changes upon ultrasonication, indicating that the ring-opening reaction of benzopyran is mechanochemical in nature. The slight increase in absorbance at shorter wavelengths in this case is characteristic of background reactions typically observed with sonication. We next set out to investigate the acidochromism of **MC** by treating the sonicated **P1** solution with hydrochloric acid in dioxane to provide a final concentration of

15 mM HCl (Figure S2.3). A substantial change was observed in the visible absorption spectrum with a new peak appearing at 558 nm putatively corresponding to the formation of **MCH**$^+$ as illustrated in Scheme 1 (Figure 2.2b). DFT calculations suggest that protonation of **MC** results in a smaller HOMO-LUMO energy gap with extended electron density on the aryl rings, consistent with the bathochromically shifted absorption peak (Figure S2.4). Addition of triethylamine to the sonicated, acidified solution of **P1** caused the solution immediately to become yellow, reflecting the putative regeneration of **MC**. However, compared to the merocyanine dye generated directly by the mechanochemical activation of **P1**, the recovered product was more

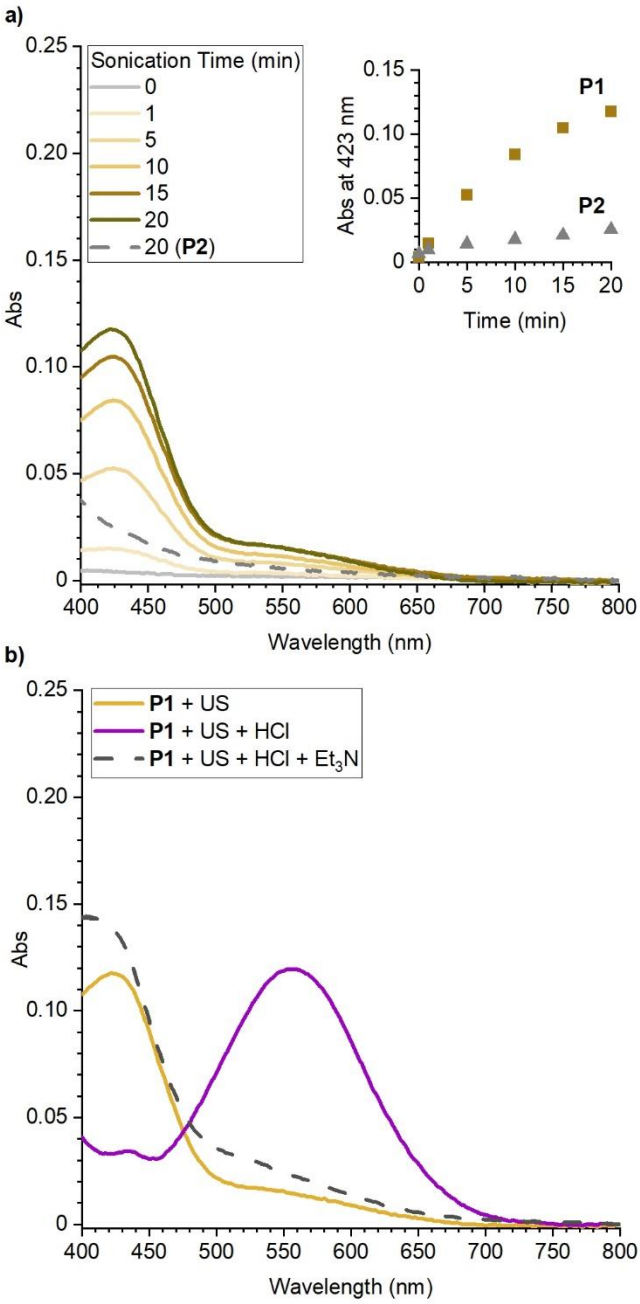

Figure 2.2 (a) UV-vis absorption spectra of **P1** and **P2** in CH_3CN (2 mg/mL with 30 mM BHT) during continuous ultrasonication at −15 °C for 20 min. Inset shows the changes in absorbance at characteristic wavelength of 423 nm (**MC**) for **P1** and **P2**. (b) The subsequent treatment of mechanically activated **P1** with HCl (15 mM) generates the protonated merocyanine product **MCH**$^+$ with an absorption maximum at 558 nm. Subsequent neutralization with triethylamine (30 mM) immediately converts the solution into its yellow form, indicating the putative regeneration of **MC**.

thermally persistent and exhibited a slightly different absorption spectrum (Figure S2.5). We note that irreversible loss of color is observed from **MCH**$^+$ over time in the absence of added base, suggesting an acid-mediated decomposition pathway (see Figure S2.3). In direct contrast to the responses of **P1**, negligible changes in absorption were observed for chain-end functional control polymer **P2** under the same conditions, suggesting that the acidochromic behavior observed post-sonication originates exclusively from protonation of the mechanically generated merocyanine dye (Figure S2.6).

To further characterize the reaction that occurs upon treating the sonicated and acidified solution of **P1** with triethylamine, we leveraged photochemical experiments that afforded a cleaner reactivity profile compared to sonication. A solution of **P1** was photoirradiated with UV light (311 nm) for 2 min and then subsequently treated with HCl followed by triethylamine. The absorption spectrum of the photoirradiated, acidified solution of **P1** closely matches the spectrum obtained after ultrasonication of **P1** followed by treatment

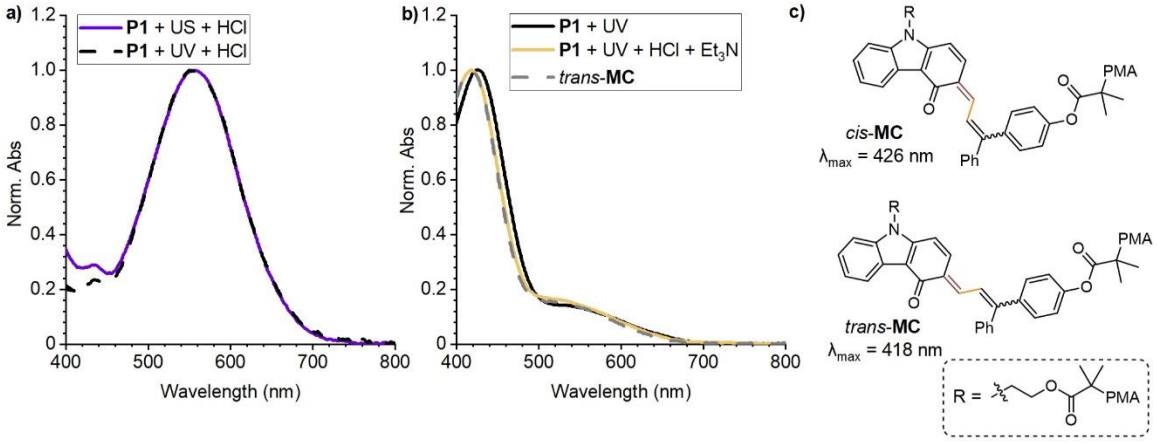

Figure 2.3 (a) Photoirradiation of **P1** with UV light (311 nm, 2 min) followed by treatment with HCl (15 mM) generates an absorption peak at 558 nm, closely matching the spectrum obtained after ultrasonication of **P1** with the same acid treatment. (b) Treatment of a photoirradiated solution of **P1** successively with HCl (15 mM) and triethylamine (30 mM) results in an 8 nm hypsochromic shift in absorption, matching the spectrum of the photochemically generated *trans*-merocyanine dye (*trans*-**MC**). (c) Structures of merocyanine isomers with *cis* and *trans* exocyclic alkene geometry.

with HCl, suggesting that the same protonated merocyanine dye (**MCH**$^+$) is generated in both cases (Figure 2.3a). Treating the solution of **MCH**$^+$ with triethylamine caused the purple solution to immediately become yellow as expected, reflecting the putative regeneration of neutral **MC** (Figure S2.7). Interestingly, the absorption peak of the chemically regenerated dye product is hypsochromically shifted by approximately 8 nm relative to the photoirradiated solution of **P1** that was not subsequently exposed to acid and base (Figure 2.3b). By comparison, naphthopyrans generate a mixture of merocyanine isomers with *cis* and *trans* exocyclic alkene geometry upon extended photoirradiation, which usually exhibit slight differences in absorption varying by ~10 nm.[43] While *cis* merocyanine isomers typically revert to the colorless naphthopyran rapidly at ambient temperatures, the *trans* isomers are more thermally persistent. To probe the idea that acid-base treatment of the merocyanine was leading to *cis*-to-*trans* isomerization of the exocyclic alkene, a solution of **P1** was photoirradiated with UV light (311 nm) for 30 min and then allowed to equilibrate in the dark for 30 min to accumulate the thermally persistent *trans*-merocyanine product (Scheme S2.1 and Figure S2.8).[52,53] Indeed, the absorption spectrum of this *trans*-merocyanine product is identical to the spectrum obtained upon neutralization of **MCH**$^+$ (Figure 2.3b). In addition, the slow color-fading and reversion to the colorless ring-closed state upon irradiation with white light indicates that the merocyanine isomer with *trans* exocyclic alkene geometry is formed during the acidification and neutralization process (Figure S2.9). On the other hand, adding HCl and triethylamine to a solution of **P1** without UV photoirradiation does not trigger the ring-opening reaction, and subsequent photochemical activation of this solution of **P1** generates

a merocyanine product with similar absorption and reversion properties as that obtained in the absence of acid-base treatment. These results suggest that generation of **MCH**$^+$ is a critical step for alkene isomerization (Figure S2.10 and Scheme S2.2).[54]

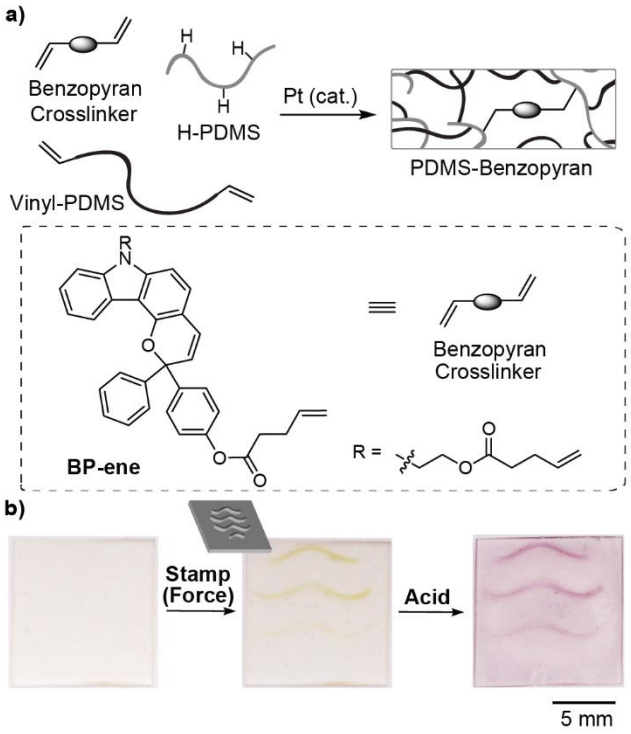

Figure 2.4 (a) Polydimethylsiloxane (PDMS) elastomers crosslinked with mechanophore **BP-ene** (1.3 wt%) prepared via Pt-catalyzed hydrosilylation. (b) Photographs of a PDMS film before and after mechanical force was applied via compression using an embossed stamp, and subsequent treatment with HCl. A schematic representation of the stamp is shown.

Encouraged by the results of the solution-phase experiments, we sought to investigate the stimuli-responsive properties of the indole-fused benzopyran mechanophore in bulk polymeric materials and demonstrate its potential for chromomorphic patterning. Crosslinker **BP-ene** containing two terminal vinyl groups was prepared and covalently incorporated into elastomeric polydimethylsiloxane (PDMS) polymer networks (1.3 wt% loading) via Pt-catalyzed hydrosilylation (Figure 2.4a). Mechanical activation of the PDMS films via compression using an embossed stamp produced yellow coloration in the regions where force was applied, corresponding to the mechanochemical generation of merocyanine dye **MC** (Figure 2.4b). Immersion of the mechanically activated PDMS film in a dilute solution of hydrochloric acid (15 mM in DCM) converted the yellow-colored pattern into a purple-colored pattern, reflecting the conversion of neutral merocyanine **MC** to the protonated

merocyanine, **MCH**$^+$ (Figure 2.4b). The purple-colored pattern faded completely after ~10 min at ambient temperature. The multicolor chromomorphic behavior of this mechanophore in response to both force and acid enables the fabrication of stimuli-responsive polymeric materials with complex switching properties.

2.3 Conclusions

In contrast to naphthopyran molecular switches that exhibit pronounced photochromic and mechanochromic behavior, 2*H*-1-benzopyrans (chromenes) have received relatively little attention because they typically only exhibit weak stimuli-responsive behavior at room temperature. In limited examples, however, hetero-annulation has been demonstrated to be an effective strategy for achieving photochromism of benzopyrans. Inspired by these reports, herein we design and investigate an indole-annulated 2*H*-1-benzopyran mechanophore that not only undergoes a ring-opening reaction under mechanical force, but the mechanically generated merocyanine dye also exhibits acidochromic behavior transforming from yellow to purple upon protonation with acid. Neutralization with base recovers the yellow-colored merocyanine isomer with *trans* exocyclic alkene geometry through an acid-mediated mechanism. The reactivity of this indole-fused benzopyran mechanophore is characterized in polymers using both solution-phase ultrasonication methods and in solid elastomeric silicone materials where the multi-staged stimuli-responsive properties are leveraged to realize chromomorphic patterns created by mechanical compression and transformed in color upon acid treatment. This study expands the existing repertoire of mechanochromic mechanophores to include the understudied benzopyran scaffold and enables the design of stimuli-responsive polymeric materials with complex switching properties.

2.4 Supplementary Figures

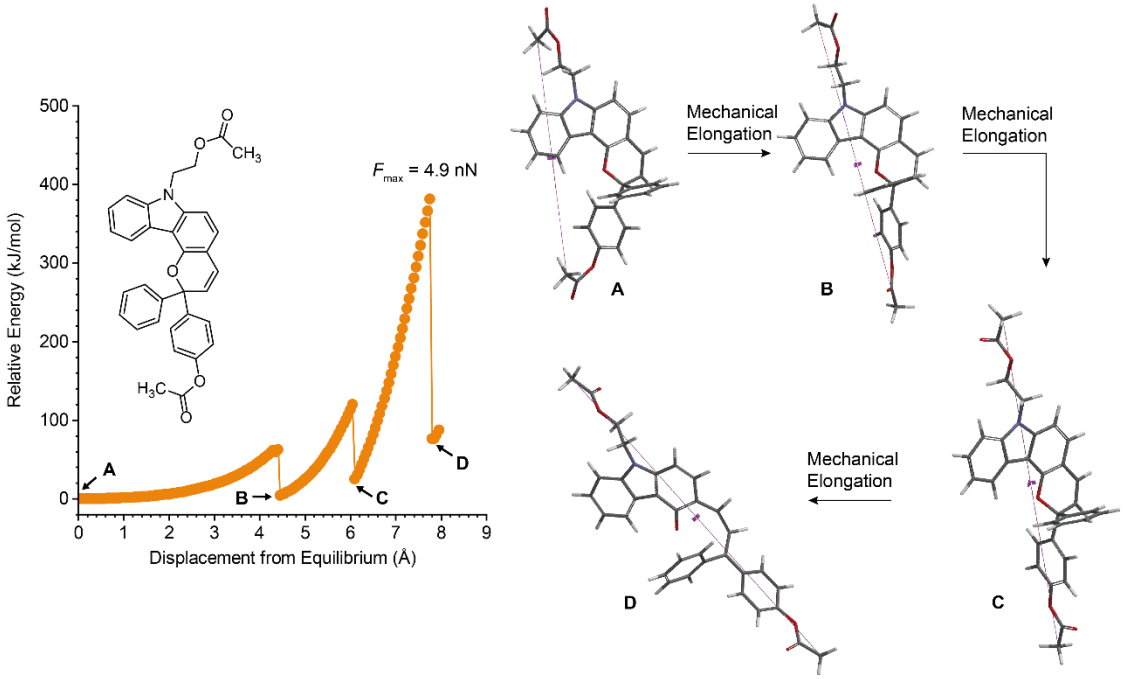

Figure S2.1 Density functional theory (DFT) calculations using the constrained geometries simulate external force (CoGEF) method performed on an indole-fused benzopyran models predict a ring-opening reaction upon mechanical elongation. The structures at various points in the CoGEF profile are shown at right, corresponding to the positions labeled A–D. Calculations were performed at the B3LYP/6-31G* level of theory. The carbon atoms of the terminal methyl groups were used to define the distance constraint. The features at ~4.4 and ~6.0 Å displacement associated with the formation of structures B and C, respectively, correspond to minor conformational changes.

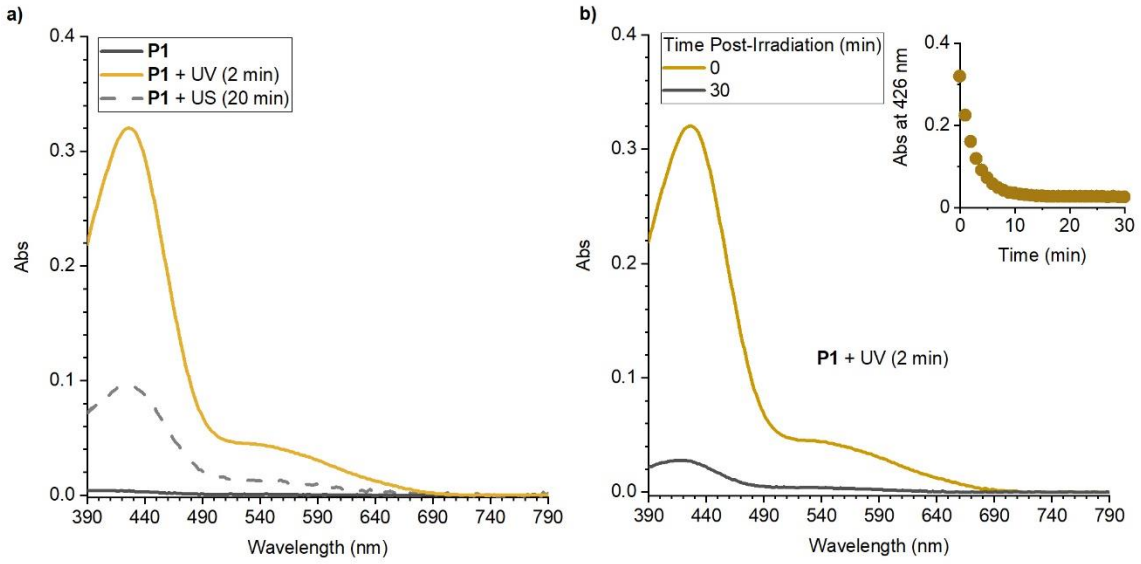

Figure S2.2 (a) UV-vis absorption spectra of **P1** (2 mg/mL in CH_3CN with 30 mM BHT) before and after photoirradiation with 311 nm UV light at room temperature for 2 min, compared to after continuous ultrasonication at −15 °C for 20 min. (b) Upon cessation of photoirradiation (20 ºC), **MC** reverts to the ring-closed benzopyran rapidly in the dark. Inset shows the fading profile of **MC** monitored at 426 nm upon cessation of photoirradiation.

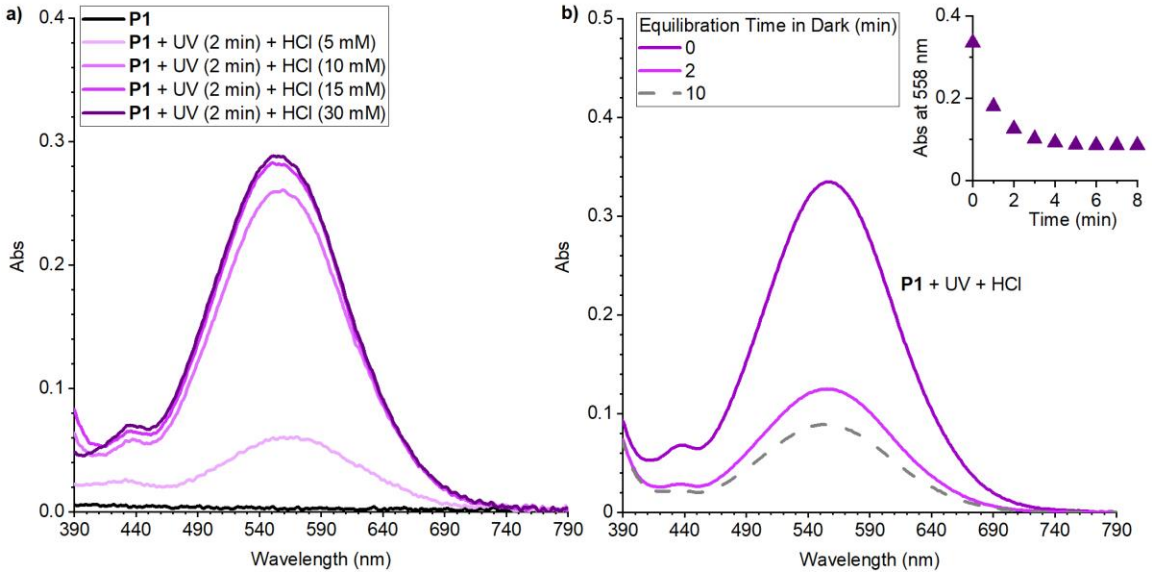

Figure S2.3 (a) UV-vis absorption spectra of **P1** (2 mg/mL in CH_3CN with 30 mM BHT) before and after photoirradiation with 311 nm UV light for 2 min and subsequent treatment with hydrochloric acid to produce a solution with the indicated concentration, resulting in a new absorption peak at 558 nm. (b) UV-Vis absorption behavior of **P1** following photoirradiation with 311 nm UV light for 2 min and subsequent treatment with HCL (15 mM) during subsequent equilibration in the dark (20 ºC). Attenuation of the visible absorption peak at 558 nm is observed without added base, suggesting an acid-mediated decomposition pathway.

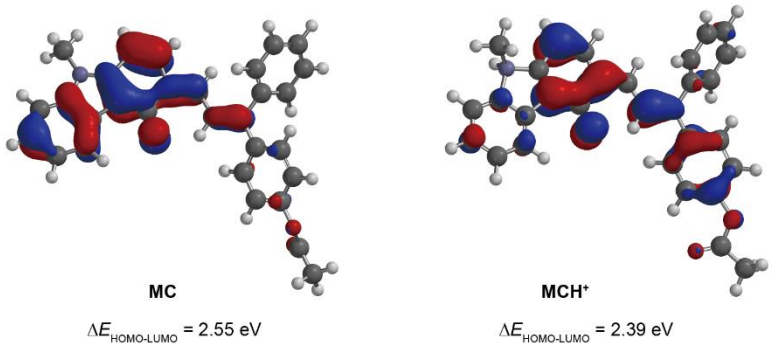

Figure S2.4 HOMO diagrams for **MC** and **MCH**$^+$. Protonation of **MC** results in a smaller HOMO-LUMO energy gap and greater electron delocalization, consistent with the bathochromically shifted absorption peak observed experimentally. Geometries are optimized at the B3LYP/6-31G* level of theory using Spartan.

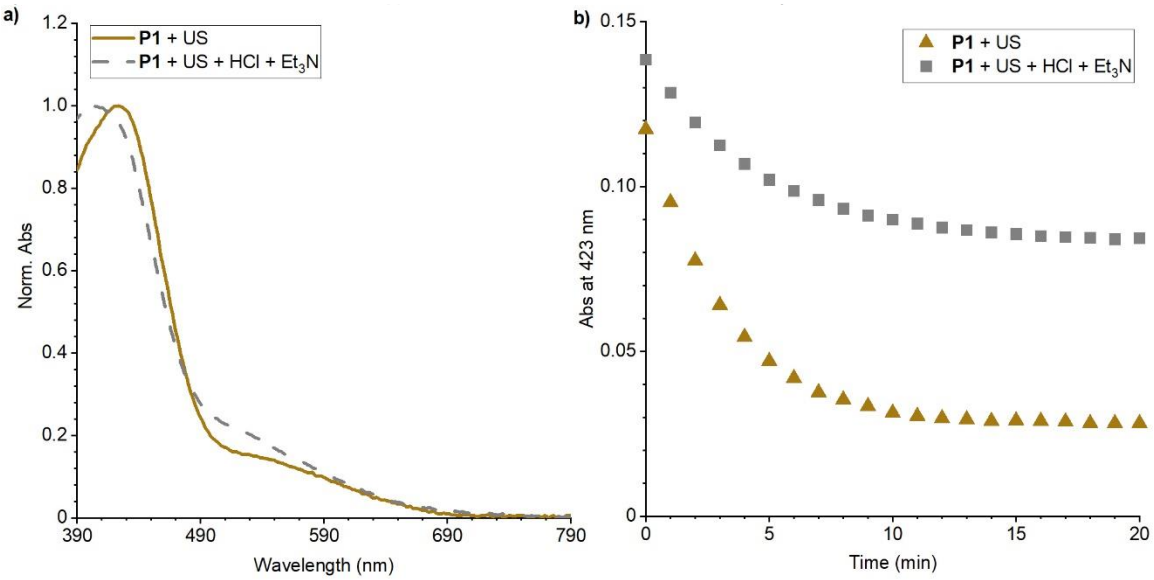

Figure S2.5 (a) UV-vis absorption spectra of a sonicated solution of **P1** in CH_3CN (2 mg/mL with 30 mM BHT, continuous ultrasonication at −15 °C for 20 min) before and after treatment with HCl (15 mM) and Et_3N (30 mM). (b) Fading profiles of mechanically generated **MC** and regenerated **MC** by treating **MCH**$^+$ with Et_3N (30 mM) as described in Figure 2. Changes in absorbance are monitored at 423 nm at room temperature in the dark.

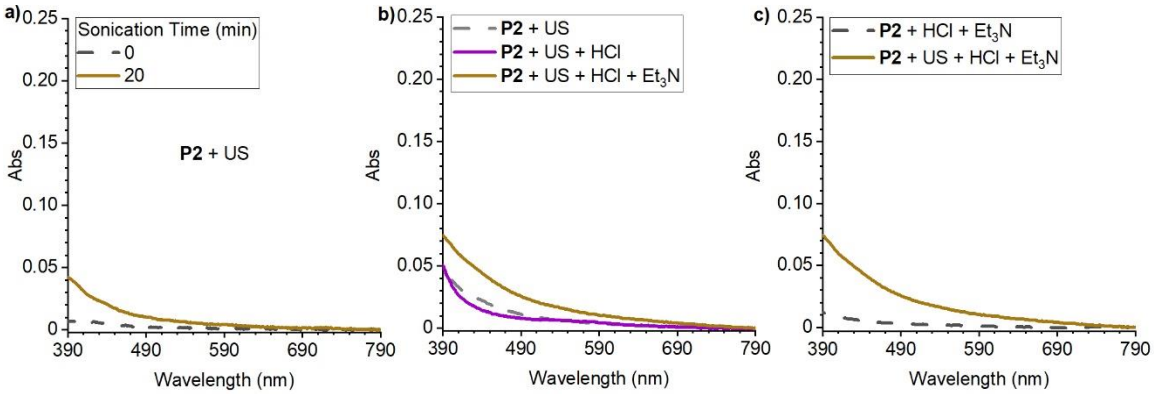

Figure S2.6 (a) UV-vis absorption spectra of chain-end control polymer **P2** in CH_3CN (2 mg/mL with 30 mM BHT) before and after continuous ultrasonication at −15 °C for 20 min. (b) UV-vis absorption spectra of sonicated **P2** in CH_3CN (2 mg/mL with 30 mM BHT) before and after successive treatment with HCl (15 mM) and Et_3N (30 mM), indicating that the acidochromic behavior originates exclusively from the mechanically activated benzopyran. (c) UV-vis absorption spectra obtained after treating a similar solution of **P2** with HCl (15 mM) and Et_3N (30 mM) successively, with and without first being subjected to ultrasonication.

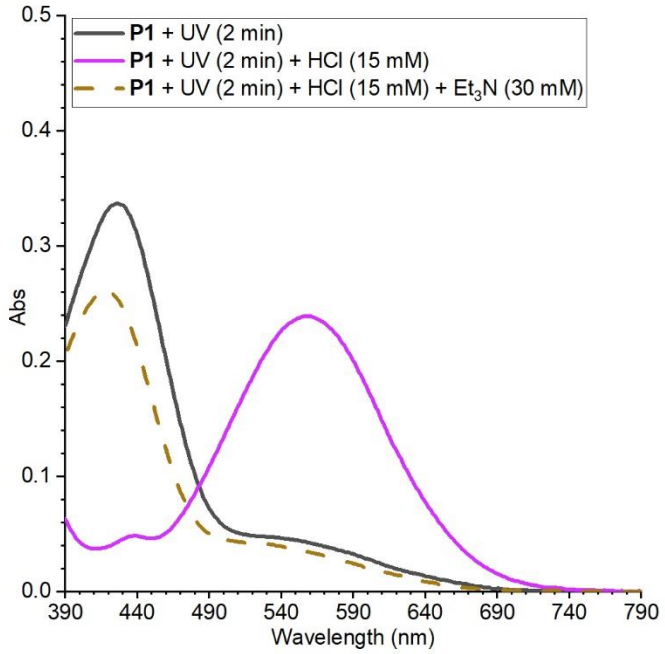

Figure S2.7 UV-vis absorption spectra of **P1** (2 mg/mL in CH_3CN with 30 mM BHT) after irradiation with 311 nm UV light for 2 min and successive treatment with HCl (15 mM) and triethylamine (30 mM). The absorption peak of the regenerated **MC** upon treatment with triethylamine is hypsochromically shifted by 8 nm compared to the photogenerated **MC**, similar to results from sonication experiments.

Scheme S2.1 Photochemical ring-opening reaction and alkene isomerization reaction to generate *cis*- and *trans*-merocyanine products.

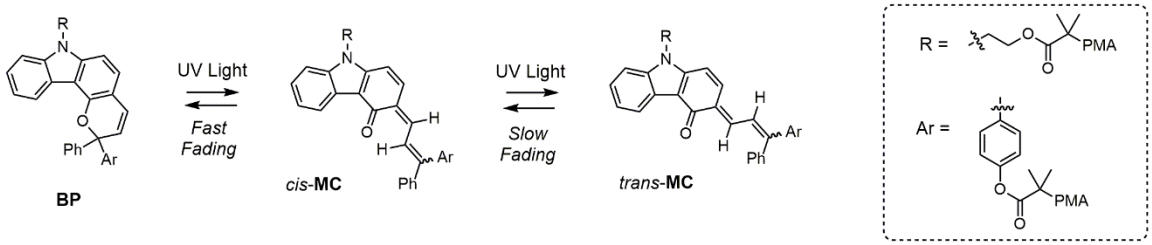

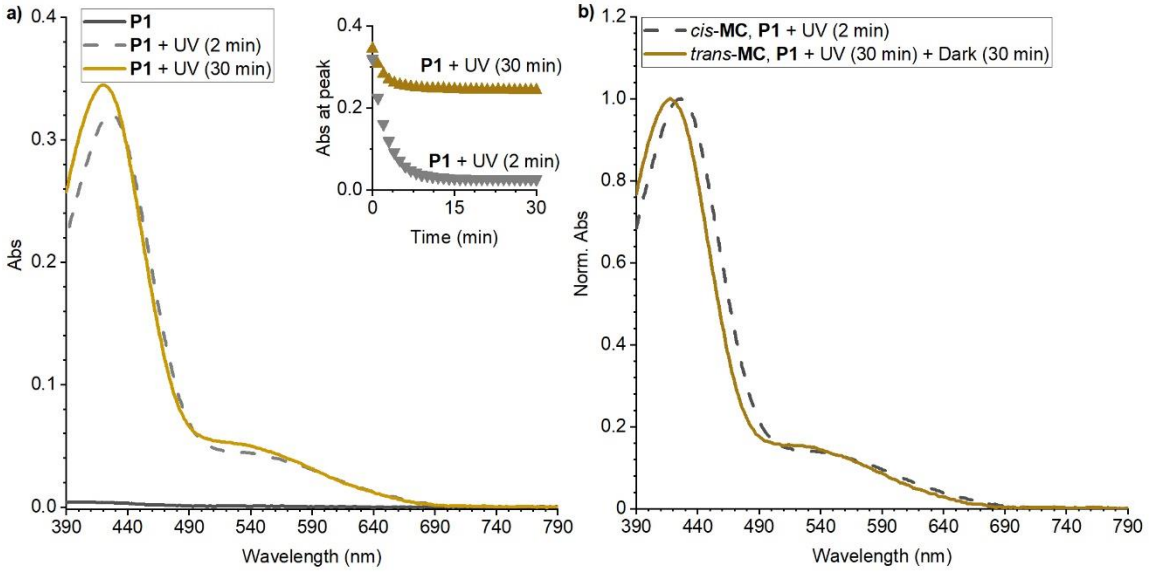

Figure S2.8 (a) UV-vis absorption spectra of **P1** (2 mg/mL in CH_3CN with 30 mM BHT) before and after photoirradiation with 311 nm UV light (2 min or 30 min) to generate a mixture of *cis*- and *trans*-**MC**. Extended photoirradiation favors the formation of *trans*-**MC**. The inset shows comparison of fading profiles monitored at λ_{max}. The more thermally persistent species is attributed to *trans*-**MC**. (b) Normalized spectra of *cis*- and *trans*-**MC** generated upon photoirradiation of **P1** with 311 nm UV light. The absorption peak of **MC** with *trans* exocyclic alkene geometry is hypsochromically shifted to 418 nm.

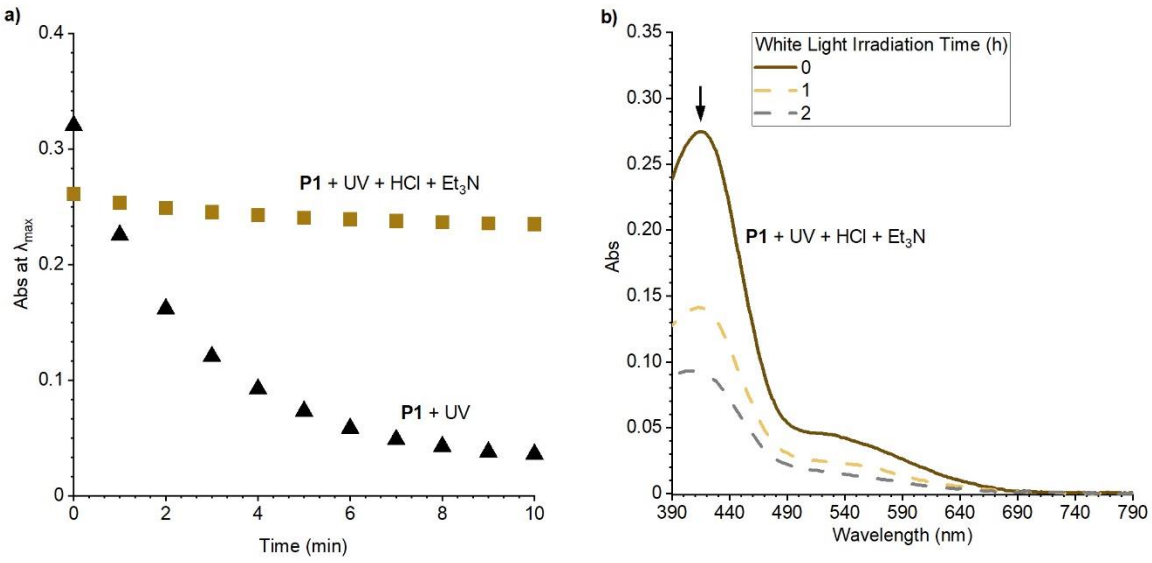

Figure S2.9 (a) Fading profiles of photogenerated **MC** (311 nm, 2 min) before and after treatment with HCl (15 mM) and Et_3N (30 mM) as illustrated in Figure S6. Changes in absorbance are monitored at λ_{max} at room temperature in the dark. (b) Photoirradiation of the solution of **P1** previously subjected to UV light/HCl/Et_3N using white light for the indicated time results in attenuation of the visible absorbance at 418 nm.

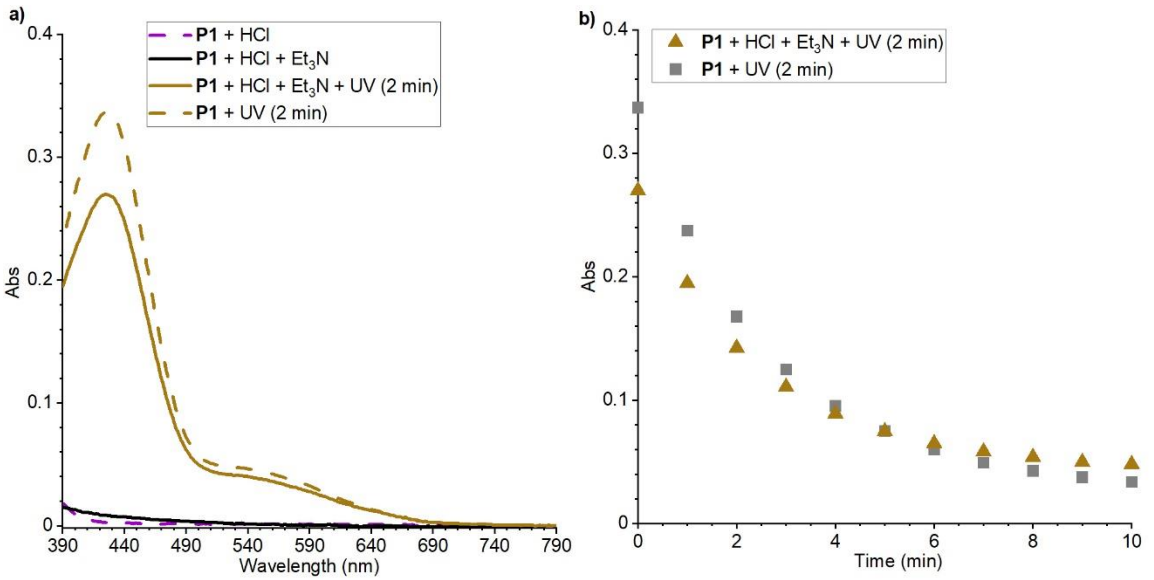

Figure S2.10 Control experiments illustrating that treatment of **P1** in CH_3CN (2 mg/mL with 30 mM BHT) with hydrochloric acid (15 mM) followed by triethylamine (30 mM) generates minimal changes in visible absorption. Photoirradiation (311 nm, 2 min) of this same solution produces a merocyanine product with similar absorption and reversion properties as that produced without prior acid-base treatment.

Scheme S2.2 Proposed mechanism of acid-mediated alkene isomerization.

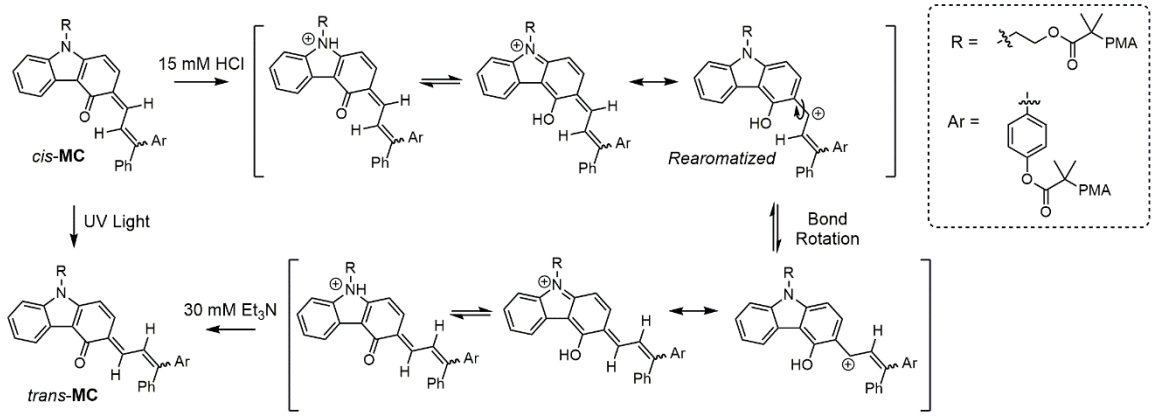

2.5 Experimental Section

2.5.1 General Experimental Details

Reagents from commercial sources were used without further purification unless otherwise stated. Methyl acrylate was passed through a short plug of basic alumina to remove inhibitor immediately prior to use. Copper wire was soaked in 1 M HCl for 30 min and then rinsed consecutively with water and acetone immediately prior to use. Dry solvents were obtained from a Pure Process Technology solvent purification system. All reactions were performed under a N_2 atmosphere unless specified otherwise. Column chromatography was performed on a Biotage Isolera system using SiliCycle SiliaSep HP flash cartridges.

NMR spectra were recorded using a 400 MHz Bruker Avance III HD with Prodigy Cryoprobe or a 600 MHz Varian spectrometer with 5 mm triple resonance inverse probe. All ^{1}H NMR spectra are reported in δ units, parts per million (ppm), and were measured relative to the signals for residual chloroform (7.26 ppm), acetone (2.05 ppm), dichloromethane (5.32 ppm), or dimethyl sulfoxide (2.50 ppm) in deuterated solvent. All ^{13}C NMR spectra were measured in deuterated solvents and are reported in ppm relative to the signals for chloroform (77.16 ppm), acetone (206.26 ppm), dichloromethane (53.84 ppm), or dimethyl sulfoxide (39.52 ppm).

High resolution mass spectra (HRMS) were obtained via direct injection on an Agilent 1260 Infinity II Series HPLC coupled to a 6230 LC/TOF system in electrospray ionization (ESI+) mode.

Analytical gel permeation chromatography (GPC) was performed using an Agilent 1260 series pump equipped with two Agilent PLgel MIXED-B columns (7.5 x 300 mm), an

Agilent 1200 series diode array detector, a Wyatt 18-angle DAWN HELEOS light scattering detector, and a Optilab rEX differential refractive index detector. The mobile phase was THF at a flow rate of 1 mL/min. Molecular weights and molecular weight distributions were calculated by light scattering using a dn/dc value of 0.062 mL/g (25 °C) for poly(methyl acrylate).

UV-vis absorption spectra were recorded on a Thermo Scientific Evolution 220 spectrometer.

Ultrasound experiments were performed using a Vibra Cell 505 liquid processor equipped with a 0.5-inch diameter solid probe (part #630-0217), sonochemical adapter (part #830-00014), and a Suslick reaction vessel made by the Caltech glass shop (analogous to vessel #830-00014 from Sonics and Materials). A Thermo Scientific EK45 Immersion Cooler (part #3281452) was used to maintain a constant temperature bath for sonication experiments. Photoirradiation with UV light was performed using a Philips PL-S 9W/01/2P UVB bulb with a narrow emission of 305–315 nm and a peak at 311 nm under ambient conditions unless indicated otherwise. Irradiation with white light was carried out using a 13 W broadband fluorescent lamp (Bayco Model BA-506) filtered through a 425 nm bandpass filter.

Compounds **4**, **8**, 2-tetrahydropyranyloxy-1-iodoethane, and *N*-methyl-4-hydroxycarbazole were synthesized following the procedures reported in the literature.[19,55,56]

2.5.2 Synthesis and Characterization of Initiators and Polymers

Scheme S2.3 Synthesis of compounds used in the study not included in Scheme S2.2.

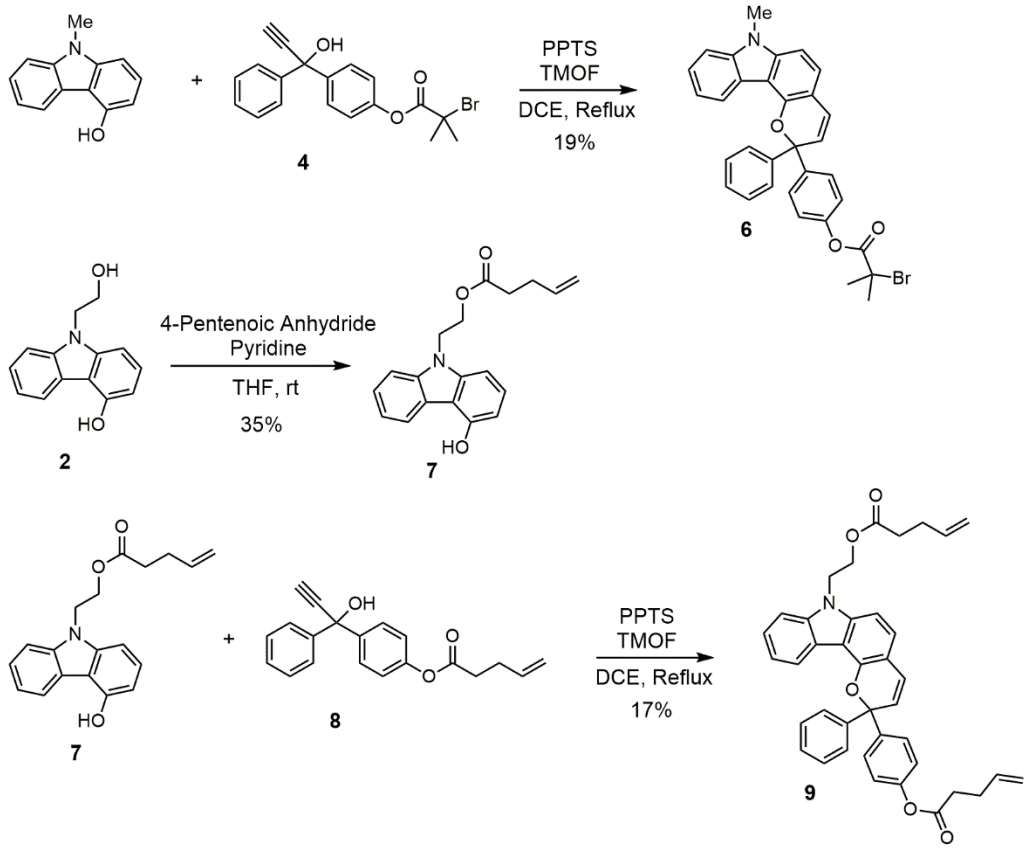

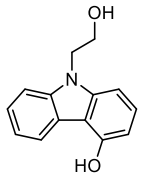

2

9-(2-hydroxyethyl)-9H-carbazol-4-ol (2). A flame-dried round-bottom flask equipped with a stir bar was charged with **1** (570 mg, 3.11 mmol). The flask was evacuated and backfilled with N_2 three times. Dry THF (10 mL) was added via syringe, followed by the addition of dry DMF (0.30 mL, 3.9 mmol) under N_2. The flask was subsequently cooled in an ice bath, a suspension of NaH (300 mg, 12.5 mmol) in 5 mL dry THF was added slowly via syringe, and the mixture was warmed to room temperature. After stirring for 10 min, 2-tetrahydropyranyloxy-1-iodoethane[55] (790 mg, 3.10 mmol) dissolved separately in 5 mL dry THF was added via syringe to the mixture. After the complete addition, the mixture was heated to reflux overnight. Upon completion, the flask was removed from heat and the reaction was subsequently cooled in an ice bath, quenched with H_2O, and diluted with ethyl acetate. HCl (1 M) was added until the pH of the aqueous phase was < 5, and the aqueous phase was extracted with ethyl acetate three times. The organic layers were combined, washed with H_2O three times, dried over Na_2SO_4, filtered, and concentrated under reduced pressure. Next, the crude mixture and pyridinium *p*-toluenesulfonate (100 mg, 0.398 mmol) were added to a round-bottom flask and the flask was evacuated and backfilled with N_2 three times. MeOH (10 mL) was added via syringe and the mixture was heated to reflux. After 12 h, the flask was cooled to room temperature and concentrated under reduced pressure. The

crude mixture was then purified by column chromatography on silica gel (0–30% ethyl acetate/hexanes) to produce the title compound as a light brown solid (192 mg, 27%).

TLC (40% EtOAc/hexanes): R_f = 0.47

^{1}H NMR (400 MHz, acetone-d_6) δ: 9.03 (s, 1H), 8.35 – 8.23 (m, 1H), 7.60 – 7.49 (m, 1H), 7.38 (ddd, *J* = 8.3, 7.1, 1.3 Hz, 1H), 7.24 (dd, *J* = 8.0 Hz, 1H), 7.17 (ddd, *J* = 8.0, 7.1, 1.0 Hz, 1H), 7.07 (dd, *J* = 8.2, 0.7 Hz, 1H), 6.67 (dd, *J* = 7.8, 0.7 Hz, 1H), 4.46 (t, *J* = 5.8 Hz, 2H), 4.09 – 4.02 (m, 1H), 4.01 – 3.93 (m, 2H).

^{13}C{^{1}H} NMR (101 MHz, acetone-d_6) δ: 154.4, 143.6, 141.0, 127.1, 125.1, 123.4, 123.2, 119.4, 112.0, 109.4, 105.2, 101.6, 61.0, 46.4.

HRMS (ESI, *m/z*): calcd for $[C_{14}H_{14}NO_2]^+$ $(M+H)^+$, 228.1019; found, 228.1027.

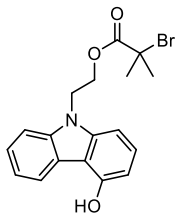

3

2-(4-hydroxy-9H-carbazol-9-yl)ethyl 2-bromo-2-methylpropanoate (3). A oven-dried vial equipped with a stir bar was charged with **2** (45 mg, 0.20 mmol) and the vial was evacuated and backfilled with N_2 three times. Dry THF (2 mL) was added via syringe, followed by the addition of pyridine (25 uL, 0.31 mmol) under N_2. The flask was subsequently cooled in an ice bath, α-bromoisobutyryl bromide (29 μL, 0.23 mmol) was added via syringe, and the mixture was warmed to room temperature. After stirring for 72 h,

the solid precipitate was filtered off and discarded. The filtrate was diluted with ethyl acetate and washed with water. The organic layer was dried over Na_2SO_4, filtered, and concentrated under reduced pressure. The crude mixture was purified by column chromatography (0–15% EtOAc/hexanes) to afford title compound as a pale yellow solid (45 mg, 60%).

TLC (25% EtOAc/hexanes): $R_f = 0.55$

^{1}H NMR (400 MHz, CD_2Cl_2) δ: 8.32 – 8.23 (m, 1H), 7.52 – 7.44 (m, 2H), 7.36 – 7.21 (m, 2H), 7.07 (d, J = 8.2 Hz, 1H), 6.62 (d, J = 7.8 Hz, 1H), 4.65 – 4.59 (m, 2H), 4.58 – 4.53 (m, 2H), 1.70 (s, 6H).

^{13}C{^{1}H} NMR (101 MHz, CD_2Cl_2) δ: 172.0, 152.5, 142.8, 140.2, 126.9, 125.4, 123.1, 122.5, 119.9, 111.5, 108.8, 105.6, 102.0, 64.1, 56.1, 42.0, 30.7.

HRMS (ESI, *m/z*): calcd for $[C_{18}H_{19}BrNO_3]^+$ $(M+H)^+$, 376.0543; found, 376.0647.

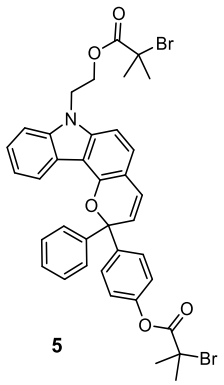

5

4-(7-(2-((2-bromo-2-methylpropanoyl)oxy)ethyl)-2-phenyl-2,7-dihydropyrano[3,2-c]carbazol-2-yl)phenyl 2-bromo-2-methylpropanoate (5). A flame-dried round-bottom flask equipped with a stir bar was charged with **3** (70 mg, 0.19 mmol), **4**[19] (83 mg, 0.22 mmol), and pyridinium *p*-toluenesulfonate (6 mg, 0.02 mmol). The flask was evacuated and

backfilled with N_2 three times. Dichloroethane (10 mL) was added via syringe, followed by the addition of trimethyl orthoformate (0.15 mL, 1.1 mmol) under N_2. After stirring at reflux for 1.5 h, the flask was removed from heat and the crude mixture was concentrated under reduced pressure, and purified by column chromatography on silica gel (0–15% ethyl acetate/hexanes) followed by a reverse-phase chromatographic separation on a C18 column (60–95% acetonitrile/H_2O) to produce the title compound as a yellow solid (23 mg, 27%).

TLC (15% EtOAc/hexanes): R_f = 0.46

^{1}H NMR (400 MHz, CD_2Cl_2) δ: 8.46 – 8.40 (m, 1H), 7.67 – 7.57 (m, 4H), 7.50 – 7.44 (m, 2H), 7.38 – 7.31 (m, 2H), 7.30 – 7.23 (m, 2H), 7.18 (d, *J* = 8.2 Hz, 1H), 7.11 – 7.04 (m, 2H), 7.00 (d, *J* = 8.2 Hz, 1H), 6.83 (d, *J* = 9.8 Hz, 1H), 6.14 (d, *J* = 9.7 Hz, 1H), 4.60 – 4.55 (m, 2H), 4.55 – 4.49 (m, 2H), 2.02 (s, 6H), 1.66 (d, *J* = 2.2 Hz, 6H).

^{13}C{^{1}H} NMR (101 MHz, Chloroform-*d*) δ: 171.8, 170.3, 150.0, 148.8, 145.3, 143.5, 142.5, 140.3, 128.4, 127.6, 127.0, 125.5, 124.9, 124.6, 124.5, 123.3, 122.3, 120.8, 120.2, 112.6, 111.8, 108.5, 101.6, 83.1, 63.6, 55.6, 55.5, 41.5, 30.7, 30.6.

HRMS (ESI, *m/z*): calcd for $[C_{37}H_{34}Br_2NO_5]^+$ $(M+H)^+$, 730.0798; found, 730.0801.

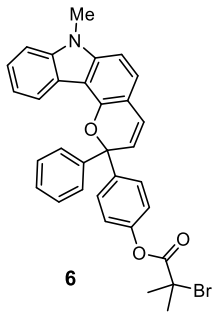

6

4-(7-methyl-2-phenyl-2,7-dihydropyrano[3,2-c]carbazol-2-yl)phenyl 2-bromo-2-methylpropanoate (6). A flame-dried round-bottom flask equipped with a stir bar was charged with *N*-methyl-4-hydroxycarbazole[56] (30 mg, 0.15 mmol), **4** (60 mg, 0.17 mmol), and pyridinium *p*-toluenesulfonate (14 mg, 0.056 mmol). The flask was evacuated and backfilled with N_2 for three times. Dichloroethane (5 mL) was added via syringe, followed by the addition of trimethyl orthoformate (0.20 mL, 1.9 mmol) under N_2. After stirring at reflux for 1 h, the flask was removed from heat and the crude mixture was concentrated under reduced pressure, and purified by column chromatography on silica gel (0–15% ethyl acetate/hexanes) followed by a reverse-phase chromatographic separation on a C18 column (60–95% acetonitrile/H_2O) to produce the title compound as a yellow solid (16 mg, 19%).

TLC (15% EtOAc/hexanes): R_f = 0.57

^{1}H NMR (400 MHz, CD_2Cl_2) δ: 8.46 – 8.38 (m, 1H), 7.69 – 7.57 (m, 4H), 7.51 – 7.43 (m, 1H), 7.41 – 7.38 (m, 1H), 7.37 – 7.31 (m, 2H), 7.29 – 7.22 (m, 2H), 7.18 (d, *J* = 8.2 Hz, 1H), 7.11 – 7.05 (m, 2H), 6.95 (d, *J* = 8.2 Hz, 1H), 6.83 (d, *J* = 9.8 Hz, 1H), 6.14 (d, *J* = 9.7 Hz, 1H), 3.79 (s, 3H), 2.02 (s, 6H).

^{13}C{^{1}H} NMR (101 MHz, CD_2Cl_2) δ: 170.6, 150.4, 148.7, 145.6, 144.0, 143.5, 141.4, 128.7, 128.5, 127.9, 127.1, 125.6, 125.1, 125.0, 124.7, 123.2, 122.0, 121.1, 119.9, 112.6, 111.6, 108.7, 102.0, 83.2, 56.1, 30.8, 29.6.

HRMS (ESI, *m/z*): calcd for $[C_{32}H_{27}BrNO_3]^+$ $(M+H)^+$, 552.1169; found, 552.1205.

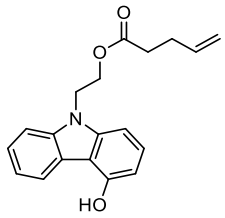

7

2-(4-hydroxy-9H-carbazol-9-yl)ethyl pent-4-enoate (7). A oven-dried vial equipped with a stir bar was charged with **2** (94 mg, 0.41 mmol) and the vial was evacuated and backfilled with N_2 three times. Dry THF (2 mL) was added via syringe, followed by the addition of pyridine (35 uL, 0.44 mmol) under N_2. The flask was subsequently cooled in an ice bath, 4-pentenoic anhydride (75 µL, 0.41 mmol) was added via syringe and the mixture was warmed to room temperature. After stirring for 72 h, the filtrate was diluted with ethyl acetate and washed with water. The organic layer was dried over Na_2SO_4, filtered, and concentrated under reduced pressure. The crude mixture was purified by column chromatography (0–20% EtOAc/hexanes) to afford title compound as a pale yellow solid (45 mg, 35%).

TLC (15% EtOAc/hexanes): R_f = 0.48

^{1}H NMR (400 MHz, acetone-d_6) δ: 9.11 (s, 1H), 8.40 – 8.23 (m, 1H), 7.61 – 7.51 (m, 1H), 7.45 – 7.36 (m, 1H), 7.29 – 7.23 (m, 1H), 7.22 – 7.16 (m, 1H), 7.08 (d, *J* = 7.9 Hz, 1H), 6.68 (d, *J* = 7.9 Hz, 1H), 5.68 (ddt, *J* = 16.6, 10.2, 6.3 Hz, 1H), 4.97 – 4.80 (m, 2H), 4.65 (t, *J* = 5.5 Hz, 2H), 4.49 (t, *J* = 5.5 Hz, 2H), 2.25 – 2.18 (m, 2H), 2.17 – 2.11 (m, 2H).

^{13}C{^{1}H} NMR (101 MHz, CD_2Cl_2) δ: 173.1, 152.5, 142.8, 140.3, 137.1, 126.9, 125.4, 123.1, 122.4, 119.8, 115.5, 111.5, 108.7, 105.4, 101.9, 62.4, 42.4, 33.6, 28.9.

HRMS (ESI, *m/z*): calcd for $[C_{19}H_{20}NO_3]^+$ $(M+H)^+$, 310.1438; found, 310.1475.

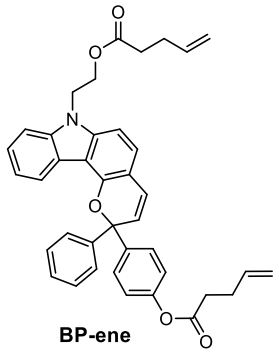

4-(7-(2-(pent-4-enoyloxy)ethyl)-2-phenyl-2,7-dihydropyrano[3,2-c]carbazol-2-yl)phenyl pent-4-enoate (BP-ene). A flame-dried round-bottom flask equipped with a stir bar was charged with **7** (49 mg, 0.16 mmol), **8**[19] (58 mg, 0.19 mmol), and pyridinium *p*-toluenesulfonate (5 mg, 0.02 mmol). The flask was evacuated and backfilled with N_2 three times. Dichloroethane (10 mL) was added via syringe, followed by the addition of trimethyl orthoformate (0.10 mL, 0.95 mmol) under N_2. After stirring at reflux for 2 h, the flask was removed from heat and the crude mixture was concentrated under reduced pressure, and purified by column chromatography on silica gel (0–25% ethyl acetate/hexanes) followed by a reverse-phase chromatographic separation on a C18 column (60–95% acetonitrile/H_2O) to produce the title compound as a yellow waxy solid (16 mg, 17%).

TLC (25% EtOAc/hexanes): R_f = 0.33

^{1}H NMR (400 MHz, acetone-d_6) δ: 8.52 – 8.41 (m, 1H), 7.70 – 7.64 (m, 4H), 7.61 – 7.57 (m, 1H), 7.51 – 7.43 (m, 1H), 7.38 – 7.32 (m, 2H), 7.30 – 7.23 (m, 2H), 7.21 (d, *J* = 8.3 Hz, 1H), 7.14 – 7.06 (m, 3H), 6.88 (d, *J* = 9.8 Hz, 1H), 6.28 (d, *J* = 9.8 Hz, 1H), 5.89 (ddt, *J* = 16.8, 10.3, 6.5 Hz, 1H), 5.66 (ddt, *J* = 16.6, 10.2, 6.3 Hz, 1H), 5.15 – 5.06 (m, 1H), 5.03 – 4.96 (m,

1H), 4.92 – 4.79 (m, 2H), 4.63 (t, *J* = 5.4 Hz, 2H), 4.48 (t, *J* = 5.4 Hz, 2H), 2.64 (t, *J* = 7.3 Hz, 2H), 2.46 – 2.38 (m, 2H), 2.24 – 2.19 (m, 2H), 2.16 – 2.10 (m, 2H).

$^{13}C\{^{1}H\}$ NMR (101 MHz, Chloroform-*d*) δ: 173.0, 171.6, 150.0, 148.8, 145.4, 143.2, 142.6, 140.4, 136.5, 136.4, 128.3, 128.2, 127.6, 127.0, 125.4, 124.9, 124.5, 124.3, 123.3, 122.3, 121.3, 120.0, 116.1, 115.7, 112.4, 111.7, 108.3, 101.4, 83.2, 62.1, 41.9, 33.7, 33.4, 29.0, 28.7.

HRMS (ESI, *m/z*): calcd for $[C_{39}H_{36}NO_5]^+$ $(M+H)^+$, 598.2588; found, 598.2677.

General Procedure for the Synthesis of Poly(Methyl Acrylate) (PMA) Polymers Incorporating a Benzopyran Unit. Polymers were synthesized by controlled radical polymerization following the procedure by Nguyen *et al*.[57] A flame-dried Schlenk flask equipped with a stir bar was charged with freshly cut 20 G copper wire (2 cm), initiator, DMSO, and methyl acrylate. The flask was sealed and the solution was degassed via three freeze-pump-thaw cycles, then backfilled with nitrogen and warmed to room temperature. Me_6TREN was added via microsyringe and the reaction was stirred at room temperature for the indicated amount of time. Upon completion of the polymerization, the flask was opened to atmosphere and diluted with a minimal amount of DCM. The polymer was precipitated 3x into methanol cooled with dry ice and then dried under vacuum. The GPC traces for each polymer are shown below in Figure S11.

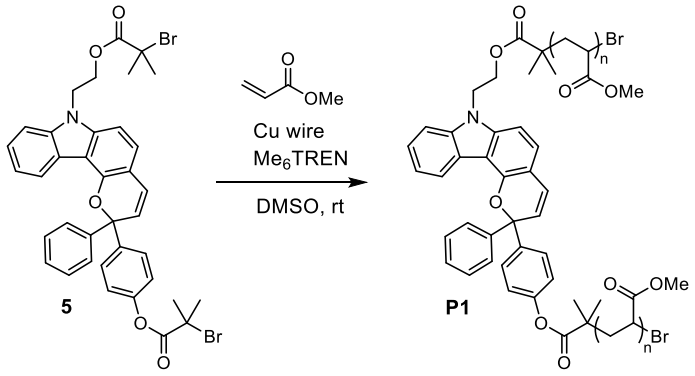

P1. Synthesized according to the general procedure using bis-initiator **5** (9.0 mg, 0.012 mmol), Me_6TREN (13 μL, 0.048 mmol), DMSO (3.50 mL), and methyl acrylate (3.50 mL, 37.0 mmol). Polymerization for 4 h afforded the title polymer as a tacky white solid (1.25 g, 37%). M_n = 149 kg/mol, $Đ$ = 1.25.

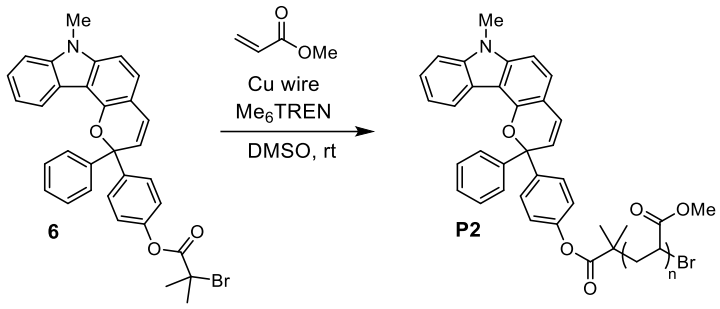

P2. Synthesized according to the general procedure using mono-functional initiator **6** (2.5 mg, 0.0045 mmol), Me_6TREN (5.0 μL, 0.018 mmol), DMSO (1.50 mL), and methyl acrylate (1.50 mL, 13.6 mmol). Polymerization for 110 min afforded the title polymer as a tacky pale yellow solid (380 mg, 27%). M_n = 191 kg/mol, $Đ$ = 1.29.

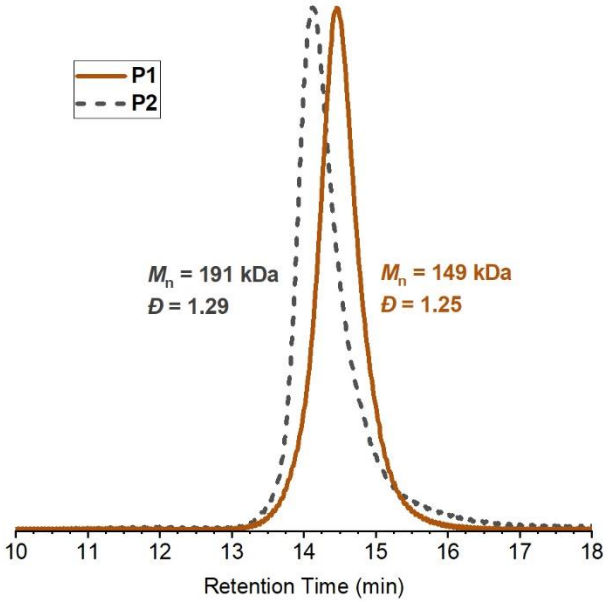

Figure S2.11 GPC traces (RI response) normalized to peak height for **P1** and **P2**.

2.5.3 PDMS Materials

PDMS materials incorporating 2*H*-benzopyran (~1.3 wt%) were prepared following previously reported procedures using the two-part Sylgard® 184 elastomer kit (Dow Corning).[16,26] PDMS sheets approximately 0.5 mm thick were cut into 1 cm x 1 cm samples for testing.

General Procedure for Preparation of PDMS Materials. Benzopyran crosslinker **BP-ene** (10 mg) was dissolved in xylenes (0.1 mL) in a 20 mL scintillation vial. Sylgard® 184 prepolymer base (752 mg) was added and the mixture was thoroughly mixed in a vortex mixer to form a homogenous, pale brown opaque dispersion. Sylgard® 184 curing agent (78 mg) was added and the contents were mixed vigorously using a vortex mixer for 10 min. The mixture was then pipetted onto a 2.5 cm x 2.5 cm Delrin plate which was placed inside a vacuum chamber and evacuated under high vacuum (< 50 mTorr) for 3 h. The Delrin plate was then transferred to an oven and cured at 80 ° C overnight. After curing, the plate was removed from the oven and the PDMS film was peeled off and cut into 1 cm x 1 cm samples with a razor blade.

Details of the Patterning Procedure Applied to PDMS Films. The stamp used in the patterning experiments to apply localized compression was 3D printed from poly(lactic acid) with embossed features in the shape of a wavy pattern,[58] as illustrated in Figure 2.3 in the main text. The stamp was manually compressed into a 1 cm^2 film under a weight of ~75 kg to achieve mechanochemical activation without causing irreversible deformation or tearing of the PDMS. After compression, the films were immersed in a solution of hydrochloric acid (15 mM in DCM) for 20 s and subsequently dried with paper towel. All steps were conducted

under ambient light and atmosphere. The hydrochloric acid solution was prepared by adding a 4 M HCl solution in dioxane to DCM to afford the indicated concentration.

2.5.4 DFT Calculations (CoGEF)

CoGEF calculations were performed using Spartan ′20 Parallel Suite according to previously reported methods.[59,60] Ground state energies were calculated using DFT at the B3LYP/6-31G* level of theory. Truncated models of each mechanophore with terminal acetoxy groups were used in the calculations. The equilibrium conformations of the unconstrained molecule were initially calculated using molecular mechanics (MMFF) followed by optimization of the equilibrium geometries using DFT (B3LYP/6-31G*). Starting from the equilibrium geometry of the unconstrained molecules (energy = 0 kJ/mol), the distance between the carbon atoms in the terminal methyl groups of the truncated structures was increased in increments of 0.05 Å and the energy was minimized at each step. The maximum force associated with the mechanochemical reaction was calculated from the slope of the curve immediately prior to bond cleavage.

2.5.5 Details for Photoirradiation and Sonication Experiments

General Procedure for Sonication Experiments. A sonication vessel was placed onto the sonication probe and charged with a 2 mg/mL solution of polymer in CH_3CN containing 30 mM BHT (20.0 mL), which was added to minimize decomposition side reactions resulting from free radicals generated during sonication.[61,62] The sonication vessel was submerged in a −45 °C bath and degassed by sparging with N_2 for 30 min. The inert gas line was then

removed into the headspace of the reaction vessel and the system was maintained under an inert atmosphere throughout the sonication experiment. Continuous sonication was then initiated (20 kHz, 20% amplitude, 8.4 ± 0.4 W/cm^2). The temperature inside the reaction vessel equilibrated to −15 °C, as measured by a thermocouple inserted into the solution (Digi-Sense EW-91428-02 thermometer with Digi-Sense probe EW-08466-83). The entire system was kept in the dark for the duration of the experiment. Aliquots (0.4 mL) were removed at 0, 1, 5, 10, 15, 20 min. The aliquots were added directly into the quartz cuvette inside of the UV-vis spectrometer and the collection of absorption spectra was immediately initiated. After the intended amount of time, sonication was stopped. A quartz cuvette charged with freshly sonicated solution (1 mL) was immediately treated with hydrochloric acid (4 N in dioxane) via microsyringe to provide a concentration of 15 mM HCl. If applicable, triethylamine (Et_3N) was added immediately to the cuvette with the freshly acidified solution via microsyringe to provide a concentration of 30 mM Et_3N. UV-vis absorption spectra were acquired immediately after the treatment with acid or base. Sonication intensity was calibrated according to the literature method.[63]

General Procedure for Photoirradiation Experiments. Photoirradiation experiments were performed in a quartz cuvette at room temperature in batch. A quartz cuvette was charged with a solution of polymer (2 mg/mL in CH_3CN containing 30 mM BHT, 1 mL total volume). The quartz cuvette was then exposed to a UV light source (λ = 311 nm) positioned ~2 in away. After the intended amount of time, photoirradiation was stopped and a UV-vis absorption spectrum was immediately recorded. Hydrochloric acid solution was prepared by adding 4 M HCl in dioxane into CH_3CN to make an HCl stock solution (1 M in CH_3CN) and

the HCl stock solution was added to the quartz cuvette containing the freshly irradiated solution via microsyringe to provide an indicated concentration of HCl. If applicable, triethylamine (Et_3N) was added immediately to the cuvette containing the freshly acidified solution via microsyringe to provide a concentration of 30 mM Et_3N. UV-vis absorption spectra were acquired immediately after the treatment with acid or base.

2.6 ^{1}H and ^{13}C NMR Spectra

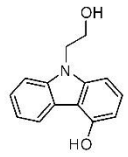

2

^{1}H (400 MHz, acetone-d_6)

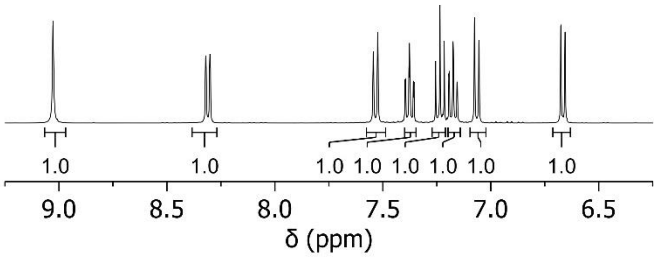

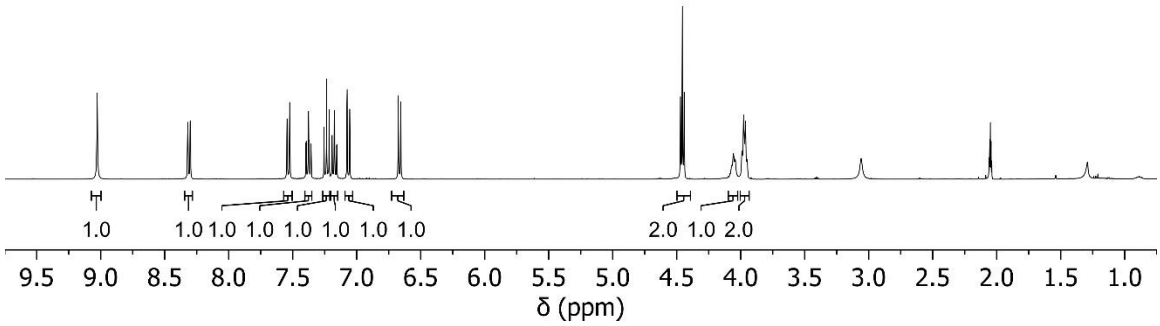

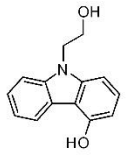

2

^{13}C (101 MHz, acetone-d_6)

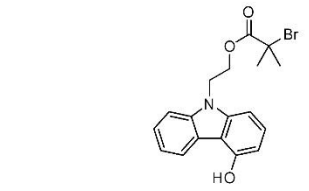

3

^{1}H (400 MHz, CD_2Cl_2)

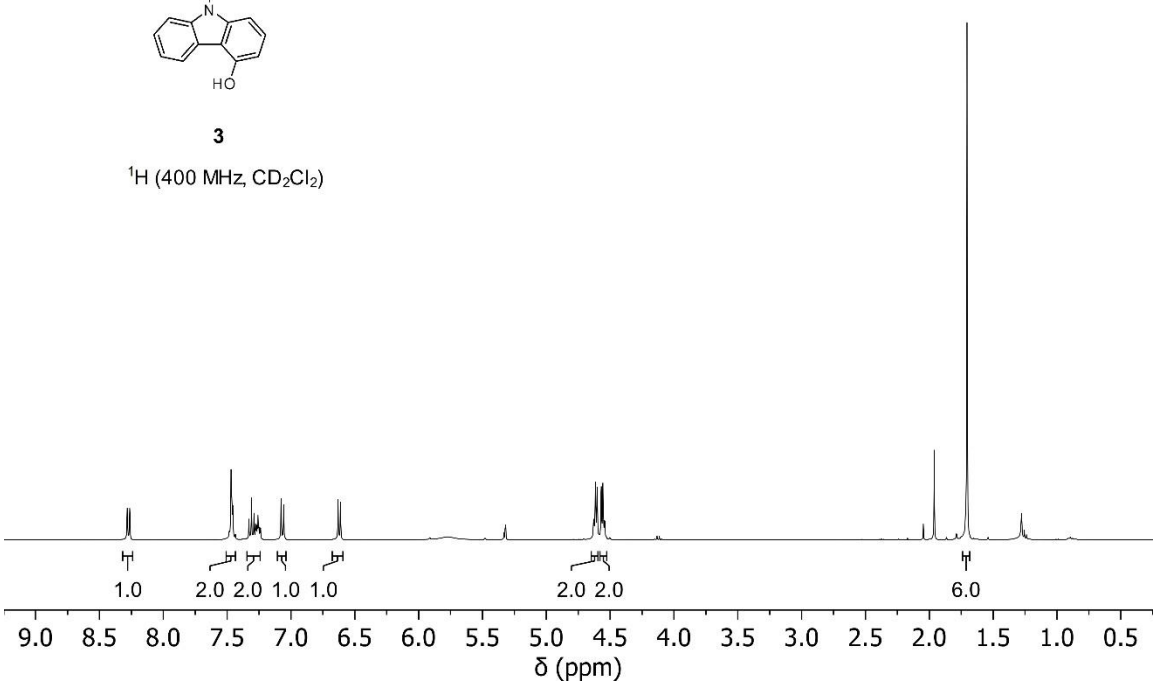

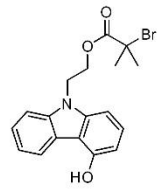

3

^{13}C (101 MHz, CD_2Cl_2)

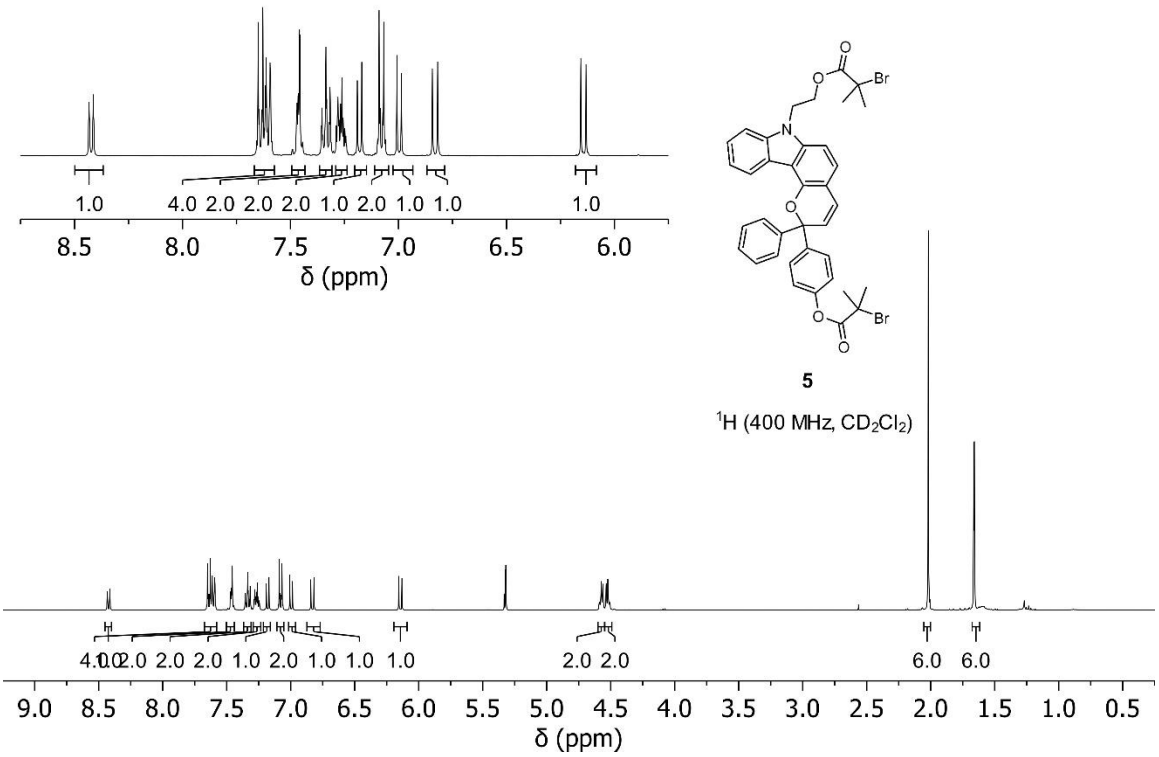
1.0
4.0 2.0 2.0 2.0 1.0 2.0 1.0 1.0
1.0
8.5
8.0
7.5
7.0
6.5
6.0
δ (ppm)
5
^{1}H (400 MHz, CD_2Cl_2)
4.0 2.0 2.0 2.0 1.0 2.0 1.0 1.0 1.0
2.0 2.0
6.0 6.0
9.0 8.5 8.0 7.5 7.0 6.5 6.0 5.5 5.0 4.5 4.0 3.5 3.0 2.5 2.0 1.5 1.0 0.5
δ (ppm)

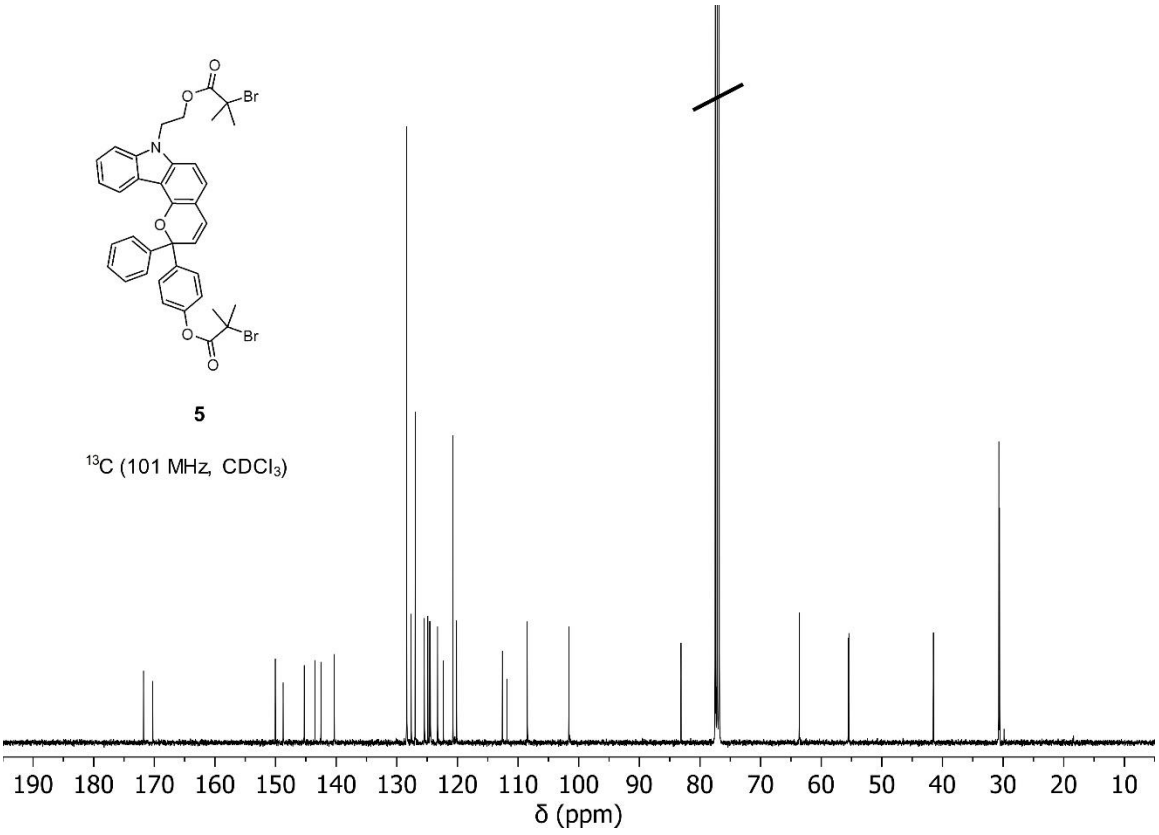
5
^{13}C (101 MHz, $CDCl_3$)
190 180 170 160 150 140 130 120 110 100 90 80 70 60 50 40 30 20 10
δ (ppm)

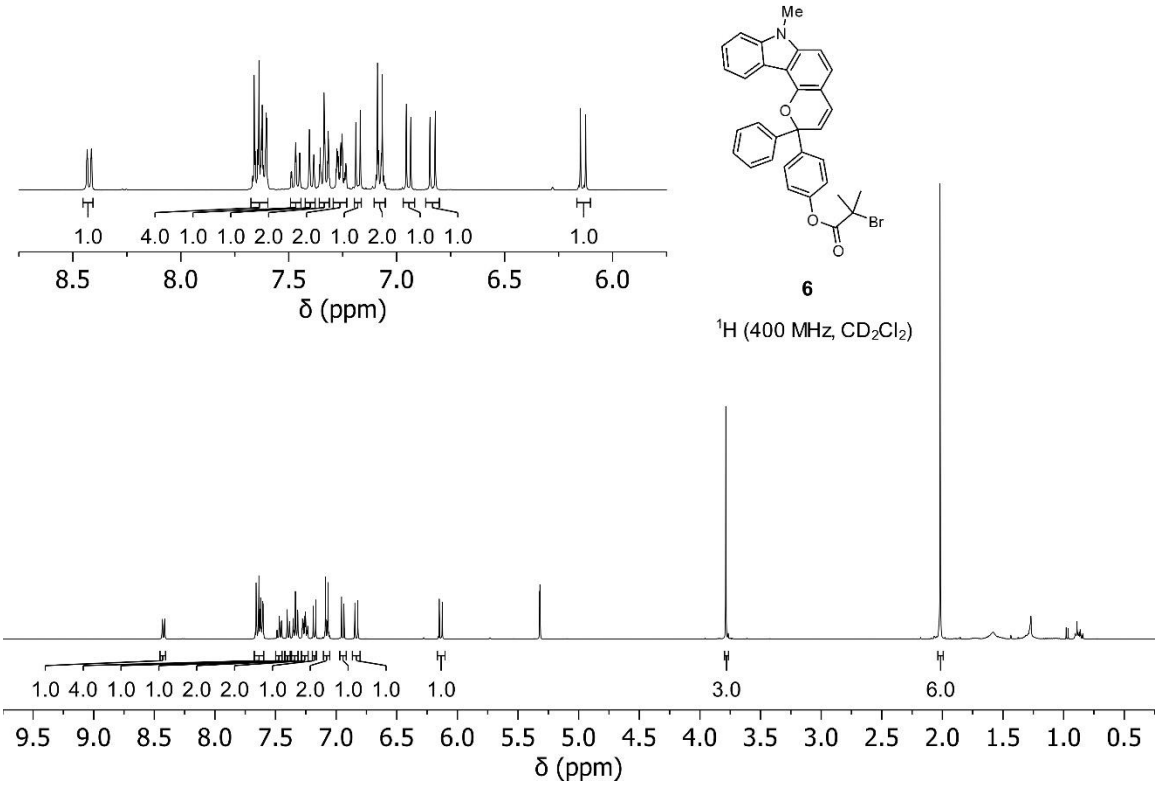
Me
N
O
O
O
Br
1.0 4.0 1.0 1.0 2.0 2.0 1.0 2.0 1.0 1.0 1.0
8.5 8.0 7.5 7.0 6.5 6.0
δ (ppm)
6
^{1}H (400 MHz, CD_2Cl_2)
1.0 4.0 1.0 1.0 2.0 2.0 1.0 2.0 1.0 1.0 1.0 3.0 6.0
9.5 9.0 8.5 8.0 7.5 7.0 6.5 6.0 5.5 5.0 4.5 4.0 3.5 3.0 2.5 2.0 1.5 1.0 0.5
δ (ppm)

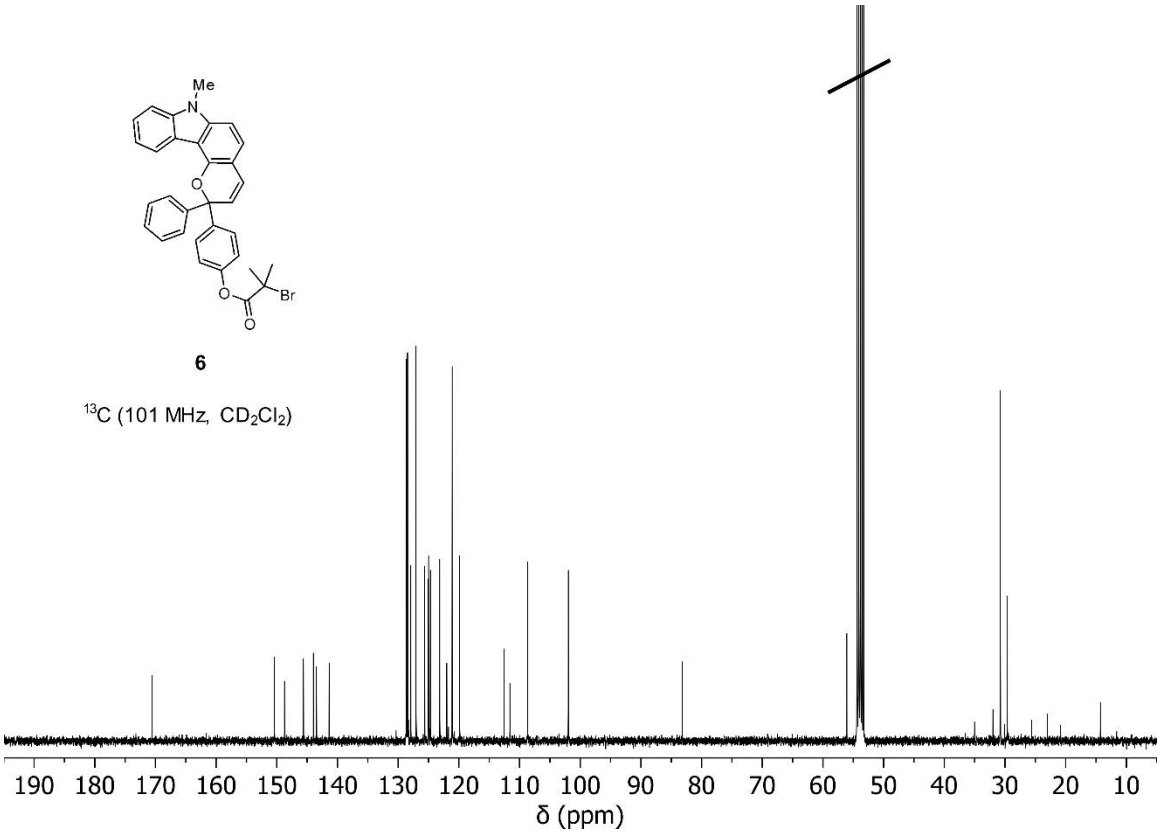
Me
N
O
O
O
Br
6
^{13}C (101 MHz, CD_2Cl_2)
190 180 170 160 150 140 130 120 110 100 90 80 70 60 50 40 30 20 10
δ (ppm)

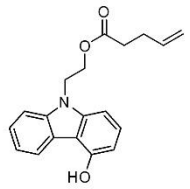

7

^{1}H (400 MHz, acetone-d_6)

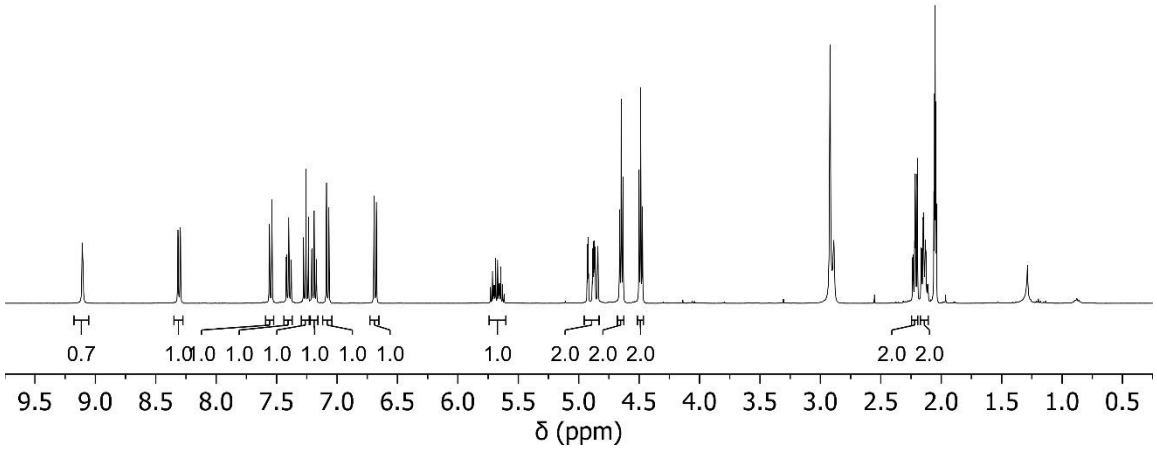

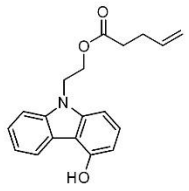

7

^{13}C (101 MHz, CD_2Cl_2)

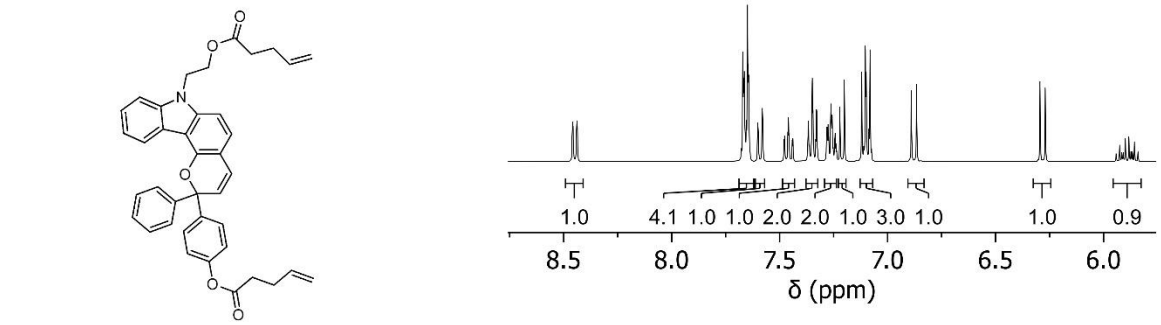

BP-ene

^{1}H (400 MHz, acetone-d_6)

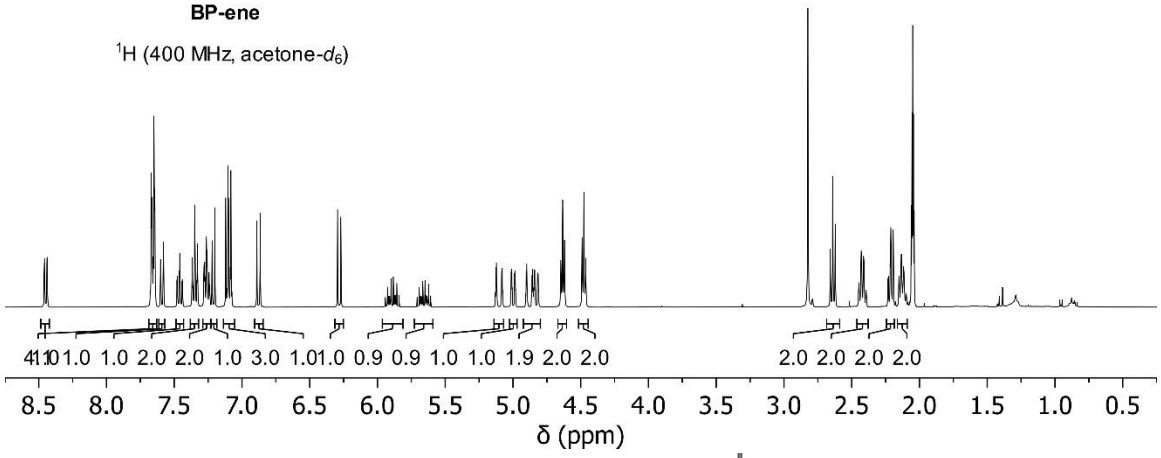

BP-ene

^{13}C (101 MHz, $CDCl_3$)

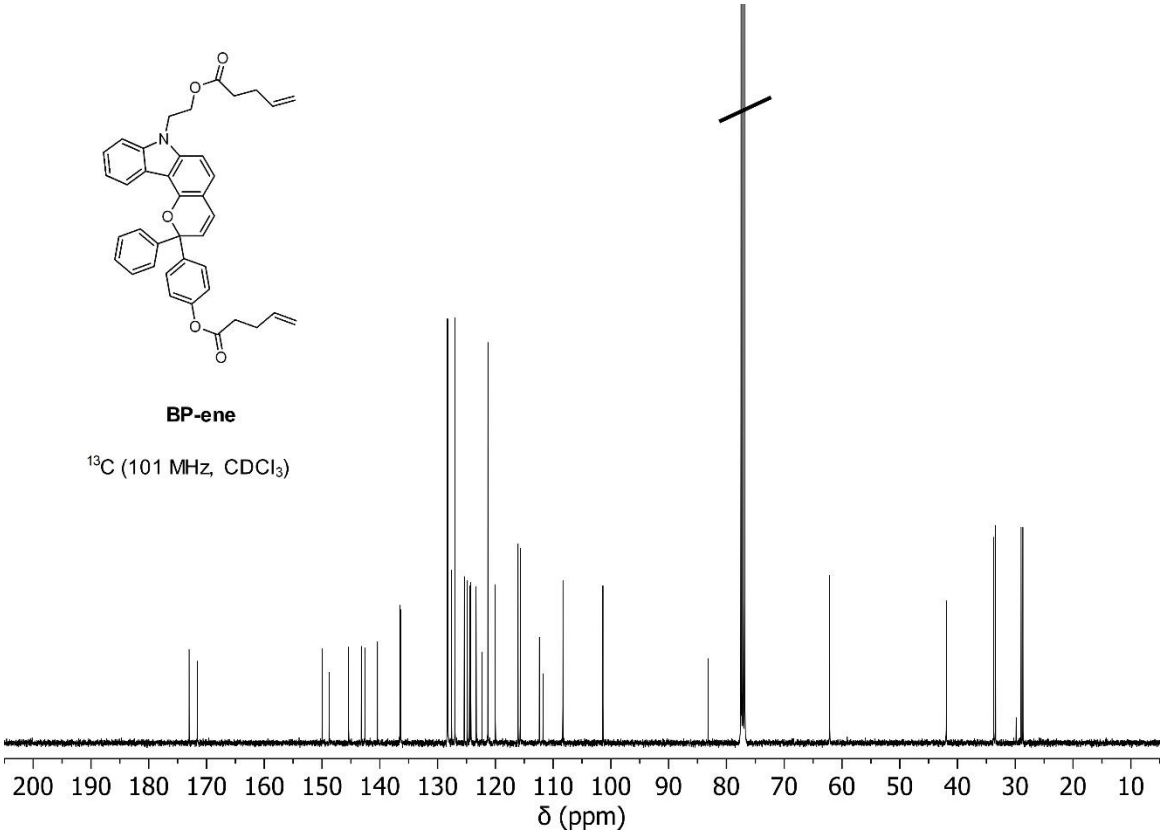

2.7 References

(1) Wei, M.; Gao, Y.; Li, X.; Serpe, M. J. Stimuli-Responsive Polymers and Their Applications. *Polymer Chemistry* **2017**, *8*, 127–143.

(2) Hu, J.; Liu, S. Responsive Polymers for Detection and Sensing Applications: Current Status and Future Developments. *Macromolecules* **2010**, *43* (20), 8315–8330. https://doi.org/10.1021/ma1005815.

(3) Bayat, M.; Mardani, H.; Roghani-Mamaqani, H.; Hoogenboom, R. Self-Indicating Polymers: A Pathway to Intelligent Materials. *Chem. Soc. Rev.* **2024**, *53* (8), 4045–4085. https://doi.org/10.1039/d3cs00431g.

(4) Cook, A. B.; Decuzzi, P. Harnessing Endogenous Stimuli for Responsive Materials in Theranostics. *ACS Nano* **2021**, *15* (2), 2068–2098. https://doi.org/10.1021/acsnano.0c09115.

(5) Wang, Y.; Weng, J.; Wen, X.; Hu, Y.; Ye, D. Recent Advances in Stimuli-Responsive *in Situ* Self-Assembly of Small Molecule Probes for *in Vivo* Imaging of Enzymatic Activity. *Biomater. Sci.* **2021**, *9* (2), 406–421. https://doi.org/10.1039/D0BM00895H.

(6) Versaw, B. A.; Zeng, T.; Hu, X.; Robb, M. J. Harnessing the Power of Force: Development of Mechanophores for Molecular Release. *J. Am. Chem. Soc.* **2021**, *143* (51), 21461–21473. https://doi.org/10.1021/jacs.1c11868.

(7) Introduction to Stimuli-Responsive Materials and Their Biomedical Applications. In *ACS Symposium Series*; American Chemical Society: Washington, DC, 2023; pp 1–30. https://doi.org/10.1021/bk-2023-1436.ch001.

(8) Fatima, M.; Almalki, W. H.; Khan, T.; Sahebkar, A.; Kesharwani, P. Harnessing the Power of Stimuli-Responsive Nanoparticles as an Effective Therapeutic Drug Delivery System. *Advanced Materials* **2024**, *36* (24). https://doi.org/10.1002/adma.202312939.

(9) Fihey, A.; Perrier, A.; Browne, W. R.; Jacquemin, D. Multiphotochromic Molecular Systems. *Chem. Soc. Rev.* **2015**, *44* (11), 3719–3759. https://doi.org/10.1039/C5CS00137D.

(10) Erbas-Cakmak, S.; Kolemen, S.; Sedgwick, A. C.; Gunnlaugsson, T.; James, T. D.; Yoon, J.; Akkaya, E. U. Molecular Logic Gates: The Past, Present and Future. *Chem. Soc. Rev.* **2018**, *47* (7), 2228–2248. https://doi.org/10.1039/C7CS00491E.

(11) Nie, H.; Self, J. L.; Kuenstler, A. S.; Hayward, R. C.; Read De Alaniz, J. Multiaddressable Photochromic Architectures: From Molecules to Materials. *Advanced Optical Materials* **2019**, *7* (16), 1900224. https://doi.org/10.1002/adom.201900224.

(12) Beyer, M. K.; Clausen-Schaumann, H. Mechanochemistry: The Mechanical Activation of Covalent Bonds. *Chem. Rev.* **2005**, *105* (8), 2921–2948. https://doi.org/10.1021/cr030697h.

(13) Caruso, M. M.; Davis, D. A.; Shen, Q.; Odom, S. A.; Sottos, N. R.; White, S. R.; Moore, J. S. Mechanically-Induced Chemical Changes in Polymeric Materials. *Chem. Rev.* **2009**, *109* (11), 5755–5798. https://doi.org/10.1021/cr9001353.

(14) Li, J.; Nagamani, C.; Moore, J. S. Polymer Mechanochemistry: From Destructive to Productive. *Acc. Chem. Res.* **2015**, *48* (8), 2181–2190. https://doi.org/10.1021/acs.accounts.5b00184.

(15) Barber, R. W.; McFadden, M. E.; Hu, X.; Robb, M. J. Mechanochemically Gated Photoswitching: Expanding the Scope of Polymer Mechanochromism. *Synlett* **2019**, *30* (15), 1725–1732. https://doi.org/10.1055/s-0037-1611858.
(16) Robb, M. J.; Kim, T. A.; Halmes, A. J.; White, S. R.; Sottos, N. R.; Moore, J. S. Regioisomer-Specific Mechanochromism of Naphthopyran in Polymeric Materials. *J. Am. Chem. Soc.* **2016**, *138* (38), 12328–12331. https://doi.org/10.1021/jacs.6b07610.
(17) McFadden, M. E.; Robb, M. J. Force-Dependent Multicolor Mechanochromism from a Single Mechanophore. *J. Am. Chem. Soc.* **2019**, *141* (29), 11388–11392. https://doi.org/10.1021/jacs.9b05280.
(18) Versaw, B. A.; McFadden, M. E.; Husic, C. C.; Robb, M. J. Designing Naphthopyran Mechanophores with Tunable Mechanochromic Behavior. *Chem. Sci.* **2020**, *11* (17), 4525–4530. https://doi.org/10.1039/D0SC01359E.
(19) McFadden, M. E.; Robb, M. J. Generation of an Elusive Permanent Merocyanine via a Unique Mechanochemical Reaction Pathway. *J. Am. Chem. Soc.* **2021**, *143* (21), 7925–7929. https://doi.org/10.1021/jacs.1c03865.
(20) Osler, S. K.; McFadden, M. E.; Robb, M. J. Comparison of the Reactivity of Isomeric 2 *H* - and 3 *H* -naphthopyran Mechanophores. *Journal of Polymer Science* **2021**, *59* (21), 2537–2544. https://doi.org/10.1002/pol.20210417.
(21) Osler, S. K.; McFadden, M. E.; Zeng, T.; Robb, M. J. Mechanochemical Reactivity of a Multimodal 2 *H* -Bis-Naphthopyran Mechanophore. *Polym. Chem.* **2023**, *14* (22), 2717–2723. https://doi.org/10.1039/D3PY00344B.
(22) Sun, Y.; McFadden, M. E.; Osler, S. K.; Barber, R. W.; Robb, M. J. Anomalous Photochromism and Mechanochromism of a Linear Naphthopyran Enabled by a Polarizing Dialkylamine Substituent. *Chem. Sci.* **2023**, *14* (38), 10494–10499. https://doi.org/10.1039/D3SC03790H.
(23) Osler, S. K.; Ballinger, N. A.; Robb, M. J. The Role of Torsion on the Force-Coupled Reactivity of a Fluorenyl Naphthopyran Mechanophore. *J. Am. Chem. Soc.* **2025**, *147* (4), 3904–3911. https://doi.org/10.1021/jacs.4c18395.
(24) Potisek, S. L.; Davis, D. A.; Sottos, N. R.; White, S. R.; Moore, J. S. Mechanophore-Linked Addition Polymers. *J. Am. Chem. Soc.* **2007**, *129* (45), 13808–13809. https://doi.org/10.1021/ja076189x.
(25) Davis, D. A.; Hamilton, A.; Yang, J.; Cremar, L. D.; Van Gough, D.; Potisek, S. L.; Ong, M. T.; Braun, P. V.; Martínez, T. J.; White, S. R.; Moore, J. S.; Sottos, N. R. Force-Induced Activation of Covalent Bonds in Mechanoresponsive Polymeric Materials. *Nature* **2009**, *459* (7243), 68–72. https://doi.org/10.1038/nature07970.
(26) Gossweiler, G. R.; Hewage, G. B.; Soriano, G.; Wang, Q.; Welshofer, G. W.; Zhao, X.; Craig, S. L. Mechanochemical Activation of Covalent Bonds in Polymers with Full and Repeatable Macroscopic Shape Recovery. *ACS Macro Lett.* **2014**, *3* (3), 216–219. https://doi.org/10.1021/mz500031q.
(27) Zhang, H.; Gao, F.; Cao, X.; Li, Y.; Xu, Y.; Weng, W.; Boulatov, R. Mechanochromism and Mechanical-Force-Triggered Cross-Linking from a Single Reactive Moiety Incorporated into Polymer Chains. *Angew Chem Int Ed* **2016**, *55* (9), 3040–3044. https://doi.org/10.1002/anie.201510171.

(28) Wang, Z.; Ma, Z.; Wang, Y.; Xu, Z.; Luo, Y.; Wei, Y.; Jia, X. A Novel Mechanochromic and Photochromic Polymer Film: When Rhodamine Joins Polyurethane. *Advanced Materials* **2015**, *27* (41), 6469–6474. https://doi.org/10.1002/adma.201503424.
(29) Wang, T.; Zhang, N.; Dai, J.; Li, Z.; Bai, W.; Bai, R. Novel Reversible Mechanochromic Elastomer with High Sensitivity: Bond Scission and Bending-Induced Multicolor Switching. *ACS Appl. Mater. Interfaces* **2017**, *9* (13), 11874–11881. https://doi.org/10.1021/acsami.7b00176.
(30) Wu, M.; Li, Y.; Yuan, W.; Bo, G. D.; Cao, Y.; Chen, Y. Cooperative and Geometry-Dependent Mechanochromic Reactivity through Aromatic Fusion of Two Rhodamines in Polymers. *J. Am. Chem. Soc.* **2022**, *144*, 17120−17128.
(31) Qian, H.; Purwanto, N. S.; Ivanoff, D. G.; Halmes, A. J.; Sottos, N. R.; Moore, J. S. Fast, Reversible Mechanochromism of Regioisomeric Oxazine Mechanophores: Developing in Situ Responsive Force Probes for Polymeric Materials. *Chem* **2021**, *7* (4), 1080–1091. https://doi.org/10.1016/j.chempr.2021.02.014.
(32) Qi, Q.; Sekhon, G.; Chandradat, R.; Ofodum, N. M.; Shen, T.; Scrimgeour, J.; Joy, M.; Wriedt, M.; Jayathirtha, M.; Darie, C. C.; Shipp, D. A.; Liu, X.; Lu, X. Force-Induced Near-Infrared Chromism of Mechanophore-Linked Polymers. *J. Am. Chem. Soc.* **2021**, *143* (42), 17337–17343. https://doi.org/10.1021/jacs.1c05923.
(33) Göstl, R.; Sijbesma, R. P. π-Extended Anthracenes as Sensitive Probes for Mechanical Stress. *Chem. Sci.* **2016**, *7* (1), 370–375. https://doi.org/10.1039/C5SC03297K.
(34) Baumann, C.; Stratigaki, M.; Centeno, S. P.; Göstl, R. Multicolor Mechanofluorophores for the Quantitative Detection of Covalent Bond Scission in Polymers. *Angew Chem Int Ed* **2021**, *60* (24), 13287–13293. https://doi.org/10.1002/anie.202101716.
(35) Hemmer, J. R.; Rader, C.; Wilts, B. D.; Weder, C.; Berrocal, J. A. Heterolytic Bond Cleavage in a Scissile Triarylmethane Mechanophore. *J. Am. Chem. Soc.* **2021**, *143* (45), 18859–18863. https://doi.org/10.1021/jacs.1c10004.
(36) Imato, K.; Irie, A.; Kosuge, T.; Ohishi, T.; Nishihara, M.; Takahara, A.; Otsuka, H. Mechanophores with a Reversible Radical System and Freezing-Induced Mechanochemistry in Polymer Solutions and Gels. *Angew Chem Int Ed* **2015**, *54* (21), 6168–6172. https://doi.org/10.1002/anie.201412413.
(37) Imato, K.; Kanehara, T.; Ohishi, T.; Nishihara, M.; Yajima, H.; Ito, M.; Takahara, A.; Otsuka, H. Mechanochromic Dynamic Covalent Elastomers: Quantitative Stress Evaluation and Autonomous Recovery. *ACS Macro Lett.* **2015**, *4* (11), 1307–1311. https://doi.org/10.1021/acsmacrolett.5b00717.
(38) McFadden, M. E.; Osler, S. K.; Sun, Y.; Robb, M. J. Mechanical Force Enables an Anomalous Dual Ring-Opening Reaction of Naphthodipyran. *J. Am. Chem. Soc.* **2022**, *144* (49), 22391–22396. https://doi.org/10.1021/jacs.2c08817.
(39) He, W.; Yuan, Y.; Wu, M.; Li, X.; Shen, Y.; Qu, Z.; Chen, Y. Multicolor Chromism from a Single Chromophore through Synergistic Coupling of Mechanochromic and Photochromic Subunits. *Angew Chem Int Ed* **2023**, *62* (11), e202218785. https://doi.org/10.1002/anie.202218785.

(40) Kocak, G.; Tuncer, C.; Bütün, V. pH-Responsive Polymers. *Polym. Chem.* **2017**, *8* (1), 144–176. https://doi.org/10.1039/C6PY01872F.
(41) Hepworth, J. D.; Heron, B. M. Photochromic Naphthopyrans. In *Functional Dyes*; Elsevier Science, 2006; pp 85–135. https://doi.org/10.1016/B978-044452176-7/50004-8.
(42) Becker, R. S.; Michl, J. Photochromism of Synthetic and Naturally Occurring 2H-Chromenes and 2H-Pyrans. *J. Am. Chem. Soc.* **1966**, *88* (24), 5931–5933. https://doi.org/10.1021/ja00976a044.
(43) McFadden, M. E.; Barber, R. W.; Overholts, A. C.; Robb, M. J. Naphthopyran Molecular Switches and Their Emergent Mechanochemical Reactivity. *Chem. Sci.* **2023**, *14* (37), 10041–10067. https://doi.org/10.1039/D3SC03729K.
(44) Oliveira, M. M.; Carvalho, L. M.; Moustrou, C.; Samat, A.; Guglielmetti, R.; Oliveira-Campos, A. M. F. Synthesis and Photochromic Behaviour of Novel 2H-1-Benzopyrans (=2H-Chromenes) Derived from Carbazololes. *HCA* **2001**, *84* (5), 1163–1171. https://doi.org/10.1002/1522-2675(20010516)84:5<1163::AID-HLCA1163>3.0.CO;2-T.
(45) Pozzo, J.-L.; Samat, A.; Guglielmetti, R.; Lokshin, V.; Minkin, V. Furo-Fused 2 *H* -Chromenes: Synthesis and Photochromic Properties. *Can. J. Chem.* **1996**, *74* (9), 1649–1659. https://doi.org/10.1139/v96-182.
(46) Pozzo, J.-L.; Lokshin, V.; Samat, A.; Guglielmetti, R.; Dubest, R.; Aubard, J. Effect of Heteroaromatic Annulation with Five-Membered Rings on the Photochromism of 2H-[1] -Benzopyrans. *J. Photochem. Photobiol. A: Chem.* **1998**, *114* (3), 185–191. https://doi.org/10.1016/S1010-6030(98)00215-9.
(47) Beyer, M. K. The Mechanical Strength of a Covalent Bond Calculated by Density Functional Theory. *The Journal of Chemical Physics* **2000**, *112* (17), 7307–7312. https://doi.org/10.1063/1.481330.
(48) Klein, I. M.; Husic, C. C.; Kovács, D. P.; Choquette, N. J.; Robb, M. J. Validation of the CoGEF Method as a Predictive Tool for Polymer Mechanochemistry. *J. Am. Chem. Soc.* **2020**, *142* (38), 16364–16381. https://doi.org/10.1021/jacs.0c06868.
(49) May, P. A.; Moore, J. S. Polymer Mechanochemistry: Techniques to Generate Molecular Force via Elongational Flows. *Chem. Soc. Rev.* **2013**, *42* (18), 7497. https://doi.org/10.1039/c2cs35463b.
(50) Zhao, W.; Carreira, E. M. Facile One-Pot Synthesis of Photochromic Pyrans. *Org. Lett.* **2003**, *5* (22), 4153–4154. https://doi.org/10.1021/ol035599x.
(51) Nguyen, N. H.; Rosen, B. M.; Lligadas, G.; Percec, V. Surface-Dependent Kinetics of Cu(0)-Wire-Catalyzed Single-Electron Transfer Living Radical Polymerization of Methyl Acrylate in DMSO at 25 °C. *Macromolecules* **2009**, *42* (7), 2379–2386. https://doi.org/10.1021/ma8028562.
(52) Brazevic, S.; Nizinski, S.; Szabla, R.; Rode, M. F.; Burdzinski, G. Photochromic Reaction in 3 *H* -Naphthopyrans Studied by Vibrational Spectroscopy and Quantum Chemical Calculations. *Phys. Chem. Chem. Phys.* **2019**, *21* (22), 11861–11870. https://doi.org/10.1039/C9CP01451A.
(53) Brazevic, S.; Baranowski, M.; Sikorski, M.; Rode, M. F.; Burdziński, G. Ultrafast Dynamics of the Transoid- *Cis* Isomer Formed in Photochromic Reaction from 3 *H* -

Naphthopyran. *ChemPhysChem* **2020**, *21* (13), 1402–1407. https://doi.org/10.1002/cphc.202000294.

(54) Sanchez, A. M.; Barra, M.; De Rossi, R. H. On the Mechanism of the Acid/Base-Catalyzed Thermal *Cis* − *Trans* Isomerization of Methyl Orange. *J. Org. Chem.* **1999**, *64* (5), 1604–1609. https://doi.org/10.1021/jo982069j.

(55) Green, S. A.; Huffman, T. R.; McCourt, R. O.; Van Der Puyl, V.; Shenvi, R. A. Hydroalkylation of Olefins To Form Quaternary Carbons. *J. Am. Chem. Soc.* **2019**, *141* (19), 7709–7714. https://doi.org/10.1021/jacs.9b02844.

(56) Araki, K.; Maebayashi, H.; Masaki, A.; Koiso, N.; Nakagame, R.; Yamomoto, M.; Sasaki, I.; Iwanaga, K. Rare Earth Complex. US2025/0074925A1, 2025.

(57) Nguyen, N. H.; Rosen, B. M.; Lligadas, G.; Percec, V. Surface-Dependent Kinetics of Cu(0)-Wire-Catalyzed Single-Electron Transfer Living Radical Polymerization of Methyl Acrylate in DMSO at 25 °C. *Macromolecules* **2009**, *42* (7), 2379–2386. https://doi.org/10.1021/ma8028562.

(58) Overholts, A. C.; Granados Razo, W.; Robb, M. J. Mechanically Gated Formation of Donor–Acceptor Stenhouse Adducts Enabling Mechanochemical Multicolour Soft Lithography. *Nat. Chem.* **2023**. https://doi.org/10.1038/s41557-022-01126-5.

(59) Beyer, M. K. The Mechanical Strength of a Covalent Bond Calculated by Density Functional Theory. *The Journal of Chemical Physics* **2000**, *112* (17), 7307–7312. https://doi.org/10.1063/1.481330.

(60) Klein, I. M.; Husic, C. C.; Kovács, D. P.; Choquette, N. J.; Robb, M. J. Validation of the CoGEF Method as a Predictive Tool for Polymer Mechanochemistry. *J. Am. Chem. Soc.* **2020**, *142* (38), 16364–16381. https://doi.org/10.1021/jacs.0c06868.

(61) Yang, J.; Horst, M.; Werby, S. H.; Cegelski, L.; Burns, N. Z.; Xia, Y. Bicyclohexene-*Peri* -Naphthalenes: Scalable Synthesis, Diverse Functionalization, Efficient Polymerization, and Facile Mechanoactivation of Their Polymers. *J. Am. Chem. Soc.* **2020**, *142* (34), 14619–14626. https://doi.org/10.1021/jacs.0c06454.

(62) Overholts, A. C.; McFadden, M. E.; Robb, M. J. Quantifying Activation Rates of Scissile Mechanophores and the Influence of Dispersity. *Macromolecules* **2022**, *55* (1), 276–283. https://doi.org/10.1021/acs.macromol.1c02232.

(63) Berkowski, K. L.; Potisek, S. L.; Hickenboth, C. R.; Moore, J. S. Ultrasound-Induced Site-Specific Cleavage of Azo-Functionalized Poly(Ethylene Glycol). *Macromolecules* **2005**, *38* (22), 8975–8978. https://doi.org/10.1021/ma051394n.